EXPERIMENTAL AND NUMERICAL STUDY ON STRETCH FORMING PROCESS

A MASTER'S THESIS

in

Manufacturing Engineering

Atilim University

by

CELAL ONUR ALKAŞ

MARCH 2013

EXPERIMENTAL AND NUMERICAL STUDY ON STRETCH FORMING PROCESS

A THESIS SUBMITTED TO

THE GRADUATE SCHOOL OF NATURAL AND APPLIED SCIENCES

OF

ATILIM UNIVERSITY

BY

CELAL ONUR ALKAŞ

IN PARTIAL FULFILLMENT OF THE REQUIREMENTS FOR THE DEGREE OF

MASTER OF SCIENCE

IN

THE DEPARTMENT OF MANUFACTURING ENGINEERING

MARCH 2013

Approval of the Graduate School of Natural and Applied Sciences, Atılım University.

_____

Prof. Dr. K. İbrahim Akman

Director

I certify that this thesis satisfies all the requirements as a thesis for the degree of Master of Science.

_____

Prof. Dr. Gülhan Özbayoğlu

Vice Chairman

This is to certify that we have read the thesis "Experimental and Numerical Study on Stretch Forming Process" submitted by "Celal Onur Alkaş" and that in our opinion it is fully adequate, in scope and quality, as a thesis for the degree of Master of Science.

_____	_____
Asst. Prof. Dr. Caner Şimşir	Asst. Prof. Dr. Celalettin Karadoğan
Co-Supervisor	Supervisor

Examining Committee Members

Prof. Dr. Bilgin Kaftanoğlu	_____
Asst. Prof. Dr. Kazım Tur	_____
Asst. Prof. Dr. Celalettin Karadoğan	_____
Asst. Prof. Dr. Caner Şimşir	_____
Dr. Ömer Music	_____

Date: 22.03.2013

I declare and guarantee that all data, knowledge and information in this document has been obtained, processed and presented in accordance with academic rules and ethical conduct. Based on these rules and conduct, I have fully cited and referenced all material and results that are not original to this work.

Celal Onur Alkaş

ABSTRACT

EXPERIMENTAL AND NUMERICAL INVESTIGATION OF STRETCH FORMING PROCESS

Alkas, Celal Onur

M.S., Manufacturing Engineering Department

Supervisor: Asst. Prof. Dr. Celalettin Karadoğan

Co-Supervisor: Asst. Prof. Dr. Caner Şimşir

March 2013, 125 pages

Stretch forming process is commonly used in the aircraft industry for the manufacturing of large sheet panels. The success of this process is highly dependent on the process parameters like mechanical properties of sheet material, the friction condition between tools-part interfaces and relative motions between tool and jaws. Determining the best parameters by trial - error procedure is quite difficult and costly, so that finite element analysis is needed.

The scope of this study is to establish finite element model (FEM) for stretch forming process. For this purpose, accurate material and reliable friction modeling are required. Material characterization tests of mostly used aluminum alloys are conducted to prepare input to the model. Standard tensile, stack compression, hydraulic bulge test (HBT) and forming limit diagram (FLD) tests are performed in order to identify deformation behavior and anisotropy properties of aluminum sheet materials. High accuracy CCD cameras are used to obtain material deformation during determination of FLDs and flow curves from HBT. Also, friction coefficients are determined for various lubrication conditions encountered in stretch forming processes using inverse based analysis.

Using these inputs, numerical model of the process is established by FEM for three basic stretching tool motions, which are; stretching the sheet by jaw, stretching the sheet by form die and finally stretching the sheet material by synchronized motion of both tools.

In order to improve the model and validate the analyses results, experimental work is also performed in which the deformation of the sheet is measured optically using GOM-Argus® 3-D deformation measurement device. Then, three selected aerospace sheet parts were analyzed and success of the model for industrial applications is proved.

Keywords: Stretch forming process, finite element analyses (FEA), optical deformation measurement, stack compression test, hydraulic bulge test (HBT), forming limit diagram test (FLD)

ÖZ

GERDİREREK ŞEKİLLENDİRME PROSESİNİN DENEYSEL VE SAYISAL İNCELENMESİ

Celal Onur, Alkaş

Yüksek Lisans, İmalat Mühendisliği Bölümü

Tez Yöneticisi: Yrd. Doç. Dr. Celalettin Karadoğan

Ortak Tez Yöneticisi: Yrd. Doç. Dr. Caner Şimşir

Mart 2013, 125 sayfa

Gerdirerek şekillendirme operasyonu, yaygın olarak havacılık sektöründe kullanılmakta olan geniş sac panelleri imal etmek için kullanılan bir yöntemdir. Bu prosesin başarısı büyük ölçüde sac malzemenin mekanik özellikleri, takım-iş parçası ara yüzeyindeki sürtünme koşulu, takım ve çenelerin birbirine göre bağıl hareketleri gibi işlem parametrelerine bağlıdır. Deneme yanılma prosedürü ile en iyi proses parametrelerinin tespiti oldukça zor ve maliyetlidir, bu nedenle sonlu elemanlar analizine ihtiyaç duyulmaktadır.

Bu çalışmanın amacı, gerdirerek şekillendirme prosesi için sonlu elemanlar modeli (SEM) geliştirmektir. Bu amaç için, hassas malzeme ve güvenilir temas modeli gerekmektedir. Modele girdi oluşturabilmek için, yaygın olarak kullanılan alüminyum alaşımlarına yönelik mekanik malzeme karakterizasyon testleri yürütülmüştür. Alüminyum sac malzemenin deformasyon davranışı ve anizotropik özelliklerini elde etmek için; standart çekme, basma, hidrolik şişirme testi (HŞT) ve şekillendirme sınır diyagramı (ŞSD) testleri gerçekleştirilmiştir. Malzeme deformasyonu süresince, ŞSD'lerin ve HŞT ile akma eğrilerinin tespiti için yüksek çözünürlüklü CCD kameraları kullanılmıştır. Ayrıca, ters analiz tekniği

kullanılarak gerdirme operasyonunda karşılaşılan farklı yağlama koşulları için sürtünme katsayılarının tespiti yapılmıştır.

Bu girdiler kullanılarak; çene kullanılarak gerdirme, kalıp kullanılarak gerdirme ve senkronize edilmiş takım hareketleri ile gerdirme gibi üç temel gerdirerek şekillendirme takım hareketleri sayısal olarak modellenmiştir.

Modelin iyileştirilmesi ve analiz sonuçlarının doğrulanması amacıyla 3-B optik deformasyon ölçüm cihazı olan, GOM-Argus® kullanılarak deneysel çalışmalar gerçekleştirilmiştir. Daha sonra, seçilen üç farklı havacılık sac malzemesi analiz edilmiş ve sayısal modelin başarısı endüstriyel uygulamalar için kanıtlanmıştır.

Anahtar Kelimeler: Gerdirerek şekillendirme prosesi, sonlu elemanlar analizi (SEA), optik deformasyon ölçümleri, basma testi, hidrolik şişirme testi (HŞT), şekillendirme sınır diyagramı testi (ŞSD)

ACKNOWLEDGMENTS

I would like to express my appreciation and thankfulness to Asst. Prof. Dr. Celalettin Karadoğan for guidance and insight in supervising this thesis, his invaluable help, and kindness. I would like to thank Asst. Prof. Dr. Caner Şimşir for his kind help and support. I also would like to thank Prof. Dr. Bilgin Kaftanoğlu, Prof. Dr. A. Erman Tekkaya, Asst. Prof. Dr. Celal Soyarslan, Asst. Prof. Dr. Merih Şengönül and Asst. Prof. Dr. Besim Baranoğlu who taught me during my undergraduate and graduate education. I became a qualified manufacturing engineer and researcher by their unforgettable efforts.

The support provided by Turkish Aerospace Industry (TAI) is greatly acknowledged. I am very grateful to Industrial Operations Manager Naki Polat, Outsourcing Manager Arif Köksal, Technical Specialist Recep Akçay and Tool Design Department Chief Umut Aktan and the Team Leader Gökay Sezer for their profound trust, support and suggestions to this research. I also would like to thank to all employees of the company for their help in performing experiments and willing to inform me about their experience.

This study is also supported by TÜBİTAK TEYDEB (The Scientific and Technical Research Council of Turkey). This esteemed institution is also greatly acknowledged.

Special thanks are extended to my colleagues Hasan Ali Hatipoğlu and Tuna Eden for their precious friendship and support in virtual and real environment which made the accomplishment of this study possible. On the other hand, support of the press operator Hakan Güneş is acknowledged. Participation and contribution of research assistants to the study; M. Emin Tamer, Oğuzhan Herkiloğlu and Yahya Tunç is also acknowledged.

I would like to express my happiness to have such close friends like Anıl, Eşref, Ali Okay, Emre, Serap, Gizem, Gökhan and Osman.

Finally, I would like to appreciate my parents and sister; Pervin, Orhan and Berivan Alkaş for their patience, love, encouragement and helpful support during my thesis work and especially, I would like to thank my fiancée Gizem for her invaluable support, kindness, and for being in my life with her endless love.

To My Family

LIST OF ABBREVIATIONS

AA	-	Aluminum Alloy
ASTM	-	American Society for Testing and Materials
BC	-	Boundary Condition
BHF	-	Blank Holder Force
CCD	-	Charge Couple Device
FC	-	Friction Coefficient
DOF	-	Degree of Freedom
DP	-	Dual Phase
FCC	-	Face Centered Cubic
FD	-	Form Die
FEA	-	Finite Element Analysis
FEM	-	Finite Element Method
FLC	-	Forming Limit Curve
FLD	-	Forming Limit Diagram
FSS	-	Ferritic Stainless Steel
HBT	-	Hydraulic Bulge Test
MCT	-	Material Characterization Test
KAI	-	Korean Aerospace Industry
SS	-	Stainless Steel
SF	-	Stretch Forming
STFM	-	Stretch Form Die
STJ	-	Stretch Forming Jaw
UTS	-	Ultimate Tensile Strength

NOMENCLATURE

F_p	Force
$\sigma_{f,m}$	Mean flow stress
A_0	Initial surface area
A_1	Final surface area
η_{def}	Efficiency of deformation range
$d\varepsilon_1$	Strain Differential in Tensile Test Direction
$d\varepsilon_2$	Strain Differential in Width Direction
$d\varepsilon_3$	Strain Differential in Thickness Direction
σ_1	True Stress in Longitudinal Test Direction
σ_2	True Stress in Width Direction
σ_3	True Stress in Thickness Direction
α	Stress ratio
β,	Strain ratio
d_0	Initial diameter
d_1	Final diameter
R_0	Anisotropy coefficient in the rolling direction
R_{45}	Anisotropy coefficient in the diagonal direction
R_{90}	Anisotropy coefficient in the transverse direction
σ_{eng}	Engineering stress
P	Instantaneous Load
σ_{eng}	Engineering Strain
Δl	Increase in length
L_0	Initial length
σ	True Stress

ε	True Strain
K	Strength index
n	Strain hardening coefficient
r	Die aperture radius
t_0	Initial thickness
R_1, R_2	Corresponding radius of the curved surfaces
$\bar{\sigma}$	Equivalent stress
d_c	Diameter of the die cavity
h_d	Dome height
r_f	Fillet radius in the die cavity
F_c	Blank Holder Force
h_c	Die inner diameter
R	Bulge radius
H	Blank holder load
μ	Friction coefficient
θ	Angle which is normal to an element of shell wall makes with the vertical axis
ds	Infinitesimal length of a curved section

TABLE OF CONTENTS

LIST OF FIGURES

LIST OF TABLES

CHAPTER 1

INTRODUCTION

1.1 An Overview of Stretch Forming Process

Stretching occurs as a part of many sheet metal forming operations such as drawing, bulging, beading and embossing. In this study, the discussion of stretch forming process is limited with the operations performed on specifically designed machines for stretching purpose.

Stretch forming can simply be described as a forming process performed by the application of tensile forces to stretch the sheet metal over a form die. Stretch forming process is usually preferred to manufacture components when large radius of curvatures is desired and residual stresses together with springback are troublesome. Therefore, this process is generally used to manufacture aircraft's wing members, tail structures, skin parts, fuselage segments and engine components. Truck bumpers, structural frames for buses, windows frames, telecommunication antenna, structural building members and many appliance components can also be produced using stretch forming technique.

As it is shown in the Figure 1, stretch forming (SF) process is performed using two important tools. These are;

- Jaws; to fix and pull the sheet material at the ends,
- Form Die; to form sheet metal into the desired shape.

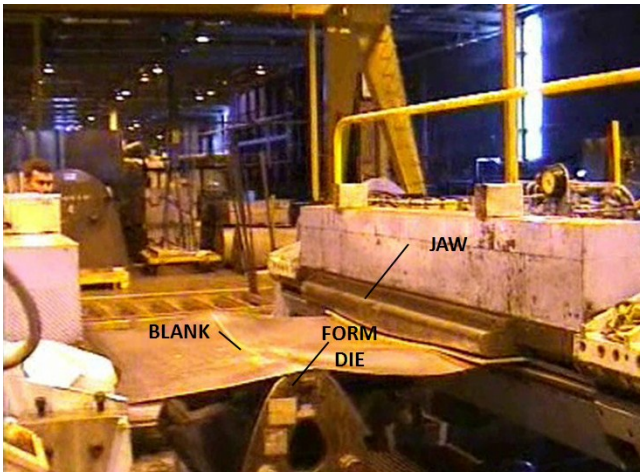

Figure 1: Stretch forming operation and stretching equipment

During the process, the sheet material is subjected to tension by jaws beyond its yield point to create plastic deformation and thinning. Since the sequence in bending and stretching is extremely important, the forces and synchronization of tool motion have to be carefully controlled during the process. The main process parameters of the process are;

- Tool motions,
- Workpiece material,
- Friction conditions,
- Geometry of final product.

Among these parameters which are mentioned above, determination of tool motions is the most important issue. Because tool motions have to be adjusted as the blank remains stretched over form die while jaws are getting closer to each other. If the amount of bending is not correctly specified, wrinkling can be observed in the sheet blank. The application of a controlled stretching of the sheet reduces the possibility of springback and failure existence such as tearing or wrinkling.

1.2 Stretch Forming of Aluminum Alloys in Aerospace Industry

Sheet metal components in different forms and properties are widely used in aerospace industry. Sheet parts with large radius of curvature and combined contours (both positive and negative contours) can be produced by stretch forming process. That's why this process is extensively used in aircraft industry. Although, large presses are used for SF process to manufacture wing members, tail structures, fuselage segments, engine components, helicopter blades, external fuel tanks for space shuttles. Different sheet metal forms obtained by SF process are illustrated in Figure 2. As it is shown, large airplane components which do not have sharp edges can be generally produced accurately. The part which will be formed with this process can be generally a part which has a large radius such as body panel shown in Figure 2 (a), also it can be a narrow part to be used in the wing structure Figure 2 (b). On the other hand, complex parts such as exhaust component illustrated in Figure 2 (c) and parts which has large bending radius Figure 2 (d) can be manufactured by using SF process.

SF process is not only limited to aircraft and aerospace industry. Other components obtained by stretch forming are; body panels such as doors, truck bumpers, fenders, structural frames for buses and recreational vehicles, monorail guide beams, window frames for mobile home, structural building members, telecommunication antenna, and many appliance components.

Increasing demand on high aero-dynamical expectations and overall affordability, significant reductions in structural weight have to be achieved. Therefore, light weight metals which provide high strength to weight ratio, are preferred in aerospace industry. Due to its good formability, low density, high strength to weight ratio, corrosion resistance, heat treatable properties and high availability, aluminum can be considered as one of the most important material for aerospace industry. For example, the world's largest twin engine airplane Boeing 777 consists of 70% aluminum alloy (Figure 3).

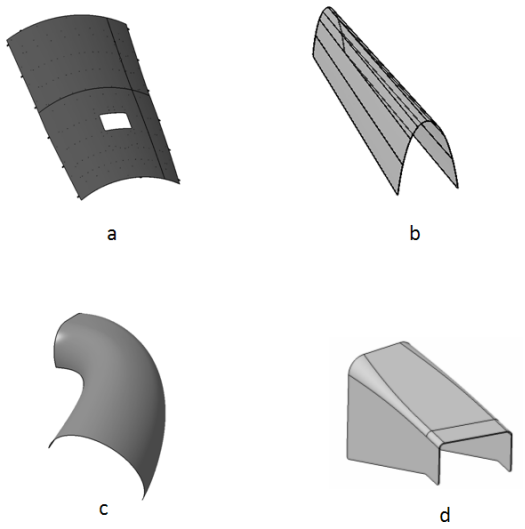

Figure 2: Stretch form parts in different geometrical properties (a) Body panel with large radius (b) Wing member with narrow edges (c) complex exhaust pipe with large radius of curvature (d) part with large bending radius

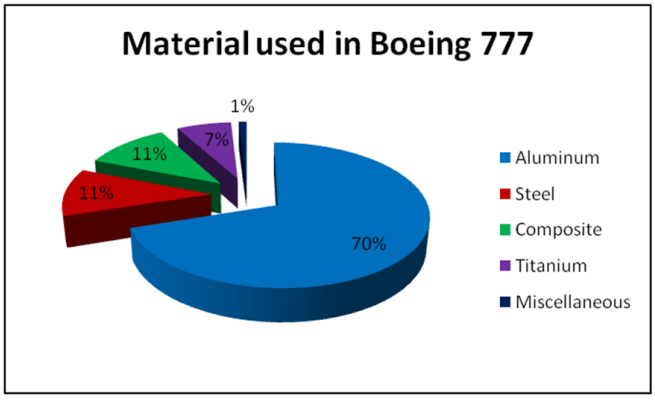

Figure 3: The percentage distribution of materials which are used in Boeing 777 [1]

Especially, 2xxx, 6xxx and 7xxx series of aluminum alloys are extensively used in skin parts, wing members, ribs, fairings and stringers which are formed into the desired shape using

stretch forming operation. The rest of the structural materials include steel, composites, titanium and other materials. With the exception of aluminum, steel and titanium parts can also be formed using SF process.

1.3 Motivation

With the effect of developing technology, high demands on the metal components which are used in aerospace industry are increasing in order to fulfill the high aero-dynamical and strength requirements. These requirements bring the necessity of manufacturing complex shaped products with materials which have higher strength to weight ratio. Stretch forming operation is the unique sheet metal forming operation when there is a need of products with compound and large curvatures. Sheet metal forms with compound curvatures bring the possibility of sheet metal forming failures such as tearing, wrinkling or spring back effect together. Excessive bending together with insufficient stretching results with wrinkling, excessive stretching results with tearing and inappropriate bending amount results with springback of the sheet material. On the other hand, the geometry of the final product, material mechanical properties, initial blank size, friction conditions and tool movement also directly affect the success of the operation. Due to this reason, the process has to be well analyzed before real manufacturing to reduce cost and production time.

Stretch forming process has many advantages compared to other sheet metal forming processes. One of the most important advantages of using SF process over other press forming processes include the production of higher quality, mechanically stronger workpiece with reduced cost. Since the material is primarily stretched, springback or formation of wrinkling does not occur. On the other hand, SF process offers better mechanical properties such as increased strength up to 10% and an increased hardness of %2. In SF process, the material is fixed from two sides, however, in other press forming processes the blank is fixed from all sides. That's why; it is also possible to obtain 15% saving from material consumption. Additionally, the material's formability is increased by the help of primarily tensile effect, hence the forming forces are reduced approximately %30-70. Exceptionally one die is usually sufficient to perform the process and since the force requirement for stretch forming is lower, die service times are longer than the other press operations.

Contrary to advantages mentioned above, SF process has some limitations. The parameters needed to be well analyzed for a successful stretch forming process can be summarized as follows;

- The tool motion and synchronization have to be determined accurately between jaws and forming die because the sheet has to remain stretched over the form die while jaws are getting closer.
- Friction condition between blank material and tools has to be carefully controlled by appropriate selection and application of lubricants.
- Die and jaw design directly influence the process quality and limits.

One of the most important difficulties in SF is that; these parameters are still found by experience through a trial-and-error approach. Since SF technique is commonly performed by aerospace companies, there is not enough public know-how and information because of the privacy policies. As a result, the cost and required time to obtain the product increases whereas the quality decreases. Therefore, the development of the knowledge is necessary to design and perform stretch forming operation to eliminate trial-error procedure. Among the above mentioned limitations, determination of tool motions is the crucial and most difficult issue for process designer. Trial-error based procedure with the estimations of press operator for tool motions results with;

- Waste of material because of wrinkling or tearing of sheet material.
- Time consumption because of implementing jaw and die motion separately.
- Reduced quality because of the insufficient stretching of the product.
- Increased operation costs because of the scrap amount.

In the light of these facts, in order to overcome such limitations and difficulties of stretch forming process, know-how development to minimize or eliminate the trial-error phase becomes an important necessity. This study focuses on preventive methods against these limitations using numerical modeling techniques.

1.4 Aim and Scope

For years, a great deal of know-how and experience has been accumulated in SF process, mostly by trial-error procedure. Process variants such as; material properties, friction conditions, relative tool motions between jaws and forming die, and initial blank geometry are determined by the operator. As it is well known, trial-error procedure even based on experience can cause the material to fail so that labor, tooling, material costs and production time directly increases while the quality of the final product decreases.

The aim of this study is as follows;

- To estimate of deformation behavior of aluminum alloys in SF process using FEM.
- To investigate the influences of process parameters such as relative tool motions, friction conditions etc. for both jaws and form die using experimental trials and FEM to obtain desired part geometry and property. (Figure 4)

So that, trial-error procedure will be eliminated by simulating the realistic simulations in CAE environment. Finite element method (FEM) is used as numerical method to simulate deformation of sheet material in SF process. In order to accomplish numerical studies successfully, virtual model must be realistic. There are especially two important process parameters which are required to be identified correctly. These are;

- Material model and material parameters,
- Contact model and its parameters.

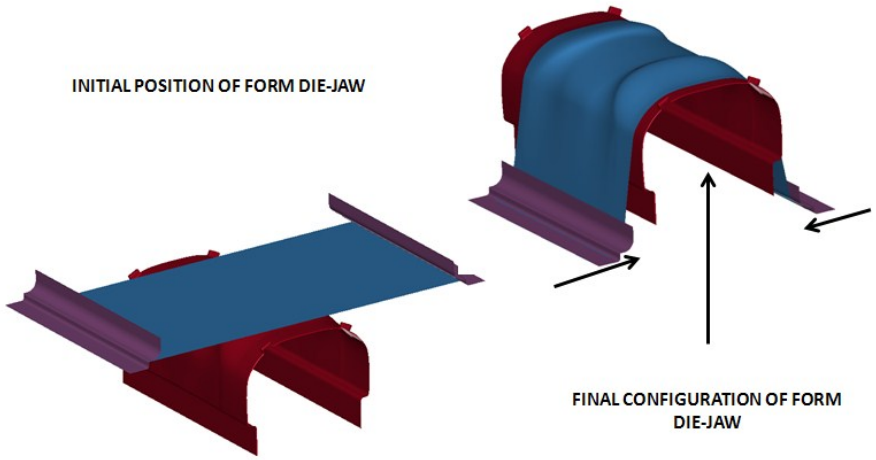

Figure 4: Initial and final configuration of tools (jaw-form die) in SF process

In this study, the method which is illustrated in Figure 5 is followed. During the studies, AA 2024, AA 6061 and AA 7075 aluminum alloys are used. Mechanical characterization tests are performed to define accurate and reliable deformation behavior for aluminum alloys. Plastic behavior of the aluminum alloys are identified using three different tests. First of all, tensile tests are performed to define elastic and plastic deformation behavior in uniaxial stretching conditions. Lankford parameters, strain hardening coefficient, strength index, elastic modulus and flow curve is obtained using tensile tests. Since the plastic strains are limited in standard tensile test, hydraulic bulge tests are also performed to define plastic flow of the material up to higher equivalent strains. Furthermore stack compression tests are performed to compare the results taken from other mechanical tests. In addition to these, forming limit diagrams are

determined experimentally for mentioned aluminum alloys in order to evaluate and interpret finite element analyses (FEA).

Secondly, friction tests are performed to define the Coulomb friction coefficient quantitatively between material-die and material-jaw interfaces. Both material characterization and friction test results are then implemented into FE software to simulate stretch forming process.

While stretch forming simulations are being executed, experimental studies are performed in order to make a comparison and verify the success of the simulations. During the experimental studies of stretch forming process, 3-D optical measurement systems are used to measure the deformation of sheet material. Strain distribution, thickness reduction and possible failure modes are compared to present success of forming simulations.

Finally, real problems which are difficult to overcome with traditional experience-oriented techniques are examined and solved by virtual tryout with the application of FEM. Work flow and the methodology being followed in this study are illustrated in Figure 5.

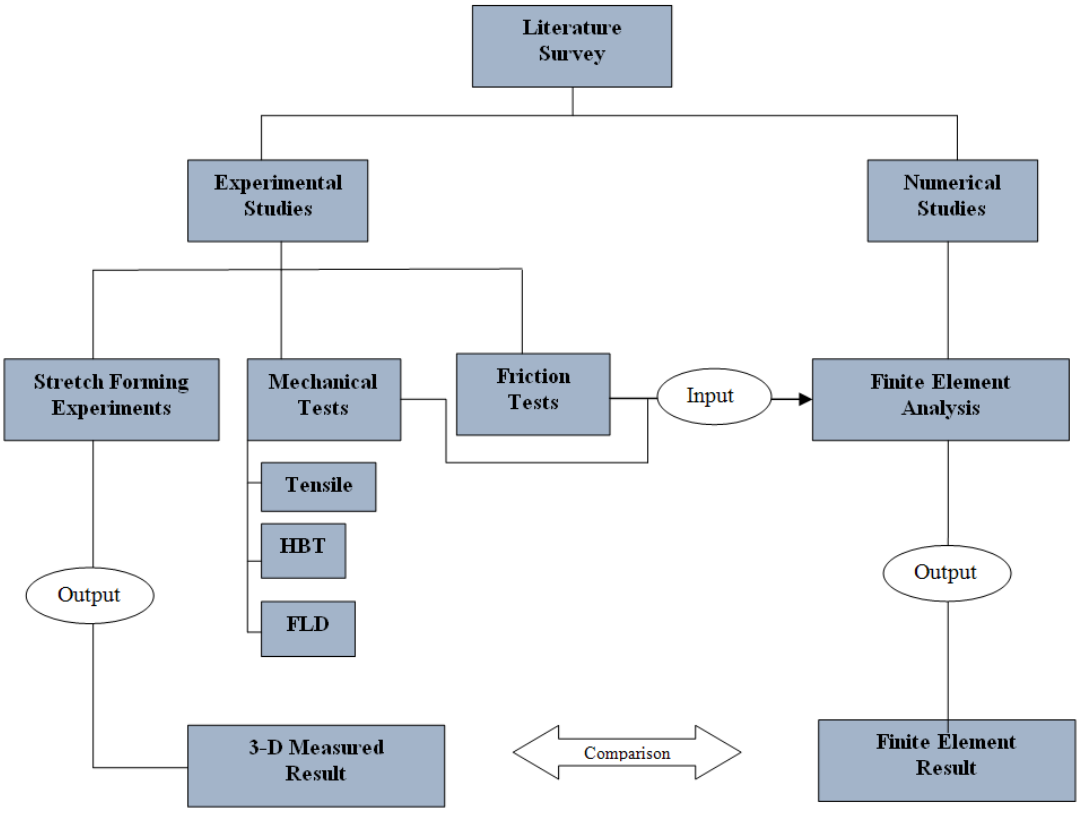

Figure 5: Content of the study which shows the work flow and their relations

1.5 Content of the Study

This study includes eight chapters. In the first chapter, brief information about the industrial importance of SF process is given. Second part of this chapter provides with literature survey and basic information on SF process. In this section, process variables, parameters and previous studies on stretch forming process are presented in detail. Mechanical material characterization is covered in the third part and in this chapter, test methods, test setups and results of these tests are worked through in detail. In the fourth chapter, in order to obtain Coulomb friction coefficient between the blank and tool interfaces for stretch forming process, an inverse technique is introduced. In the fifth Chapter, experimental studies are investigated including stretching trials, experimental setup-procedure and the results of optical measurements. In the sixth chapter, numerical analyses are performed to simulate the experimental stretching processes and the comparison between optical measurement and numerical modeling is discussed. Furthermore, the experimental and numerical investigations on selected example parts (real airplane parts) are discussed as case studies. Finally, results and findings are discussed and future works are mentioned in conclusion and outlook section.

CHAPTER 2

LITERATURE SURVEY

2.1 Introduction to Metal Forming

The word "manufacturing" comes from Latin words, manus and factus. The combination of these two words, manus-factus, means handmade. Nowadays, manufacturing can simply be described as; converting raw or semi-finished materials into more useful and valuable parts. As it is shown in the Figure 6, manufacturing processes are applied in order to transform raw or semi-finished materials into more valuable parts by changing its shape or physical-chemical properties [2].

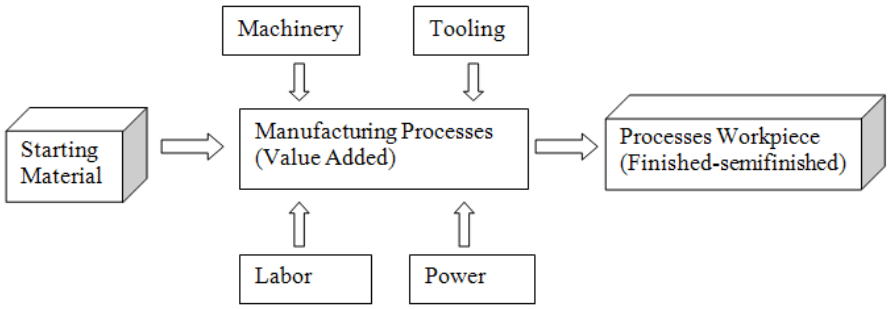

Figure 6: Schematic description of manufacturing and it's requirements to obtain a final product [2]

Manufacturing processes can be classified according to DIN 8580 as described in the Table 1 [3]. Primary forming operation refers to the casting process in which the molten metal flows into a mold where it solidifies into the desired shape. The other primary forming operation is called Powder Metallurgy. It is also metal processing technology in which the parts are manufactured under high pressure and temperature in order to sinter metallic powders.

Secondly, deforming processes refers to Metal Forming Operations which is the manufacturing by plastic change of the form of a solid body by preserving both the mass and cohesion. Deforming operations are classified (Figure 7) in accordance with DIN 8582 considering the application direction of the stress [4]. These are;

- Forming under compressive conditions,
- Forming under combined tensile and compressive conditions,
- Forming under tensile conditions,

- Forming by bending,
- Forming under shear conditions.

The third classification refers to material removal processes. The processes include conventional and non-conventional machining operations, such as plunge EDM, wire EDM and laser cutting processes. In these processes, the common feature is that the excess material is removed from the workpiece in order to obtain desired shape. Joining operations include, welding, brazing, soldering, and adhesive bonding which form a permanent joint between the parts. Coating operations are applied to provide corrosion protection and to enhance product appearance and properties by painting and plating operations. Finally, processes which are applied to change material properties are called heat treatment operations [2].

Table 1: Classification of manufacturing processes according to DIN 8580 [3]

<table>
<tr><th colspan="5">Classification of Manufacturing Processes</th></tr>
<tr><th>Creation of Cohesion</th><th>Maintenance of Cohesion</th><th>Destruction of Cohesion</th><th>Increase of Cohesion</th><th></th></tr>
<tr><td rowspan="4">1. Primary Forming</td><td colspan="3">Shape Form Modification</td><td rowspan="4">5.Coating</td></tr>
<tr><td>2. Deforming</td><td>3. Separating</td><td>4. Joining</td></tr>
<tr><td colspan="2">6. changing of Material Properties</td><td></td></tr>
<tr><td>Rearrangement of Particles</td><td>Removal of Particles</td><td>Addition of Particles</td></tr>
</table>

Among all the manufacturing methods, deforming type of processes is preferred. The reasons behind preferring deforming type of processes are;

- High material utilization,
- High productivity with short production times,
- High dimensional and shape accuracy within certain tolerances,
- Better mechanical properties can be obtained.

This thesis focuses on experimental and numerical studies on stretch forming process which is one of the important branches of “tensile forming conditions”. In this chapter, detail information is given about SF process. The basics of the process such as types, auxiliary

equipments, workpiece materials, lubrication conditions and also previous studies about stretch forming operation is investigated in detail to provide the reader better understanding for the following chapters.

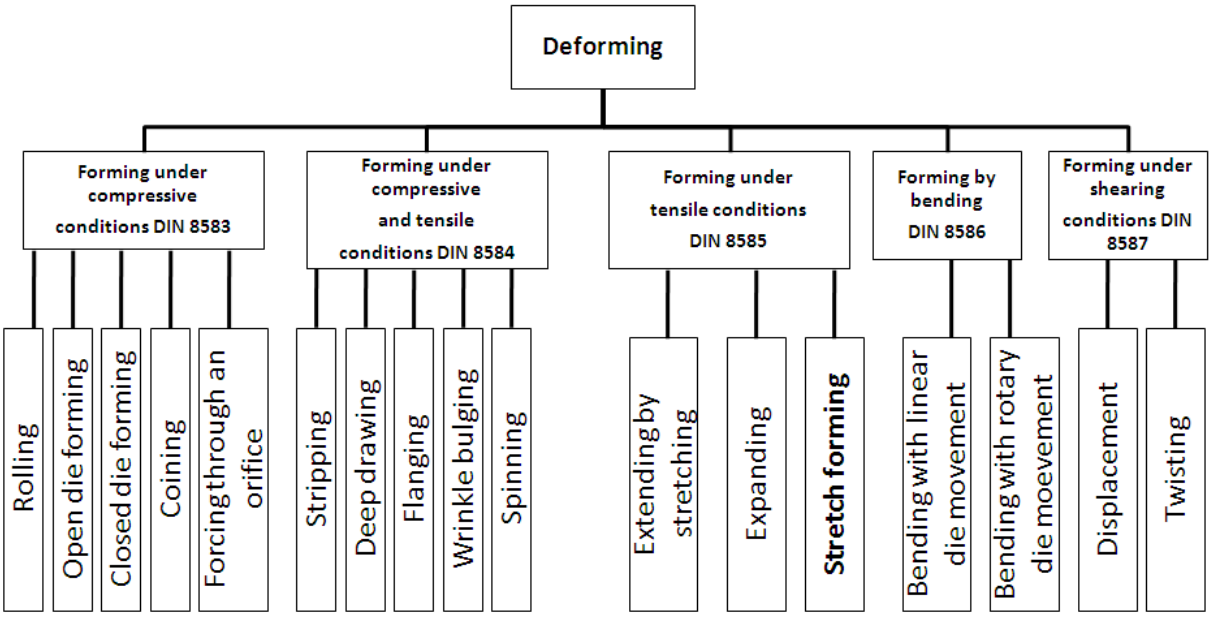

Figure 7: Classification of manufacturing processes according to DIN 8582 [4]

2.2 Stretch Forming of Sheet Materials

This part aims to give brief information about stretch forming process. Technical description, process capabilities, types, necessary equipment, process design and also previous studies on stretch forming are explained in detail in the following sections.

2.2.1 Definition, Applications and Types

According to DIN 8585, stretch forming is described as the forming of a sheet blank with a rigid form die, whereby the blank is rigidly clamped at the edges by jaws as shown in Figure 8 [5]. Process generally consists of three basic stages as illustrated in the Figure 9. In the primary stage, the sheet is clamped between rigid jaws and subjected to pre-stretching. In the second mode, form die rises and the sheet material is stretched by vertical movement of die. Finally, rigid jaws come closer to each other in order to make form die covered by sheet material. Each of these modes can be applied individually; however, it is also applicable to use combination of these modes at the same time to obtain desired part. In other words, the sheet material is stretched and formed into the desired shape by the proper trajectories of form die and jaws.

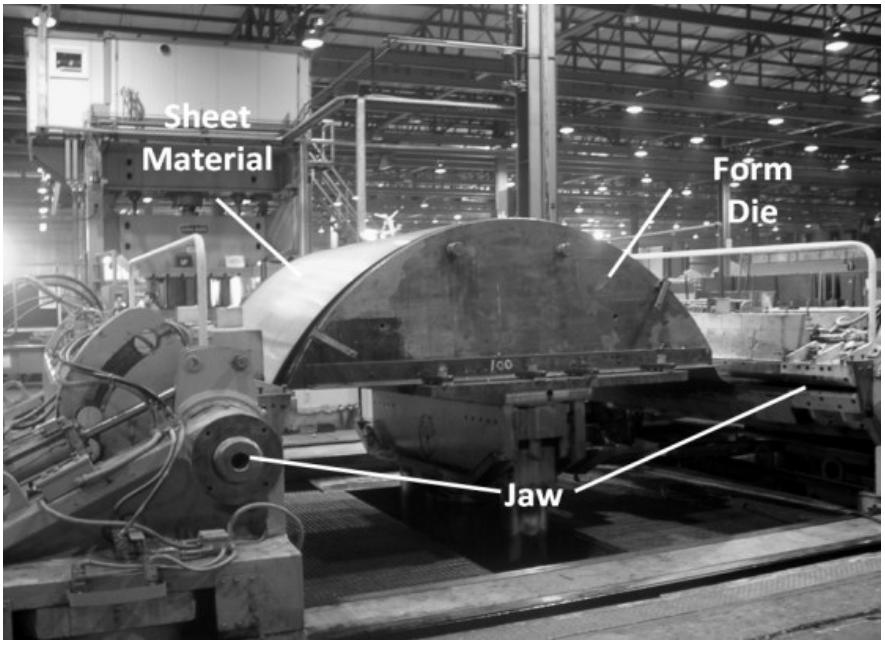

Figure 8: 750 tons capacity Cyril-Bath stretch forming press and stretching equipments

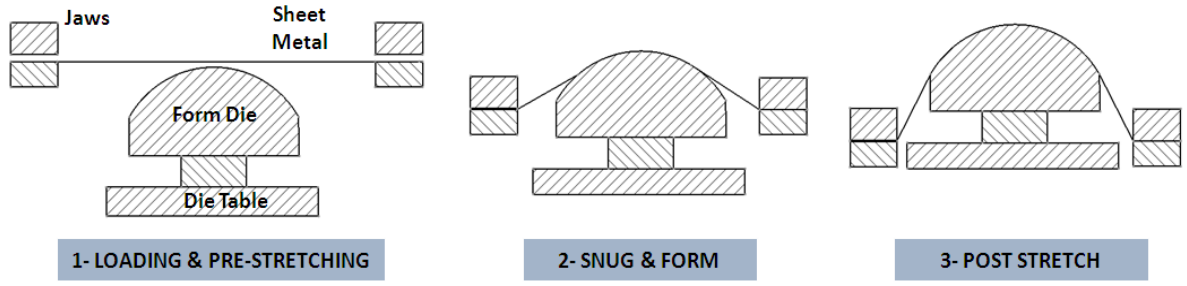

Figure 9: Stages of forming process using stretch forming process

Since the process does not have capability to produce deep contours, the general field of applications consists of relatively flat parts of large dimensions as single pieces, prototypes or for small batches whereby convex forms and large radius of curvatures are needed.

Sometimes compound curvatures are needed on the final configuration of sheet metal. Examples of such forms are; body panels for automobile and aerospace industries and parts of trains and wagons.

Different types of stretch forming dies and products are shown in Figure 10. Types of stretching forming processes are reviewed in detail [5-6-7]. There are four different types of stretch forming process;

i. Simple stretch forming,
ii. Tangential stretch forming,
iii. Stretch forming according to Cyril-Bath,
iv. Multi-sided stretch forming processes. [6]

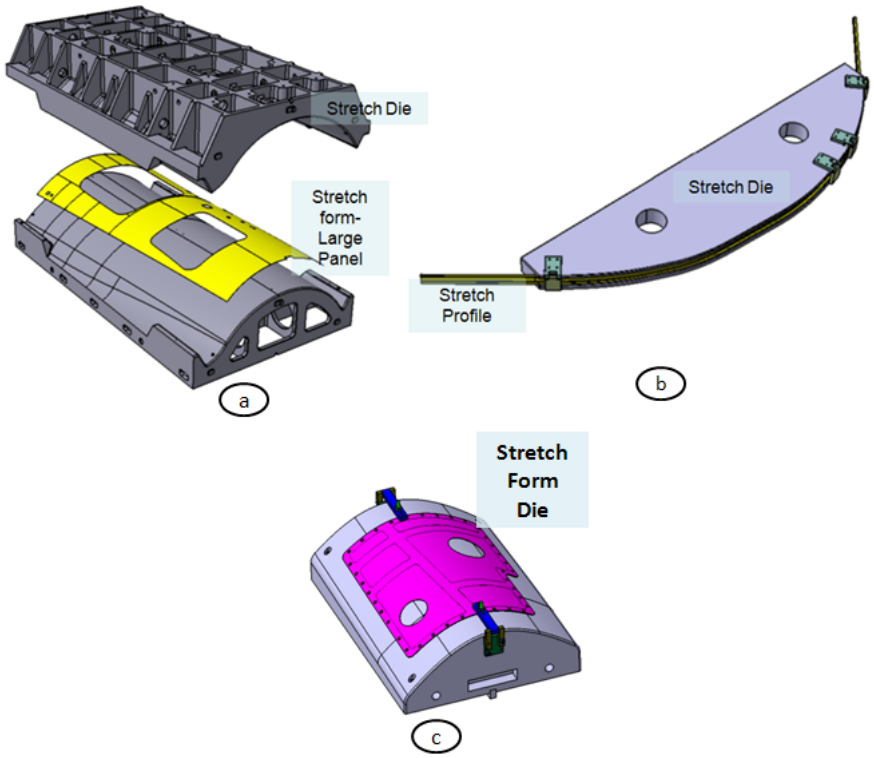

Figure 10: Examples to stretching form dies and final products

i. Simple stretch forming The sheet metal is fixed using two gripping jaws from the opposite ends. These two gripping jaws can rotate in their mounts, however, they remain stationary. The forming tool which is replaced over the die table hydraulically moves upwards to deform the sheet material. The sheet material receives its contours during the motion of the form block. In another words, the sheet material is stretched by using form block. As it is shown in the Figure 11, firstly punch contacts with the apex of the blank and then workpiece is stretched as the punch's stroke proceeds. The sheet metal receives its desired shape at the end of the stroke [6].

In simple stretch forming, in case of large deformation interface between sheet and punch, there sometimes exists very little regional deformation. This is especially the case for flat shaped form blocks when little motion allows sheet material to cover (to get in contact with) the form block completely and then during the stroke of the form block, friction forces prevents the material being stretched especially in the central region over the die. Therefore, the middle regions of the sheet materials cannot contribute to total deformation strain which leads to, non-uniform strain distribution over the cross section of the sheet, springback formation of wrinkles and insufficient work hardening. [5]

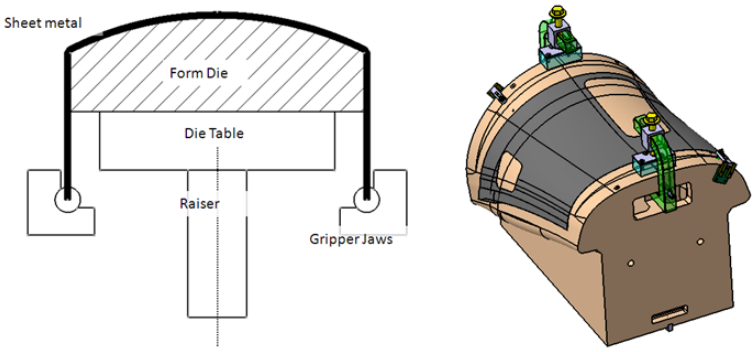

Figure 11: 2-D and 3-DiIllustrations of simple stretch forming operation

On the other hand, one of the other main disadvantages of simple stretch forming is that, it is impossible to obtain negative contours without using a counter punch. In order to form components which requires larger uniform strain limit, it is necessary to choose different material as a workpiece or the workpiece is needed to be grip from all sides. Therefore, larger deformation can be obtained before necking occurs. Also, large amount of waste material is used in simple stretch forming process.

Components which have arbitrary shapes, precise stress-strain values cannot be known, however, required force, F_p, applied by form block can be obtained using following equations [6].

$$F_p = \frac{A_1}{\eta_{def}} \sigma_{f,m} ln \frac{A_0}{A_1} \qquad (Eq\ 1)$$

Where A_0 is initial surface area of sheet, A_1 is the area of stretched-formed component, $\sigma_{f,m}$ is the mean flow stress and η_{def} is the efficiency of deformation range which varies between 0,5-0,7.

ii. Tangential stretch forming In tangential stretch forming process, the sheet material is also gripped from opposite sides and formed using a form die. The main difference from simple stretch forming process is that; both jaws and forming die can move during the process. Using the capability of movable jaws, it is possible to subject sheet material to prior strain before the real deformation process. When the blank is subjected to tensile forces by jaws, uniform strain distribution can be obtained over the whole cross section, therefore the sheet material can be uniformly elongated. In this type, load is always tangential to the contour of the tool (Figure 12) [5].

In tangential stretch forming, the deformation occurs in two distinct stages [6]. In the first step, the blank is stretched using the gripping jaws in order to provide uniform plastic strain and then in the second phase, the blank is formed into the desired shape by using forming die by exceeding the yield strain independent of the material by 2-4% or sometimes by 6%. During the second phase, the blank is still under the constant tensile stress.

In this process, the first interaction occurs between middle region of the blank and die. That's why, there is no influence of friction as it is in simple stretch forming. By the effect of the tensile stress, residual stresses are reduced and shape accuracy can be easily obtained in the absence of springback. Compared to simple stretch forming, in tangential stretch forming lower amount of waste material is used.

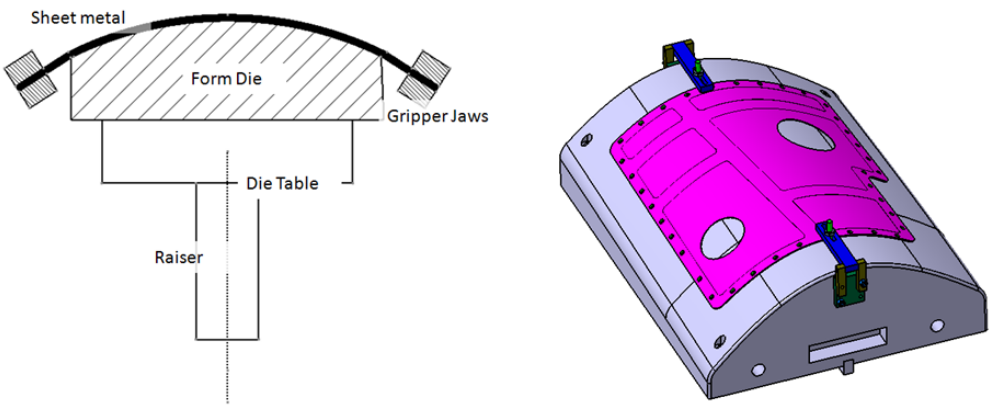

Figure 12: 2-D and 3-D illustration of tangentional stretch forming process

Tangential stretch forming machines are equipped to form large parts up to 6,100 mm wide and up to 9,300 mm long such as roofing arches for trains, door frames and planking for buses and for aerospace industry. The force requirement to form such parts can reach up to 10,000 kN [5].

iii. Cyril-Bath Process (Stretch draw process) This process is developed by Cyril Bath company to apply tangential force to the contour of the sheet metal and can be accepted as the combination of stretch forming and deep drawing processes. That's why; the processes having this ability are called stretch-draw presses. This system is simply consists of;

- Upper die which is mounted on ram,
- Lower die which is mounted on die table,
- And two gripping jaws.

The sheet is gripped using the jaws which are located in opposite ends. And the blank is formed between upper and lower dies under tensile forces. Since there is upper die, it is possible to obtain convex-concave shapes using Cyril-Bath process.

The forming steps of this process are given below.

1) The sheet blank is stretched using gripping jaws up to an elongation of e= 0,2-0,4%.
2) Without reducing the stress, the jaws move downwards to form convex shape.
3) The punch which is located on ram moves downwards to push the sheet material in order to form internal concave geometries. During this step, jaws can move in horizontal and vertical directions to prevent tearing caused by over-stressing.
4) The force applied by punch is unloaded and punch returns to its original position.
5) After releasing of the force applied by punch, the gripping jaws also release the material and return to their original positional leaving the formed piece on lower die.

The one of the most important difference obtained by Cyril bath process compared to other conventional stretch forming processes is the capability of the press mentioned in the 3rd part. By the help of this ability, the blank is subjected to constant or variable stresses even during the deformation phase.

One of the other advantages is the good forming of the middle regions of the blank which makes the process capable of attaining high amount of work hardening. Springback is also reduced in stretch draw process due to the forming characteristics in the plastic state. Furthermore, cancelling the upper and lower dies, where necessary, makes the processes faster and more economical [5].

iv. Multi-axial Stretch Forming This process is designed in order to take the advantages of both tangential stretch forming and Cyril-Bath processes. Furthermore, the disadvantages of stretching sheet material from only two sides can be removed by stretching the workpiece

from all sides. This process is performed only by using a prototype which is designed by Cyril-Bath Company. The process steps are as follows;

- The sheet blank is fixed to one of the gripping jaws and moving action of the jaws towards each other simplifies to fixing the sheet from all four sides. Then jaws move in opposite direction in order to give pre-straining to the blank.
- During the deformation process whereby the forming block moves upwards, vertical and horizontal movements of the jaws are controlled and coordinated.

2.2.2 Machines, Tools and Equipment of Stretch Forming Operation

Stretch forming press requires at least two jaws to give pre-straining to the blank by stretching and a forming die(s). According to the final configuration of the workpiece, there might be positive or negative contours on the dies. Generally, if there are positive and negative curvatures or different types of contours or joggles on product, usage of upper die become a necessity. The working principle of the machines is simple; however, they can be quite complicated according to the geometrical or mechanical complexity of the final product. First of all, the blank is fixed between the gripper that can hydraulically be activated. Secondly, the blank is stretched approximately up to its yield strength and elongated approximately up to %3 of its length. Then the forming die is activated and moves upward to form the sheet metal. The location and the movements of the jaws during the process can vary.

This process is accomplished using special purpose presses. Many different types and sizes can be used to form sheet materials. Machine selection is done considering the blank size, force requirements and the shape of the desired product. According to the analysis, required stretching type has to be determined considering economical and technological facts. Six types of presses are available for SF applications. Brief information about these presses is given below [8].

i) **Drape Forming Presses** In this type, the blank is fixed between two stationary jaws which are attached to the base structure. These machines can be considered as the simplest SF presses which are used to form large sheets with simple geometries.

ii) **Combined Stretching and Bending Presses** these machines combine the stretching and bending operations. In these operations, jaws are also activated in many directions which are designated according to the customer needs.

Since pre-straining is possible, wrinkling and springback can be minimized. In this research, all the experimental studies are performed using 750 tons capacity Cyril-Bath press.

iii) **Stretch Draw Presses** These presses are used to pre-stretched blank approximately %2-3 of their initial lengths on the lower die using stretching blank holders. Then the process is performed by forming the blank using the hydraulically activated upper die.

iv) **Stretch Wrap Forming Presses** The stretch wrap forming presses are used to combine stretching and bending operations in order to form rolled or extruded sheet stocks.

v) **Compression Forming Presses** This process is used to bend sheet metal applying compression force against die by shoes or rollers.

vi) **Radial Draw Forming Presses** These presses have the ability of combining the capability of both stretch wrap forming presses and compression forming presses. Therefore, difficult shapes such as; formation of joggle on the bended sheet can be obtained easily.

These presses has advanced from the use of hand operated control parameters such as pressure, flow rate of the hydraulic fluid and the direction of the system components to electronically controlled automatic operation. As it is known, over or under stretching can destroy the workpiece. That's why, the process parameters are needed to be correctly defined and controlled during the process. As it is mentioned before, stretch forming presses equipped with two important auxiliary components which are; jaws and form die in which the form of sheet is given by them.

Jaws

One of the most important equipments used in stretch forming process are jaws in which the material is gripped and stretched from the edges. These are the equipments which are used to stretch sheet blank in order to give pre-straining just before or during the press forming operation (Figure 13). Two opposite located jaws are used to squeeze the material applying vertical pressure from the edges. For this purpose two different jaw designs are available, which are; articulating and straight jaws. Selection of the jaws requires an analysis on the blank and desired workpiece geometries. For example, articulating jaw type is more suitable for the cases in which the blank geometry includes different curvatures due to the capability of being curved to any radius. On the other hand, jaws surface finish and surface knurls have

considerable effect on forming of different types of materials. It is a necessity to has serrated surface on a smooth jaw, when forming of aluminum alloys. Also, emery clothes or a metal in the same thickness with the aluminum sheet can be put behind the ends in order to prevent rupture.

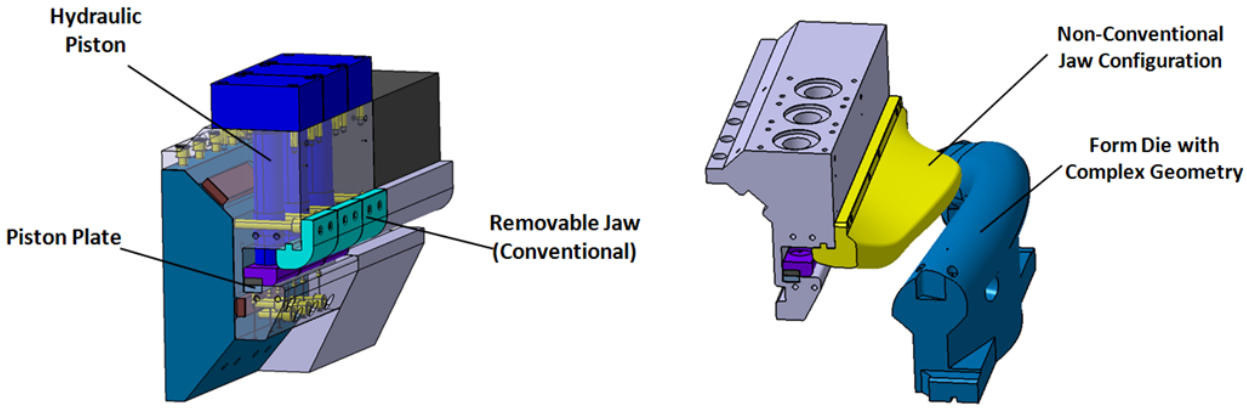

Figure 13: (a) CAD model of stretching jaws with conventional tools (b) CAD model of stretching jaws with non-conventional tools (it is used to form more complex parts)

For straight jaws, different designs can be used to form sheet material (Figure 13-a). According to the desired form of the workpiece, jaw geometries can vary. For simple geometries, straight jaw types can be used effectively, however, for complex geometries in which the edges of workpiece require to be formed with angled geometry, jaws are also needed to include similar shapes and angled geometry as shown in Figure 13-b.

Form Die

Die is the part which gives the final shape of the sheet blank. Die is mounted on the form block and move vertically during the stretch forming process. In stretch forming process, die is the part where the EOP (Edge of part) is located (Figure 14). EOP is the sign which is drawn on the die to show the desired geometry of the product and its edges. The remaining parts beyond EOP on the die is called excess regions which are used to provide uniform deformation over the sheet blank and to identify the centering holes for the coming operations (trimming) by punching holes.

Stretch forming process can be considered as near net shape because pre-straining of the sheet blank prevents springback which means the dimensional accuracy of the final product is very similar to the desired one. So that dies surface geometry kept similar to the surface geometry of the blank. Due to springback, re-work can be necessary on the forming dies.

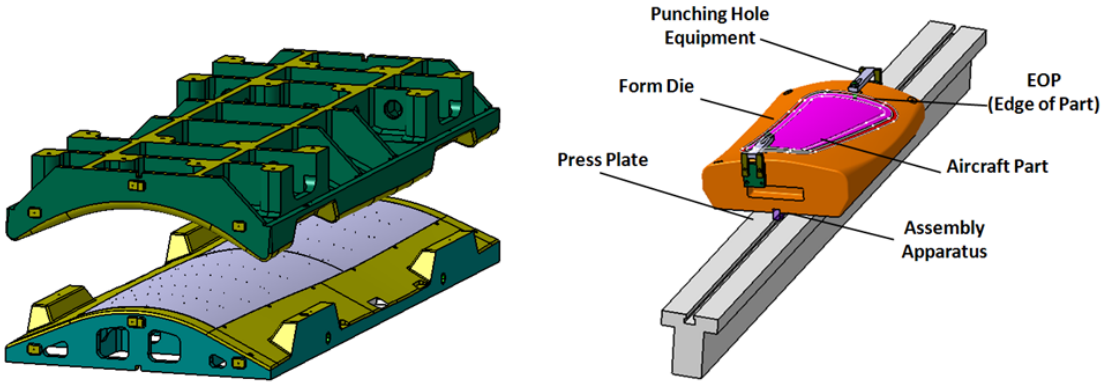

Figure 14: Stretch forming die (a) which consists of ram and form die, (b) which consists of only form die

Forming dies are manufactured considering the thickness of the sheet metal, the force required, desired geometry of the wokpiece, blank geometry and the number of the parts being produced. Die material can also be selected considering the process parameters. Common die materials used in stretch forming process are; aluminum, steel, kirksite, wood and plastic. Kirksite also called zinc alloy, are produced by using casting process. After the die is polished by hand grinding method, kirksite offers the smoothest surface among all alternatives. On the other hand, recycle of this type is possible after melting operation. Hard wood material can be used for production of small batch quantities where the force requirement is low. In order to increase the surface quality, these materials can be coated by other metals.

Plastic materials are also preferred due to ease of machining and lightweight property. One of the famous plastic materials used in stretch forming process is epoxy laminates. Steel dies especially SAE 1020 are preferred due to its superior properties such as having the highest life time. Since they are expensive, their mechanical properties make them more economical in the case of production of higher amount of parts. Dies which are made of aluminum have also high life times and they are preferred because of the easy machining of aluminum alloys. Lastly, ceramic dies are used to form materials which require prior heating such as magnesium and titanium [7].

2.2.3 Materials Used in Stretch Forming Process

The common materials which are used in stretch forming process are; aluminum alloys, stainless steels, low carbon steels, special materials such as niobium, beryllium and pure

titanium. On the other hand, heat resistant alloys and magnesium alloys can be hardly formed. Practically, it can be said that, alloys which are difficultly deform in press operations can be formed easily using stretch forming due to increased formability of sheet metal.

Formability of sheet material properties can be determined using tensile, Erichsen cupping, FLD or hydraulic bulge test. If the sheet material displays higher quantities of strain hardening exponent, uniform elongation limit and fracture strain, better material formability for stretch forming process can be obtained. If the uniform elongation is high, material tendency towards necking is lower, in other words, larger deformation amounts can be obtained in SF process.

Aluminum is the most commonly formed material using stretch forming technology. Aluminum alloys, especially, 2xxx, 6xxx and 7xxx series are commonly used in this process. In this study, mechanical properties for these alloys are obtained by using various tests. Both heat treatable and non-heat treatable alloys can be stretch formed, however, non-heat treatable alloys requires annealing before the process. In the case of forming heat treatable alloys, after solution heat treatment, 8-15% elongation can be achieved [9]. 7075 aluminum type in T6 condition is not offered for SF process. Thin sheets whose thickness is less than 0, 51 mm have a tendency to rupture from the locations where gripping jaws apply force. Therefore, additional sheet metals are put beyond the jaws or emery clothes are replaced between jaws and blank. One of the other solutions to prevent this problem is to cool sheet material up to -34 C° in refrigerator [8].

Austenitic stainless steel (ASS) can also be contoured by SF process. High ductiliy of ASS permits them to be stretch formed easily. All grades have very high ductiliy when they are in annealed condition. However, there are some limitations for ASS material which increases the required force to accomplish the process.

- Higher wear rate of the tools,
- Springback is more pronounced,
- Work hardening entails additional forming steps after annealing operations.

Among all types of stainless steels, austenitic stainless steel has the most elongation capability. 30-40% of elongation is possible, if the stretch formed material is austenitic type. Except Type 430, ferritic stainless steel (FSS) does not show so much elongation. For martensitic stainless steel, only lower carbon grades such as Type 403 and Type 410 are recommended. Precipitation hardening stainless steels are available with austenitic and

martensitic structures for SF. Last but not least, steel sheets can also be manufactured using SF process. Hot or cold rolled, low carbon steels such as AISI 1015 to 1020 can be formed.

As it is known, Ti and its alloys are also important in aerospace industry, that's why there is a need for stretch forming such materials. Ti alloys has very low stain hardening coefficient. Therefore, unexpected necking formation can occur. Depending on the alloy type, Ti alloys can be stretch formed in 200-650 C° range. Maximum elongation obtained in forming of Ti alloys varies between 4-10%. If the elongation requirement is more than %15, there is a need for annealing between operations. One of the most important hints to form Ti is that; strain rate has to be kept low.

Finally, magnesium alloys are stretch formed after they are heated up to 150-260 C° in order to prevent heat loss, die for this purpose are also heated. However, jaws are not needed because cold magnesium has higher strength and it prevents possible failures. [8]

In this study, aluminum alloys in 2xxx, 6xxx and 7xxx are used in different thicknesses, heat treatment and coating conditions. The alloying elements and advantages of aluminum alloys are summarized in APPENDIX Part-Table 8-9, respectively. Their material and contact properties are evaluated in detail in the following chapters.

2.3 Formability of Sheet Materials

Formability of sheet material vary according to the mechanical properties of workpiece material, heat treatment, geometry of final product, friction conditions and also level of cold work. Simply, properties of workpiece material and deformation mechanics identify the formability. In sheet metal forming applications, problems encountered due to instability and springback make the prediction of formability more difficult. Since the sheet material is subjected to pre-straining for eliminating springback problem in stretching operations, springback phenomena is not the primary concern of this study. So the research intensively focuses on eliminating problems which are encountered due to instability.

2.3.1 Mechanics of Sheet Metal Forming

In this study, the deformation behavior of aluminum alloys are investigated both experimentally and numerically. Mechanics of sheet metal forming is described by the equations derived from simple tension test. Mechanics of tensile test is introduced in Chapter 3. Through thickness stresses are neglected in sheet metal forming processes, since the normal

stress is very small compared to in-plane stresses in other directions. The operations such as simple tensile test in which the normal stress is missing, are called plane stress deformation.

The infinitesimal element shown in Figure 15 shows the principal directions. In sheet metal forming operations, it is assumed that up to ultimate tensile stress (UTS), instability does not exist; therefore uniform deformation takes place and the faces remains perpendicular to each other. Shear strains are neglected and the principal directions are called as 1, 2, and 3 which are longitudinal, width and through thickness respectively [10].

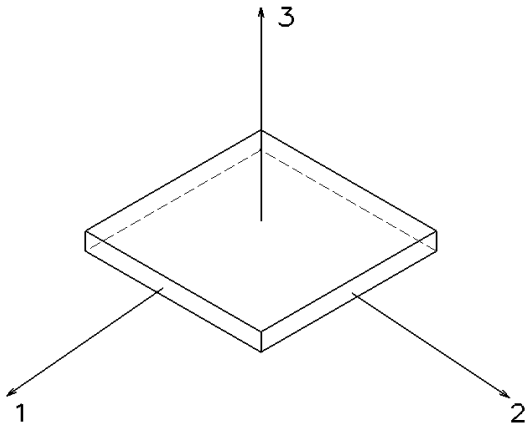

Figure 15: Principal directions in sheet metal forming (1-Longitudinal, 2-Transverse, 3-Normal direction)

Incremental strains in these directions are described by following equations;

$$d\varepsilon_1 = \frac{dl}{l} \qquad (Eq\ 2)$$

$$d\varepsilon_2 = \frac{dw}{w} \qquad (Eq\ 3)$$

$$d\varepsilon_2 = \frac{dt}{t} \qquad (Eq\ 4)$$

Where:

$d\varepsilon_1$: Strain in Tensile Test Direction

$d\varepsilon_2$: Strain in Width Direction

$d\varepsilon_3$: Strain in Thickness Direction

Volume constancy can be used for the relationship between these three strain values.

$$w.l.t = w_0.l_0.t_0 \qquad (Eq\ 5)$$

$$d(w.l.t) = d(w_0.l_0.t_{0)} = 0 \qquad (Eq\ 6)$$

$$dw.l.t + dl.w.t + dt.l.w = 0 \qquad (Eq\ 7)$$

$$\frac{dl}{l} + \frac{dw}{w} + \frac{dt}{t} = 0 \qquad (Eq\ 8)$$

$$d\varepsilon_1 + d\varepsilon_2 + d\varepsilon_3 = 0 \qquad (Eq\ 9)$$

For isotropic material, second and third components of strain will be equal to each other so;

$$-\frac{1}{2}\varepsilon_1 = \varepsilon_2 = \varepsilon_3 \qquad (Eq\ 10)$$

If mechanics of tensile test is summarized:

$$d\varepsilon_1 = \frac{dl}{l} \qquad d\varepsilon_2 = \frac{dw}{w} \qquad d\varepsilon_3 = \frac{dt}{t} \qquad (Eq\ 11)$$

$$\sigma_1 = \frac{P}{A} \qquad \sigma_2 = 0 \qquad \sigma_3 = 0 \qquad (Eq\ 12)$$

Where:

σ_1: True Stress in Tension Test Direction

σ_2: True Stress in Width Direction

σ_3: True Stress in Thickness Direction

The deformation of an infinitesimal element for a proportional process is described by either the strain ratio, β, or the stress ratio, α. The stress-strain relationship for principle directions are defined in Table 2.

Table 2: Stress-Strain Relations for Principles Directions

Plane Stress Deformation			Uniaxial Testing		
Direction 1	**Direction 2**	**Direction 3**	**Direction 1**	**Direction 2**	**Direction 3**
σ_1	$\sigma_2 = \alpha\sigma_1$	$\sigma_3 = 0$	σ_1	$\sigma_2 = 0$	$\sigma_3 = 0$
ε_1	$\varepsilon_2 = \beta\varepsilon_1$	$\varepsilon_3 = -(1+\beta)\varepsilon_1$	ε_1	$\varepsilon_2 = -\varepsilon_1/2$	$\varepsilon_3 = -\varepsilon_1/2$

Where:

$$\alpha = \frac{2\beta + 1}{2 + \beta} \qquad (Eq\ 13)$$

$$\beta = \frac{2\alpha - 1}{2 - \alpha} \qquad (Eq\ 14)$$

Principal Strains

Optical measurement device observe the dimensional change of the grids on test specimen during sheet metal forming operation as shown in Figure 16. The principal strains at the end of the process are;

$$\varepsilon_1 = ln\frac{d_1}{d_0} \qquad \varepsilon_2 = ln\frac{d_2}{d_0} \qquad \varepsilon_2 = ln\frac{t}{t_0} \qquad (Eq\ 15)$$

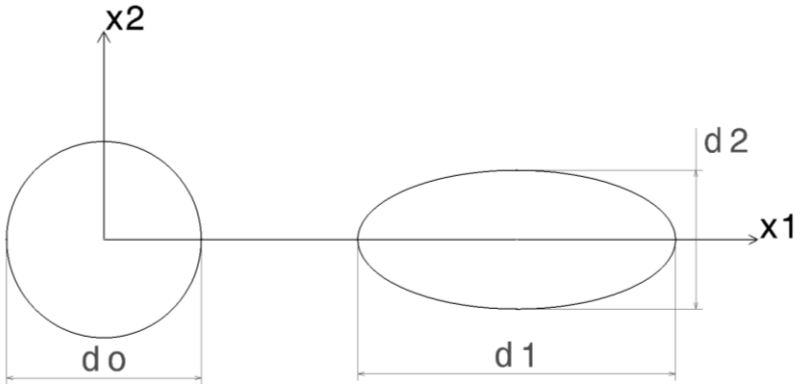

Figure 16: Dimensional change of the grids in principal directions

Thickness Strain

Thickness strain is calculated from the major and minor strains assuming volume constancy.

$$\varepsilon_3 = ln\frac{t}{t_0} = -(1+\beta)\varepsilon_1 = -(1+\beta)ln\frac{d_1}{d_0} \quad \text{(Eq 16)}$$

From Equation 16,

$$t = t_0 \exp(\varepsilon_3) = t_0 \exp[-(1+\beta)\varepsilon_3] \quad \text{(Eq 17)}$$

Since $td_1d_2=t_0d_0^2$ remains constant,

$$t = t_0 \frac{d_0^2}{d_1 d_2} \quad \text{(Eq 18)}$$

2.3.2 Failure

Sheet metal forming processes can be limited or terminated by some events during the operation. It may be very difficult to predict these which are responsible for an unsuccessful process. However, understanding the basic mechanics and controlling the process parameters according to a good proper process design can delay the failure. Following events are the major forms of failure.

- **Localized necking or tearing:** Local thinning or thickening can be observed during the deformation process. On the region where local thinning is high, tearing can be observed.
- **Wrinkling:** Wrinkling instability occurs when one of the inplane principal stresses (σ1, σ2) in an element is compressive beyond a certain value. Wrinkling appears especially in draw radius. In stretch forming process, in the case of insufficient stretching or inappropriate surface conditions, wrinkling phenomenon can be seen (Figure 17).

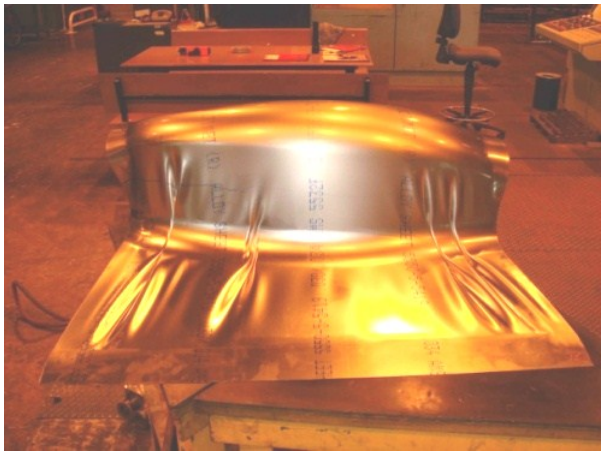

Figure 17: An example to wrinkling phenomenon

- **Fracture:** Fracture can be observed in brittle manner for a plastically deforming element. Fracture is usually preceded by local instability.

2.3.3 Anisotropy

Most industrial sheet shows different material behaviors according to the direction of measurement. This property of metallic materials is called anisotropy. Material in which the same properties are measured in any direction is called isotropic. The state of anisotropy is generally indicated by the R-value. The R-value is described as the ratio of width strain to thickness strain.

$$r = \frac{ln\frac{w}{w_0}}{ln\frac{t}{t_0}} \quad \text{(Eq 19)}$$

The direction in which the R-value is measured is indicated by a suffix according to the direction it is measured. R_o, R_{45} and R_{90} are the anisotropy values for rolling, diagonal and transverse directions respectively (Figure 18).

Planar anisotropy is defined by;

$$\Delta R = \frac{r_0 - 2r_{45} + r_{90}}{2} \quad \text{(Eq 20)}$$

Normal plastic anisotropy ratio is defined by;

$$\bar{R} = \frac{r_0 + 2r_{45} + r_{90}}{4} \quad \text{(Eq 21)}$$

Where

R_0 is the anisotropy coefficient in the rolling (0^0) direction (RD)

R_{45} is the anisotropy coefficient in the diagonal (45^0) direction (RD)

R_{90} is the anisotropy coefficient in the transverse (90^0) direction (RD)

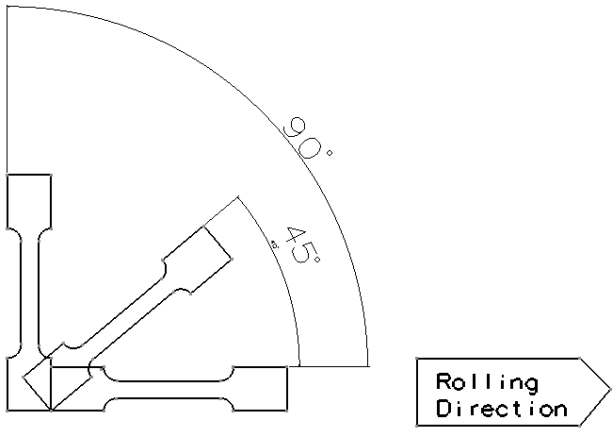

Figure 18: Alignment of tensile test specimens to determine anisotropy

In this study, aluminum alloys which exhibit anisotropic behavior are used as workpiece materials. So that Lankford parameters (anisotropy values) are determined during tensile test using width extensometer of the tensile test machine.

Anisotropic material properties are also modeled during FEM analyses using 3-Parameter-Barlat card in Ls-Dyna® and the capability of anisotropic model of commercial FEM package, Ls-Dyna®, is validated. Proportion of the width strain to the thickness strain is calculated for each stage of deformation and the results are compared with the actual anisotropy coefficients measured by extensometers of tensile test device. As shown in the APPENDIX A-Figure 112, results show good consistency.

2.3.4 Failure Modes and Troubleshooting

Uniform deformation in stretch forming process can be terminated by necking and fracture. If the blank necks before taking the desired geometry, there could be two important reasons;

i) Uniform strain limit is too low relative to the required strain,
ii) Frictional forces are high.

Relevant to the facts mentioned above, three types of failures that can be distinguished are shown in the Figure 19.

Crack formations which occur near to gripping jaws are generally resulted from excessive applied forces. This situation is only observed in materials which have good formability.

Since such types of cracks are formed out of the EOP region, the sheet components can still be used. Another type of crack is the one which appears in the apex of the form die.

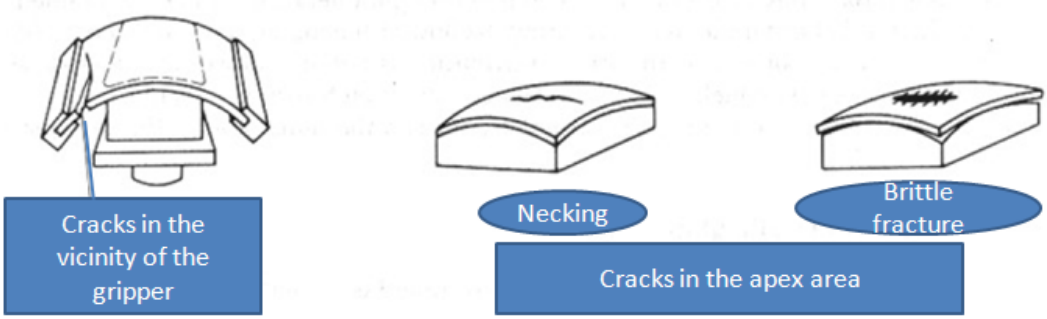

Figure 19: Common failure modes encountered in SF process

On the other hand, it is also possible to observe wrinkling during the forming of saddle shaped parts.

In stretch forming process, the operation can be terminated by many variables; however, these undesired events might be prevented by the application of suitable process parameters such as selection of the proper machine, force and set up controls and the continuous application of the lubricant. Wrinkling can be prevented by reducing the width and increasing the thickness of the workpiece material or the usage of a matching top die to clamp the sheet can be another solution.

2.4 Previous Studies on Stretch Forming Process

This study only focuses on stretch forming operation in which the material is stretched by jaws and formed with the vertical movement of die. Since SF operation is a special process which is generally performed in aerospace industry, it becomes very difficult to achieve required studies due to the privacy policy of the companies in which the relevant studies takes place. The remaining studies which are directly related with the SF operation include applications of finite element analyses and springback prediction methods for the process, die design optimization and new improvements on the auxiliary equipment of the process.

Jung represented 3-D FE simulation of stretch forming process to evaluate forming parameters using Msc. Marc. On the other hand, springback amount and failure existence were evaluated using the simulation results. In this study, influence of the angled jaw on the

formability of the sheet stretch forming process was analyzed and it was concluded that rounded jaws gave less stress concentration than the one performed with angled jaws [11].

A new process sequences design approach was developed for multi stage stretch forming operation to determine the minimum stage number and deformation amount for each stage by combining the FE method and strain distribution method. Since strain path of material deformation of longitudinal stretch forming for aircraft skin is close to uniaxial tension state, a two stage uniaxial tensile test was used to evaluate the effect of pre-strain on the limit strain for necking and the critical strain without formation of orange peel [12].

The comparison of the numerical simulations with the experimental studies showed that the approach is capable performing process design for multi-stage stretch forming of complex shapes to prevent deformation defects [13].

In another study, an optimization method was implemented for stretch forming of titanium alloy aircraft skin to determine process parameters and to reduce springback amount. A mathematical formulation of stress difference was developed and explicit FEM was used to analyze the forming process and to determine the amount of stress. Experimental trial performed with the parameters which were obtained by optimization method showed that springback amount can be controlled using this method [14].

On behalf of Boeing Company, Wade studied on the elimination of hand forming process using FE analysis to predict deformation behavior of aluminum alloys. Dynamic boundary conditions were verified using Catia to define dynamic boundary conditions for FE model. Springback prediction was also made and it was shown that .02 inch difference was obtained between numerical simulation and experimental trial [15].

Chikong et al. [16] examined influence parameters on springback occurrence during stretch forming of dorsal skins which is made out of AA 7075-W. After finite element analyses of stretch forming processes were executed under different forming loads and friction coefficients, statistical analyses were performed to observe the effect of above mentioned parameters on springback amount. They concluded that the influence of friction is less significant than force to the springback.

Hardt et al. [17] examined the various modes of control for SF process using both analytical and experimental applications. A series of lab experiments were conducted to compare the sensitivity of the three modes of operation control which are force, displacement and strain.

Yoshida and his co-workers [18] obtained fracture limits in sheet stretch bending theoretically. Their study based on the assumption that the fracture occurs when the stretching force reaches its maximum value. The limit wall stretch was determined as a function of n value and non-dimensional bending curvature t_o/R where t_o be the initial sheet thickness and R is the bending curvature. Luo and Wierzbicki adopted Modified Mohr-Coulomb ductile fracture criterion to analyze the failure behavior [19] of DP steel sheets using stretching bending operations because of the fact that shear fracture could not be identified using standard FLD test. Also, a series of parametric studies were conducted on the 3-D element model considering the tooling friction, mesh size and tension level.

Rajiv Suri and Kevin Otto [20] developed an integrated system model to simulate sheet stretch forming process. In this study, heat treatment and stretch forming operations were simulated separately and outputs from each process become inputs for the following process. The results of the analyses showed the same trend of factory floor data. Also, the predictions of the variational model accorded well with variation measurements of double curvature aircraft skin which is made of AA 2024.

Keum and Wagoner [21] developed a finite element modeling program in which triangular elements are used for simulating the sheet metal stretch forming operation. The reliability and accuracy of the FEM code was numerically tested using simple stretch forming examples. As a result of this study, an excellent agreement between measured and computed strains is obtained.

A formulation which is used to predict distortion of aluminum extrusions was presented by E. Corona [22]. The formulation was developed considering a part which is subjected to combined tension, internal pressure and bending over a die with a model die. Since the radius of the die matches with the concave side of the part, die radius is incremented until it becomes equal to the curvature of the part. The results obtained from the above mentioned formulation showed good agreement with calculations for simple tubular sections and relevant experimental results given in the literature.

Properties of laser welded steel sheet samples of different thickness and samples of same thickness were characterized considering their formability in stretch forming [23]. In this study, tensile properties of the specimens had been determined for both longitudinal and transverse directions. Microstructure and micro-hardness tests were used to evaluate weld quality. Formability of samples which were comprised of different and same thickness was

studied by performing out-of-plane stretch forming test with a hemispherical punch. The one of the most important findings of the study was the great influence of thickness difference of the blanks while surface condition had no considerable effect on the formability.

Xu Feng et al. examined the capability of implicit commercial FE code, Autoform®, to simulate stretched curve flanges [24]. In this study, analytical and numerical studies were investigated and the influences of several geometries on the formability were presented. Experimental trials showed that finite element simulations decrease the failure rate of the problematic parts to 2% from previous 10 %.

The accuracy of anisotropy types and calibration methods for the numerical modeling of stretch forming operation using Hill's yield criterion was investigated by Gilmour et al. [25]. The orthotropic response of a 2024-T3 aluminum alloy was characterized using uniaxial and biaxial tests. Flow curve of the material was obtained using standard tensile test and yield point is determined using biaxial hydraulic bulge test. They concluded that the most accurate strain prediction can be achieved using r-values determined from plastic strains. Besides, it was shown that the accuracy of the yield criterion is to be dependent on both the calibration method and the r-value types.

A new analytical model, which is based on moment and curvature relationship for stretch-bend sheet metal forming processes, was developed by Moon et al. The influence parameters on the existence of curl during stamping operations such as applied tension, yield strength of the material, elastic modulus, bending radius and sheet thickness were considered during the development of the model. The consistency of the analytical model was verified using bending under tension test set-up. It was concluded that predicted curls for dual-phase steels (DP600) and high strength low alloys (590R) using analytical model showed a good correlation between the measured curls obtained from the experimental test [26].

The study on the formability of tailor welded blanks (TWB) was presented by Panda and Kumar. During the experimental studies, strips of different thickness, grades and surface characteristics were used which were prepared by laser welding technology. In biaxial stretch forming of TWBs with difference thickness, it is found that limiting dome height decreases as the thickness ratio increases and the conclusion of the influence of weld ductility and the extent of difference are the most important parameters to form TWBs [27].

Cai et al. described the technology of flexible production system for sheet metal parts and also simulation based approach to compensate springback phenomenon was developed for the digitized die forming system. In this study, the advantages of the digitized die forming were emphasized. It was also pointed that this technology could be used in many sheet forming applications such as skins, ship hull plates and even in titanium prosthesis [28]. Paunoiu et al. introduced new method for springback compensation. Reconfigurable model based on the displacement adjustment was used to compensate springback using FE analyses. In this study, the part was measured and the distances for arbitrary points between the stretched and released sheet were calculated. After the surfaces of the tools were replaced with the same distance but in the direction opposite to the springback deformation, springback could be compensated [29].

Another study on the numerical modeling of multi-point stretch forming process was discussed by Cai et al. In this paper, numerical simulations of the processes for stretching parabolic cylinder, toroidal saddle and sphere parts were practiced using dynamic explicit FE code and the results were compared with the ones implemented for traditional dies. The dimpling effect caused by discrete punch elements were also investigated in this paper. This study can be accepted as a useful guide to determine multi-point stretch form parameters correctly and to accomplish a successful process [30].

Liu and his co-workers built a finite element model to simulate sheet metal multi stretch forming process. The influence of non-uniform deformation of elastic cushion, which is used to prevent dimpling effect, and the springback after unloading the specimen were investigated using FE analysis. Result of the analyses showed that usage of elastic cushion can effectively minimize the dimpling formation, however, non-uniform deformation caused by elastic cushion affect the precision forming of the desired part. Therefore, a method was developed to compensate non-uniform deformation of elastic cushion considering the result of the simulations [31].

Another study performed by Wang only focused on analyzing dimples and shape error. Punch element number and shape were investigated to end up with a precise and accurate final part [32].

One of the most important studies related with the technological improvements on stretch forming process was the development of short cycle stretch (SCS) forming technology Wang and Cai. Although they did not use stretch forming press with hydraulically activated jaws

and dies, they managed to obtain advantages of stretch forming process by the use of single action press with a complex die design. This technology combines a plane pre-stretching and deep drawing operation for the production of body panels. In this design, required restraining force is applied by two opposed interlocking convex bead set elements which alternately bend and unbend the blank while the tool is closing [33]. Besides, in order to improve the process and the part quality, modifications were accomplished to prevent excessive material consuming and wrinkle formation [34]. On the other hand, it is stated that SCS technology is also applicable to form aluminum alloys and it is possible to reduce the number of bead elements to provide material saving.

A new hybrid forming process which is the combination of incremental sheet forming and stretch forming was investigated by Araghi et al. [35]. In this study, new process was introduced which has the capability of forming parts which include both negative and positive contours. It was shown that, this combined process had positive impact on some limits of the operation such as material thinning, geometric accuracy and the process duration.

Kurukuri and other authors focused [36] on modeling intermediate heat treatments which were performed between different levels of stretch forming to prevent Lüder Line formation and to increase formability without any defects. Wegter yield function, which is preferred to define anisotropic and biaxial behavior of the aluminum sheet, was used to obtain accurate material model. Photogrammetric technique was used to evaluate FE analyses. Strain measurements from both experimental and numerical ways were compared and it was concluded that physics based simulations gave better results.

This study differs from previous studies which are mentioned above in many ways. In this work, finite element model is generated for conventional stretch forming operation. Material and contact parameters are determined by using reliable tests. Finally, accuracy of numerical model for stretch forming process is validated through experiments.

CHAPTER 3

MECHANICAL MATERIAL CHARACTERIZATION

3.1 Introduction

Sheet metal forming processes are widely used in many important industries such as aerospace, automotive and white good industries. Development of the technological conditions brings the high mechanical and aero-dynamical expectations together in order to obtain high technology products. This situation increases the importance of efficient manufacturing in which the costs such as scrap, labor and over production times are minimized. Therefore, FEM simulations are used to identify and prevent possible failures before the real manufacturing. However, a successful modeling of a process with finite element method has some requirements. One of the most important requirements to manage successful modeling is to obtain accurate material model. Mechanical properties such as, Young's modulus, Poisson's ratio, percent elongation, plastic deformation behavior, anisotropy (Lankford) parameters have to be determined. In this study, mechanical properties of aluminum alloys are determined using;

- Tensile test,
- Forming Limit Diagram (FLD),
- Hydraulic bulge tests (HBT).
- Stack compression test.

An in-depth understanding and mechanical material characterization are required to establish reliable material model which reflects same deformation behavior of the workpiece during actual process. In sheet metal forming operations, mechanical properties of the sheet material has an important influence on deformation. Therefore, accurate determination of the material properties is an important prerequisite for finite element simulations. There are numerous experimental methods to define deformation behavior of sheet material under different conditions. The common test methods are named as; tensile, compression, torsion, limiting dome height, plane torsion, hardness, plane strain compression and hydraulic bulge tests.

As a result, mechanical properties for aluminum alloys are obtained by using the tests mentioned above to implement successful deformation behavior into finite element software.

In this study, as workpiece materials, aluminum alloys in different chemical compositions, thicknesses and heat treatments are used. So, mechanical properties of aluminum alloys for these conditions are obtained for each case. Before detailed information on mechanical material characterization tests, brief information related with aluminum alloys and heat treatments is given.

3.1.1 Aluminum Alloys and Solution Heat Treatment Procedure

In this study; AA 2024, AA 6061 and AA 7075 are used in both 0 (annealed) and W (solution heat treated) conditions with different coatings (clad coating/non-clad coating) and thicknesses. Material tests and heat treatment processes are accomplished in Metal Forming Center of Excellence which is located in Atilim University. The sheet material is subjected to solution heat treatment by using Proterm furnace (heating up to max. 1300 C°) and Binder (working temperature between -40C° and +110 C°) refrigerator. Solution heat treatment procedure for aluminum alloys can be summarized with the following example. A specimen which is made out of 2024-0 in 1 mm thickness requires several stages to transform 2024-W condition. First of all, specimen needs to be cleaned with water and then put into heat treatment furnace. For this purpose, specially designed fixture (Figure 20) is used to complete heat treatment operation for at least 14 specimens at once. So that, time required for heat treatment phase is minimized.

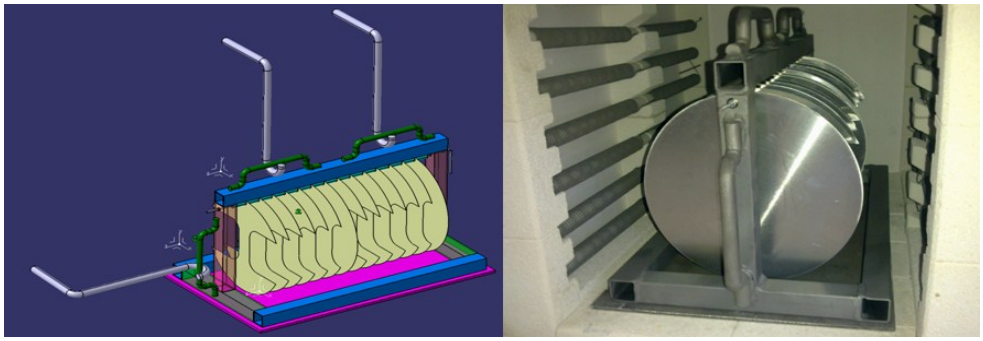

Figure 20: CAD model and actual illustration of heat treatment fixture

Test specimens are subjected to 493 C° for 35 minutes in preheating furnace. After that, the specimens are immersed into water pool as quick as possible. After 3 minutes cooling in water, they are placed in refrigerator at -20 ^{0}C. In the refrigerator, aluminum alloys can keep their W condition for 7 days. After that, they transform into T-42 condition because of aging phenomena of aluminum alloys. Solution heat treatment and forming procedure to obtain

FLD purpose are illustrated in Figure 21 and more detailed explanation is given in APPENDIX Part-Table 10. On the other hand, the success of heat treatment operation is validated through TAI Process Standard PS. 35.42 [37]. This procedure and results of measurements are summarized in APPENDIX Part-Table 11.

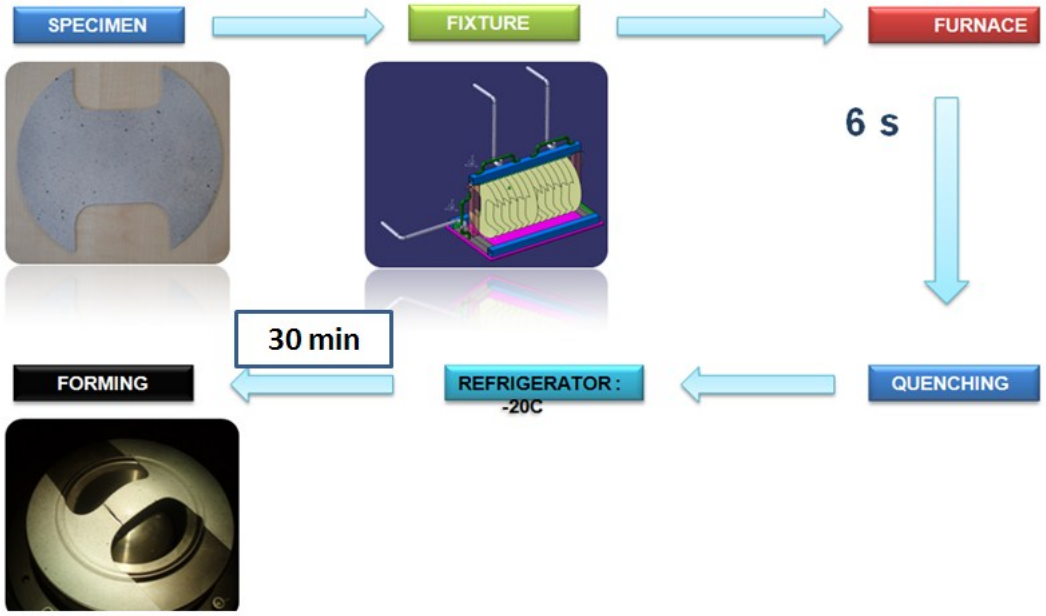

Figure 21: Solution heat treatment sequences for aluminum alloys

3.1.1 Mechanical Characterization Tests

In this section, mechanical characterization tests of mostly used aluminum alloys in aerospace industry are given in detail.

3.1.2.1 Tensile Test

Tensile test is the most common method to obtain mechanical properties of sheet material due to its simplicity and ease of application. Mechanical material properties such as; ultimate tensile strength, yield strength, percent elongation, plastic flow and anisotropy parameters can be determined using tensile test. Tensile test is simple and inexpensive method, however, only limited strain values can be obtained due to the fact that process is performed under uniaxial stress conditions [38].

Tensile test is carried out by elongating the test specimen with oppositely moving jaws by applying force (P). The tensile force applied during the test is recorded by load cells.

Meanwhile, length of the specimen in thickness (t_o) and width (w_o) direction are also monitored by the extensometer. During the test, these values are recorded by data acquisition system in order to calculate anisotropy coefficients from the proportion of width to thickness strain. Using the equations given in Eq. 22-25, load-extension, engineering stress- engineering strain and true stress-true strain curves can be obtained.

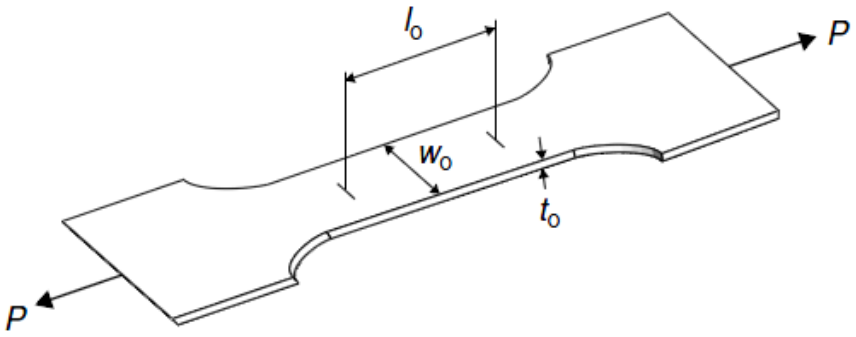

Figure 22: Illustration to tensile test specimen and test's important parameters

Engineering Stress and Engineering Strain:

$$\sigma_{eng} = \frac{P}{A_0} \qquad (Eq\ 22)$$

$$e_{eng} = \frac{\Delta l}{l_0} \times 100\% \qquad (Eq\ 23)$$

True Stress and True Strain:

$$\sigma = \frac{P}{A} \qquad (Eq\ 24)$$

$$d\varepsilon = \frac{dl}{l} ==> \varepsilon = \int_{l0}^{l} \frac{1}{l} dl = ln\frac{l}{l_0} \qquad (Eq\ 25)$$

Where;

σ_{eng}	:	Engineering Strain (MPa)	Δl	:	Increase in length (mm)
P	:	Instantaneous Load (N)	L_0	:	Initial length (mm)
A_0	:	Initial cross sectional area (mm^2)	σ	:	True Stress (MPa)
e_{eng}	:	Engineering Strain	ε	:	True Strain

In this study, tensile tests are performed in order to obtain mechanical properties of Al 2024-0, AL 6061-0 and AL 7075-0 aluminum alloys for their different heat treatment (W condition), thickness (0.8 mm-1.02 mm- 1.6 mm-2.5 mm) and coating (clad) conditions. Each test is performed three times for different rolling directions in order to obtain anisotropy parameters as it is identified in ASTM E8-04 [39]. The geometrical dimension of the test specimen is given in the APPENDIX-Part Figure 112.

It is a well-known fact that conventional machining and pressing operations can cause micro cracks on the test specimen. Therefore, non-traditional cutting method water jet is used to cut test specimen into the desired geometry [40].

Tensile tests are performed with 0, 01 sn-1 strain rate using 300 kN capacity Zwick/Z300 tensile testing device which has tangible elongation and width extensometers (Figure 23).

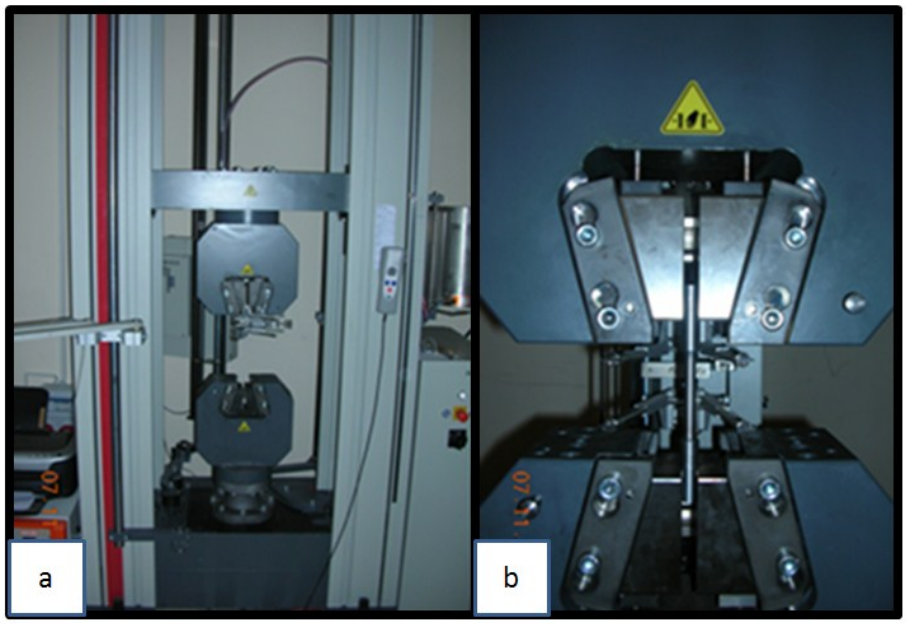

Figure 23: a) Zwick/Roell (300 kg-f capacity) tensile test machine b) Closer look to gripping jaws and extensometers

The output of the standard tensile test is the true stress-strain values. In Figure 24, true stress-true strain curve is given for AA 2024-W. Ludwik-Hollomon equation is used to express and extrapolate deformation behavior and as it is seen in Figure 25, the curve obtained by Ludwik-Hollomon equation fits the experimental curve obtained by tensile test. It can be easily said that; Ludwik-Hollomon equation give good fitting results with experimental data for aluminum alloys.

$$\sigma = K.\varepsilon^{n} \qquad (Eq\ 26)$$

- σ: Flow Stress(MPa)
- K: Strength index (MPa)
- ε: Strain
- n: Strain hardening coefficient

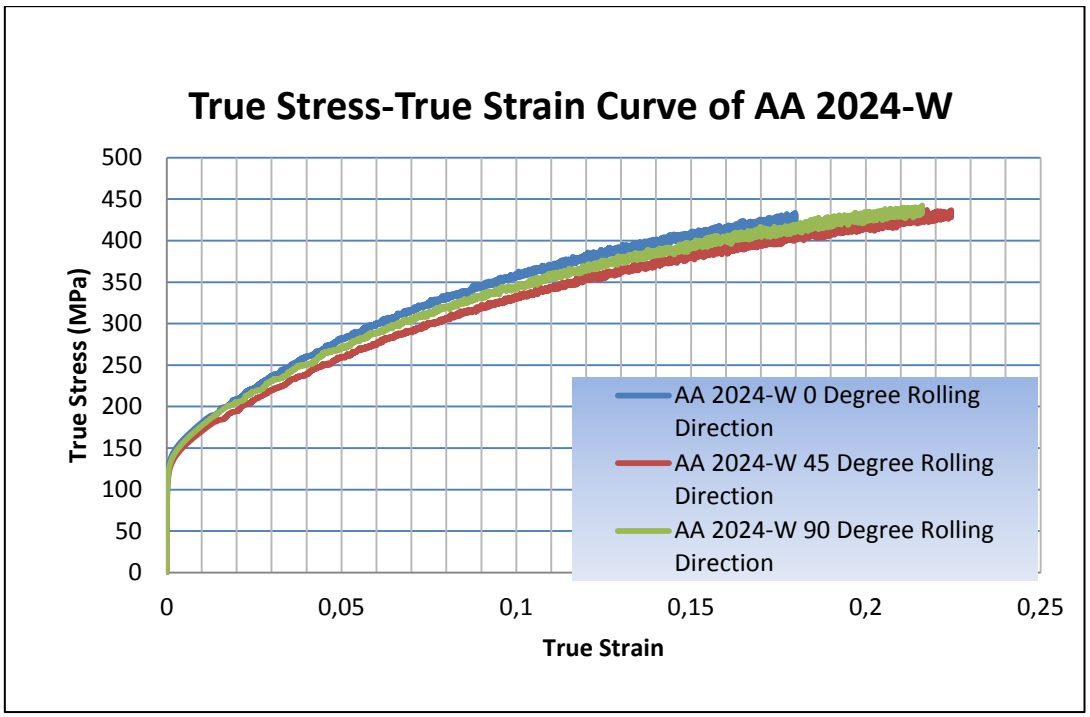

Figure 24: True stress-strain curve for AA 2024-W (obtained by tensile test)

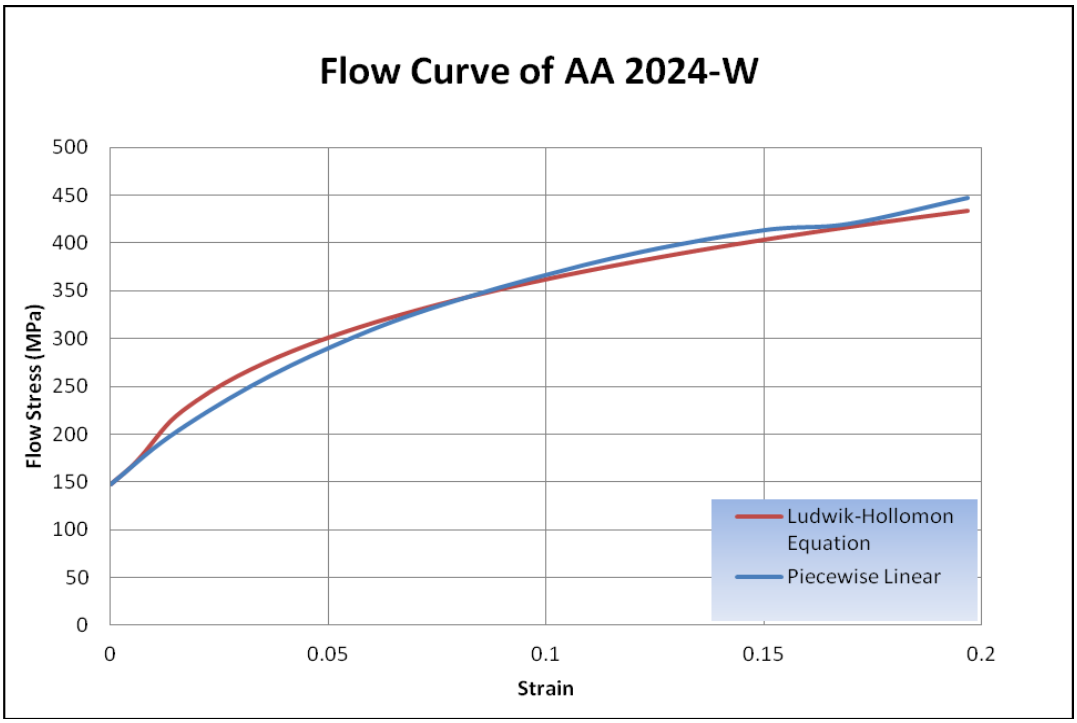

Figure 25: Flow curve of AA 2024-W (Both experimental and Ludwik-Hollomon curves are plotted)

Mechanical properties obtained by standard tensile test for both annealed and solution heat treated aluminum alloys are summarized in Table 3 and Table 4, respectively. A well-known fact which claims clad condition and material thickness have no influence on flow curve of aluminum alloys is also verified. However, alloying elements play an important role on deformation behavior. As it is shown, yield strength of AA 6061 is quite lower than the other alloys. AA 2024 and AA 7075 show similar deformation behavior. Also, it is observed that ductility of aluminum alloys considerably influenced by solution heat treatment.

Table 3: Mechanical properties of aluminum alloys in 0 (annealed) condition

Aluminum Alloy	YS (Mpa)	UTS (MPa)	Elastic Modulus (Mpa)	Poisson Ratio	R0	R45	R90	K	n
AA 2024-0	72	171	73100	0,33	0,65	0,83	0,6	326,8	0,226
AA 2024-0-CLAD	58,5	168	73100	0,33	0,63	0,75	0,65	336,5	0,257
AA 6061-0	56	121	68900	0,33	0,65	0,65	0,58	211,7	0,208
AA 7075-0	86	205	71700	0,33	0,74	0,66	1,06	378	0,218
AA 7075-0-CLAD	82	193	71700	0,33	0,76	0,61	0,98	326,5	0,198

Table 4: Mechanical properties of aluminum alloys in W (solution heat treatment) condition

Aluminum Alloy/	YS (Mpa)	UTS (Mpa)	Elastic Modulus	Poisson Rat,o	R0	R45	R90	K	n
AA 2024-W	147	447	67100	0,33	0,74	0,87	1,14	669,81	0,27
AA 2024-W-CLAD	165	518	67700	0,33	0,80	0,78	0,89	779,77	0,26
AA 6061-W	74	225	62233	0,33	0,73	0,69	0,61	339,68	0,24
AA 7075-W	145	421	69966	0,33	0,80	0,37	2,22	653,93	0,26
AA 7075-W-CLAD	138	400	69700	0,33	0,72	0,72	0,94	615,23	0,25

3.1.2.2 Hydraulic Bulge Test (HBT)

Tensile test is the most widely used one which is standardized by ASTM E8-04. Although tensile test is inexpensive and simple, it also has many limitations [41].

- Tensile test is carried out under uniaxial stress state where biaxial stress state exists in stamping operation.
- Maximum achievable strain is limited up to 30 % where up to 70 % plastic strain levels can be obtained in the tests which performed under biaxial stress state.
- Extrapolation of the data obtained from tensile test causes significant errors to define actual material behavior.
- Variation of strain hardening is difficult to discern and obviously affect the extrapolation.

In the light of these facts, the deformation behavior of sheet materials under biaxial stress state is usually carried out with the HBT. Since the test is performed by hydraulic oil instead of punch, large strain values can be obtained in frictionless environment. The one of the most important advantage of this test is that, higher plastic strains (approximately up to 70%) can be obtained before instability occurs.

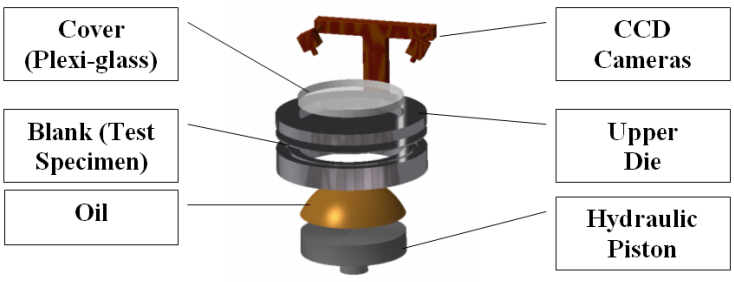

Figure 26: CAD model of HBT test set-up

The plasticity [42] and mechanical properties [43] of the sheet material are investigated using quasi-static bulge test developed in the late of 1940s. In this test, instantaneous measurement of dome apex thickness, pressure and the bulge radius are required, however, accurate measurement of these parameters are quite difficult. Therefore, several simplifications with several approximations have been developed. In Hill's approach [44], it is assumed that the shape of bulged sheet is sphere. He developed an analytical model to determine the thickness at the dome of the apex [45]. Chakrabarty and Alexandar [46] used Tresca's yield criterion and improved the model using strain hardening coefficient, n. Panknin [47] performed hydraulic bulge tests with different sheet materials which have different strain hardening coefficient and he observed that the thickness distribution over the sheet is more uniform for the materials with high strain hardening coefficient. Gutscher et al. performed VBT with experimental methods and numerical analyses to identify the test variables such as dome wall thinning, dome radius, dome height and strain hardening index. He concluded that, with high deformation velocities, strain rate becomes an important parameter and n value affects the thickness of the dome and dome height. Influence of the anisotropy on deformation is also being established. As it is known, a material with larger r-value will thin less during tensile test. Based on the simulation results, Altan et al. claim that negligible difference is obtained [45].

Atkinson [48] conducted explicit formulations for HBT to determine thickness variations and effective radius of curvature. He showed experimentally that, stress-strain relationship significantly changes by his corrections.

Güner's study [49] on HBT covers the finite element analysis of geometric and process parameters in terms of the accuracy of the flow curve. He claims that; it is not always possible to obtain accurate flow curves even with simulation results especially towards to end of the test due to existence of higher strain values. Therefore, 3-D optical measurement systems are advised to obtain more realiable data.

Koç [44] compared different approaches provided in the literature for HBT in order to determine accurate flow curves. In this study, optical measurement systems are used to obtain accurate data to evaluate the test variables experimentally. From his studies, it is determined that Panknin's bulge radius and Kruglov's thickness calculation formulations give the most reliable flow curves.

Mutrux et al. introduced a procedure for the determination of the biaxial hardening curve from the hydraulic bulge test. After surface strain at pole region was measured, the procedure investigated the congruence of the biaxial and uniaxial tensile hardening curves. Once the tensile and biaxial hardening curves were determined, the strains were related using equivalent plastic work [48].

In order to obtain flow curve using HBT, following variables are required to be measured at different strain levels of deformation. Due to volume constancy,

$$\varepsilon_{xx} + \varepsilon_{yy} + \varepsilon_{zz} = 0 \qquad (Eq\ 27)$$

$$\varepsilon_{xx} + \varepsilon_{yy} = -\varepsilon_{zz} \qquad (Eq\ 28)$$

$$\bar{\varepsilon} = -\varepsilon_{zz} = ln\left(\frac{t}{t_0}\right) \qquad (Eq\ 29)$$

Now, equivalent stress can be determined. The statement of the problem can be considered as plane stress condition; where;

$$\sigma_{zz} = \sigma_{thickness} = 0, \varepsilon_{zz} = \varepsilon_{thickness} \neq 0 \qquad (Eq\ 30)$$

Membrane theory is used to define flow stress with HBT. Therefore, bending stress is neglected and uniform stress distribution over the sheet thickness is assumed [49]. Membrane theory is only valid for thin shells and bending stresses can only be neglected, when Eq 31 holds true [51-52].

$$\frac{r_c}{t_0} > 10 \qquad (Eq\ 31)$$

Where; r is the die aperture radius and t_0 is the initial thickness.

Membrane theory is expressed by;

$$\frac{\sigma_1}{R_1} + \frac{\sigma_2}{R_2} = \frac{P}{t} \qquad (Eq\ 32)$$

Where; σ1, σ2 are principal stresses, R_1, R_2 are corresponding radius of the curved surfaces, P is the hydraulic pressure and t is the thickness of the sheet.

As it is known, two principal stress values and radius of curvature are equal at the pole. Therefore;

$$\sigma = \frac{P.R}{2t} \qquad (Eq\ 33)$$

If the dome height is spherical, then the radius in bulge rolling direction (R_{RD}) is equal to the bulge radius in transverse direction (R_{TD}).

$$R = RRD = RTD \qquad (Eq\ 34)$$

By combining Equations 33 and 34, following equation can be obtained;

$$\sigma_{xx} = \sigma_{yy} = \frac{PR}{2t} \qquad (Eq\ 35)$$

According to V. Mises Criterion, $\bar{\sigma}$(equivalent stress) can be calculated as;

$$\bar{\sigma} = \frac{1}{\sqrt{2}}\left[\begin{matrix}\left(\sigma_{xx}-\sigma_{yy}\right)^2+\left(\sigma_{yy}-\sigma_{zz}\right)^2+\\(\sigma_{zz}-\sigma_{xx})^2+6(\tau_{xy}^2+\tau_{yz}^2+\tau_{xz}^2)\end{matrix}\right]^{\frac{1}{2}} \qquad (Eq\ 36)$$

Then,

$$\bar{\sigma} = \frac{RP}{2t} \qquad (Eq\ 37)$$

Effective strain is found using the sheet thickness;

$$\varepsilon = -\varepsilon_t = \ln(\frac{t_d}{t_0}) \qquad (Eq\ 38)$$

As it is showed above, instantaneous wall thickness at the apex of the dome, instantaneous radius of curvature, instantaneous dome height and pressure is required for the equations [44].

Instantaneous radius of curvature at the top of the dome can be found by following equation if there is no fillet in the cavity of die;

$$R_d = \frac{d_c^2+4h_d^2}{8h_d} \qquad (Eq\ 39)$$

Where; d_c is the diameter of the die cavity, h_d is the dome height.

Panknin conducted HBT experimentally and he measured the radius at the apex of the dome of the bulged samples with strain gages. If there is fillet in the cavity of die, then the Eq 39 becomes;

$$R_d = \frac{\left(\frac{d_c}{2}+r_f\right)^2 + h_d^2 - 2r_f h_d}{2h_d} \qquad (Eq\ 40)$$

Where; r_f is the fillet radius in the die cavity.

Schematic illustration of hydraulic bulge test is given in Figure 27.

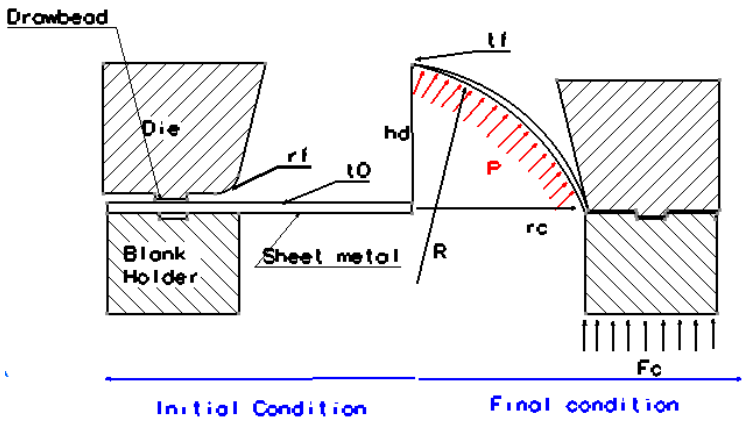

Figure 27: Schematic illustration of hydraılic bulge test

t_o	: Initial material thickness	P	: Hydraulic pressure
t_f	: Final thickness	R	: Radius of the dome
H_d	: Dome height	R_c	:die cavity radius
F_c	: Blank Holder Force (BHF)	R_f	:upper die fillet radius

As it is mentioned before, one of the most important test parameter is the determination of the thickness at the apex of the dome, however, the sheet is assumed to be formed in sphere shape. So that, Hill developed an analytical formulation which is given in Eq 41.

$$t_{d=}t_0\left(\frac{1}{1+\left(\frac{2h_d}{h_c}\right)^2}\right)^2 \qquad (Eq\ 41)$$

Where; h_c is the die inner diameter.

Moreover, this method is improved by Chakrabarty and Alexander by consideration of strain hardening coefficient, n [46].

$$t_d = t_0 \left(\frac{1}{1 + \left(\frac{2h_d}{d_c}\right)^2} \right)^{2-n} \qquad (Eq\ 42)$$

Another analytical formulation to determine instantaneous thickness at the apex of the dome is developed by Kruglov [49].

$$t = t_0 \left[\frac{\frac{r_c}{R}}{\sin^{-1}\frac{r_c}{R}} \right]^2 \qquad (Eq\ 43)$$

Where; R is the bulge radius.

Experimental Procedure

Experimental studies are performed using 600 kg-f capacity Zwick/BUP 600 test machine integrated with 3-D optical measurement device GOM/Aramis®. Experimental set-up consists of upper-lower dies, ARAMIS® module, hydraulic piston and oil (Figure 26). The sheet material is clamped between upper and lower dies and formed using oil pressure which is activated by hydraulic piston. Draw beads are used to prevent material flow from the dies.

First of all, 50 mm height of high viscosity oil is pulled on the lower die. The deformation is observed by the CCD cameras which are mounted on the press. Arcrylic-glass® material which is used to prevent oil leakage is fixed between the lower die and CCD cameras. Until the sheet tears, deformation of sheet material is observed and recorded by optical cameras. In the simplest tests, approximately 400 photographs are taken and the results taken from the controlled press are saved in each 0.01 seconds. Other test parameters of hydraulic bulge test are given below in Table 5.

Table 5: Parameters applied during hydraulic bulge test

Test Adjustments	Blank holder force (BHF)	Punch force	Cupping speed	Cupping force
-	450000N	150N	2500mm/s	550000 N

In this study, 200 mm square shaped sheet material is used. In order to prevent the reflection of light while the images are taken, test specimen is painted into white color. Black dots are formed on the specimen by spraying to enable CCD cameras measuring the deformation (Figure 28). After that, the test specimen is clamped between upper and lower dies and the blank holder force is applied. Upper and lower dies have approximately 160 mm diameter drawbead to prevent material flow in clamping region.

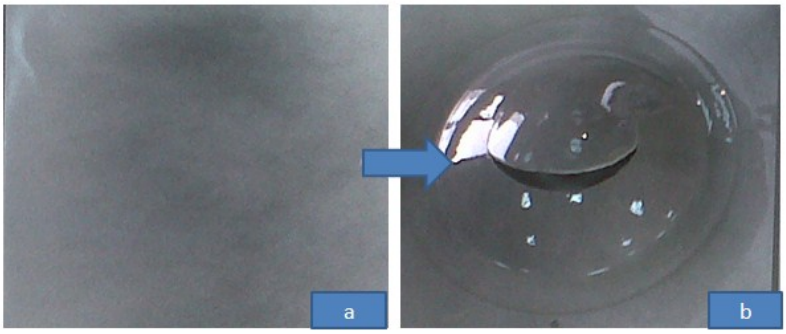

Figure 28: (a) Initial geometry of workpiece material (b) Bulged specimen

The sheet is formed by oil pressure until it fractures. In every second, 20 frames are taken by two accurate and fast optical cameras to observe the deformation until the sheet fractures.

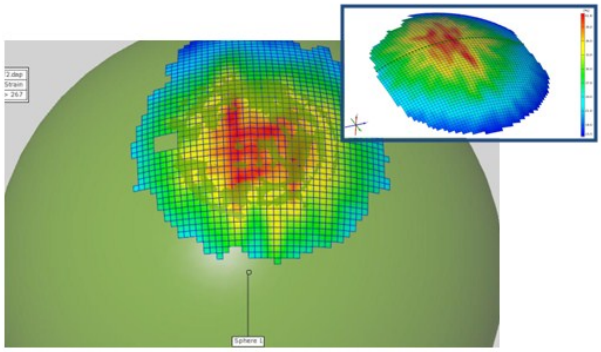

Figure 29: Aramis® best fit sphere and strain distribution measured by Aramis®

During deformation; oil pressure is recorded by the help of load cell located under the piston. Principal strain and bulge radius values are also recorded for each stage using the 3-D deformation measurement device-Aramis®. On the other hand, Aramis® gives sphere radius data for each stage. This data is calculated by Aramis® using best fit sphere formulation and gives the radius of the spherical shaped specimen (Figure 29). Using these outputs of the test, flow curve of the material can be obtained using the equation provided in the literature. Approximately up to 0.15 strain value can be achieved using standard tensile test. For a successful finite element modeling, this data needs to be extrapolated. However, as it is shown in Figures 30-31, up to 0.6 strain data can be obtained by hydraulic bulge test under biaxial stress state.

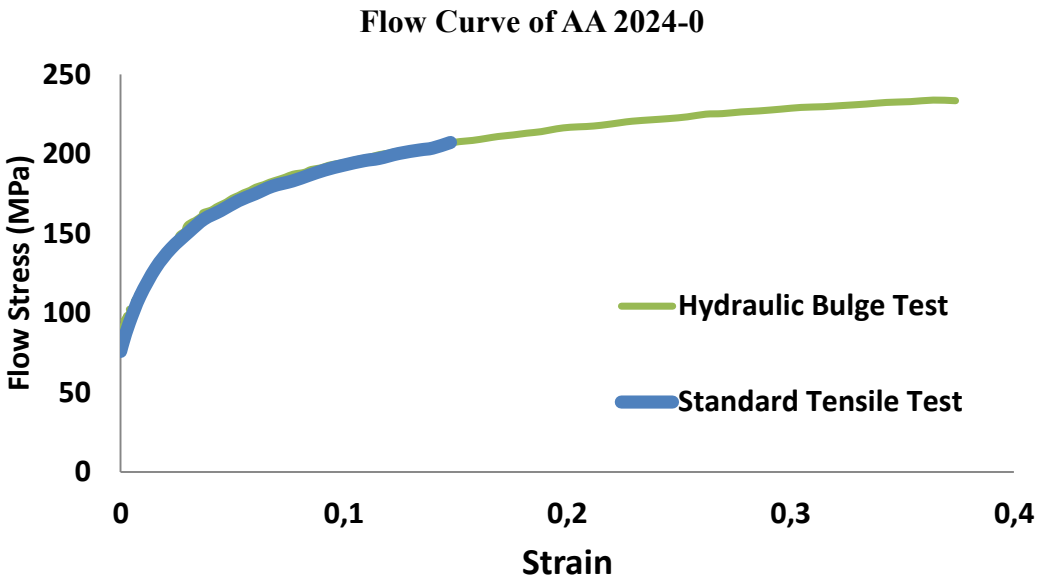

Figure 30: Flow curve of AA 2024-0 (obtained by HBT)

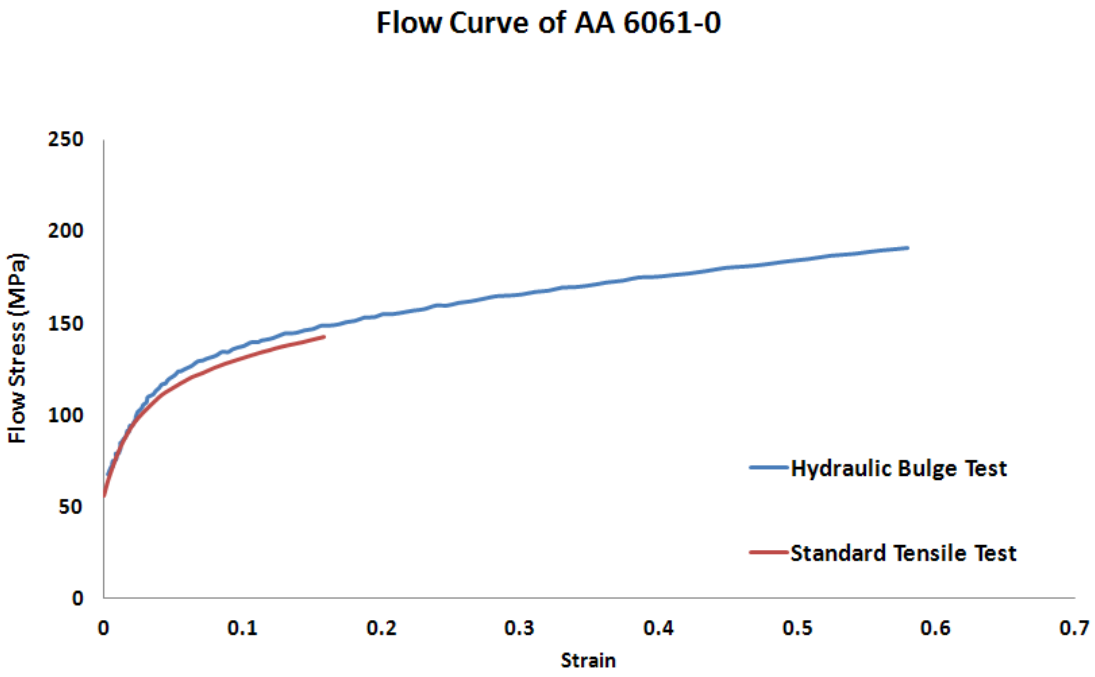

Figure 31: Flow curve of AA 6061-0 (obtained by HBT)

The FEM simulation of HBT is also performed. The results taken from the HBT experiments are compared to the values obtained by analyses and it is observed that similar curve of displacement and pressure curves are obtained. It has been validated that; reliable modeling using correct mesh type and size and material modeling provide results which is similar to real application as shown in the Figure 113 in APPENDIX Part.

3.1.2.3 Forming Limit Diagram (FLD)

Forming limit diagram is one of the most important tools which can be used to evaluate process limits considering simulation results. One of the most important and basic study on critical strain terms are performed by Keeler [53] and Goodwin [54] in 1960s. As it is mentioned above, principal strains can be determined by measuring the strains at failure using sheet parts which are covered with circular grids. During the deformation circular grids becomes ellipses. Keeler obtained major-minor strains in biaxial stretching conditions where $\varepsilon1>0$ and $\varepsilon2>0$. Plot obtained using biaxial stretching of the sheet components forms the right region of the forming limit curve. Then, Goodwin obtained the curve for the tension/compression domain where $\varepsilon1>0$ and $\varepsilon2<0$ [55]. The connection of these two plots is currently called as the Forming Limit Diagram (FLD). Since then, FLD has been widely used

for studying the formability of sheet metals. Forming limit diagram is formed using critical strain values as it is shown in the Figure 32. As it is seen in the Figure 32, the diagram represents the critical major (ε_1) and minor strains (ε_2).

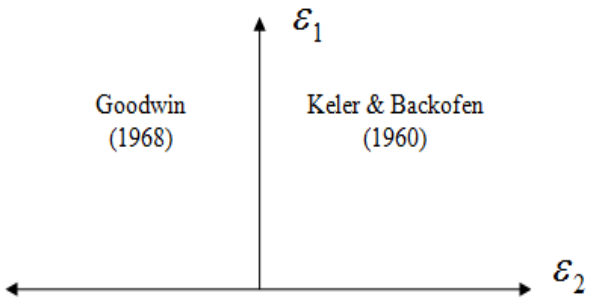

Figure 32: Goodwin-Keeler FLD

This diagram represents the deformation limits from uniaxial strain condition to biaxial strain conditions for different geometries. FLD tests are performed to identify the maximum and minimum strain levels under uniaxial and biaxial stress conditions. It is an efficient method to distinguish safe and critical regions (wrinkling or tearing) on the sheet material during the deformation. In the Figure 33 given below, marked zones are described.

i. Zone 1: shows the crack region. The points located above the forming limit curve represent failure.

ii. Zone 2: Shows the excessive thinning region. The points located between forming limit curve and the same curve is offset 10%, represents the critical zone.

iii. Zone 3: Shows the safe region. The points located below the forming limit curve represent the safe region.

iv. Zone 4: Shows the insufficient stretching region. Points located in the circle whose radius is 0.002 mm show insufficient stretching.

v. Zone 5: Shows the wrinkling tendency region. Points located above the y=-x line and below the uniaxial section represents the wrinkling tendency.

vi. Zone 6: Shows the strong wrinkling tendency region. The points located below the y=-x line represents the higher wrinkling tendency.

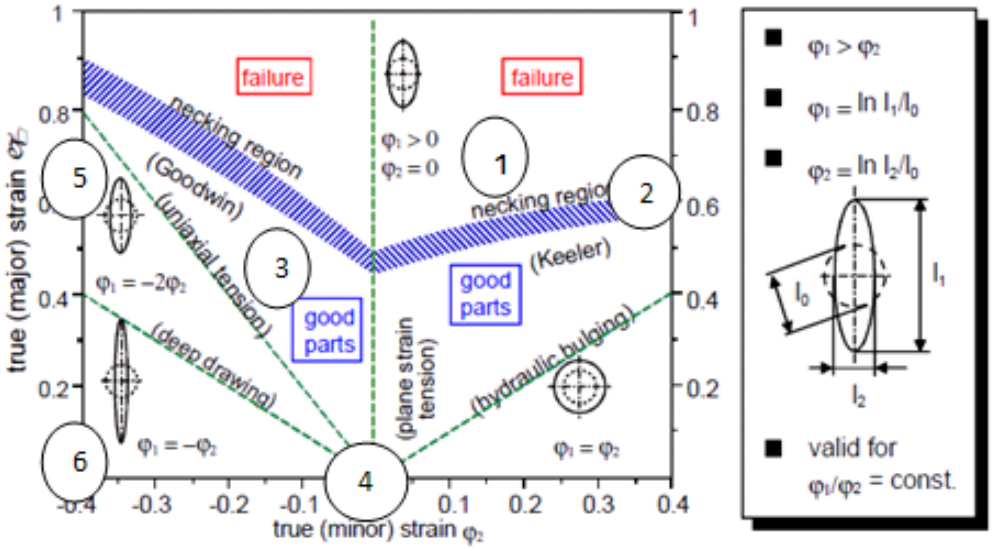

Figure 33: Represantation of FLD [6]

The determination of FLDs are standardized as ISO 12004-2, "Determination of Forming Limit Curves in the Laboratory" [56]. FLD test are accomplished using 600 kg-f capacity Zwick/BUP600 which is integrated to 3-D optical measurement system, GOM/ARAMIS® (Figure 34).

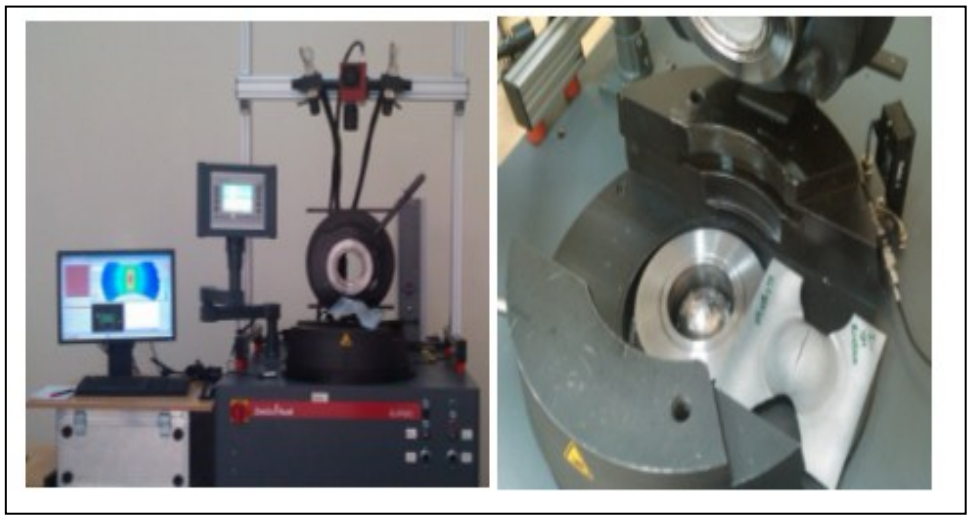

Figure 34: Experimental FLD Set-up

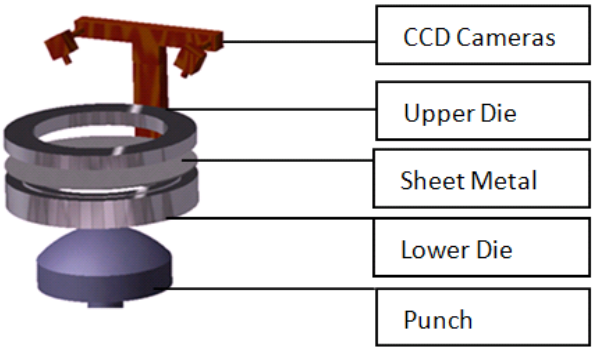

Figure 35: CAD model of FLD test set-up

Test equipment consist of; CCD cameras, upper and lower dies and hemi-spherical punch (Figure 35). First of all, sheet specimen is painted using a stochastic pattern (Figure 36).

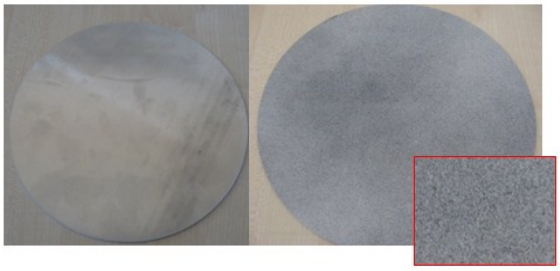

Figure 36: FLD test specimen and stoachastic pattern on the sheet material

After the painting dries, the specimen is clamped between dies and the blank holder force is set-up. Since the best lubrication condition is satisfied with Paraffin lubricant, it is used between punch and sheet material's interfaces to reduce friction coefficient. The test specimens are cut into the desired geometry with water jet- technology.

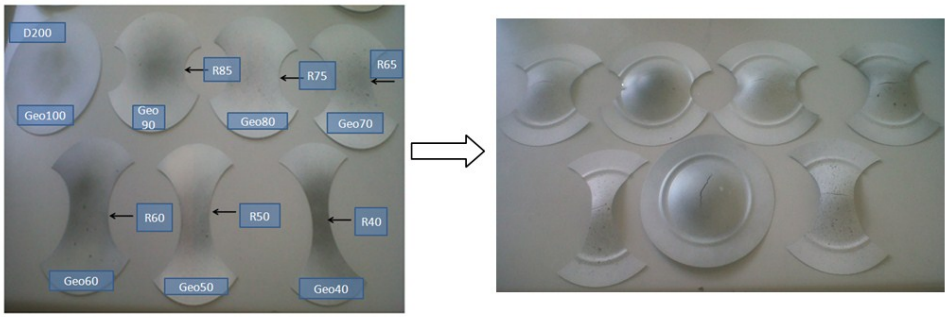

Figure 37: Nakazima test specimen (Initial and final test specimens)

As it is known, Nakajima and Marciniak test geometries give the most successful results. Therefore during the studies, Nakajima test specimens with 7 different geometries are used (Figure 37).

The sheet is clamped between dies and the blank holder force is optimized. In the case of applying higher blank holder force may cause tearing in the specimen, the lower blank holder force may cause the wrinkling of the edges. Therefore, it is a necessity to optimize blank holder force. After the blank holder force is adjusted, the punch starts to form the sheet material until it fractures. During the deformation, optical measurement cameras record the strain distribution over the specimen and determine the critical strain limits just before the fracture for each test (Figure 38-39).

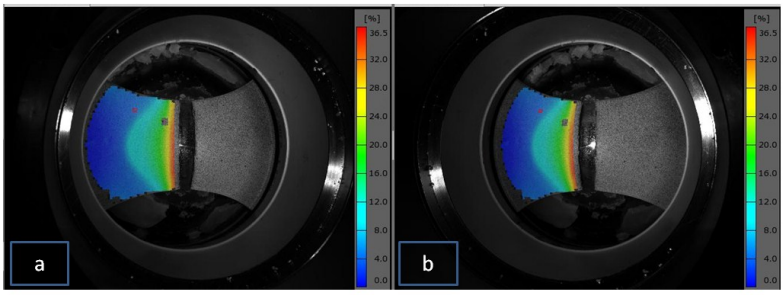

Figure 38: Left and right view of CCD cameras in instantaneous time after tearing occurs

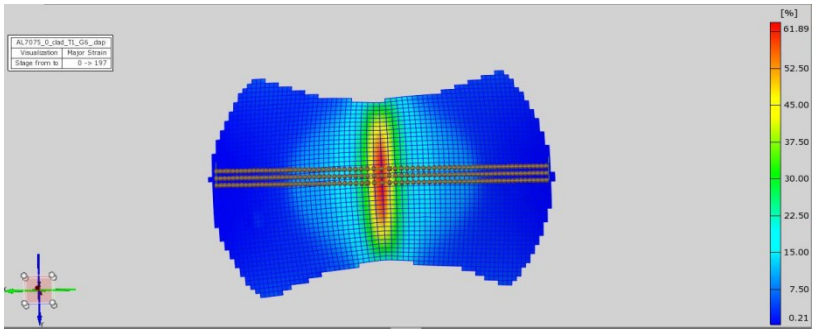

Figure 39: Section over sheet material (GOM-Aramis® result)

In this study, FLDs are obtained for aluminum alloys considering different thickness, coating and heat treatment conditions. Tests are applied according to the criteria specified in ISO 12000-2. As it is shown in the Figure 38, tearing of the test specimens are formed in the apex region due to low friction state. FLD curves which illustrates repeatability of test results and formability limits of AA 2024-0 are shown in Figure 40-41, respectively.

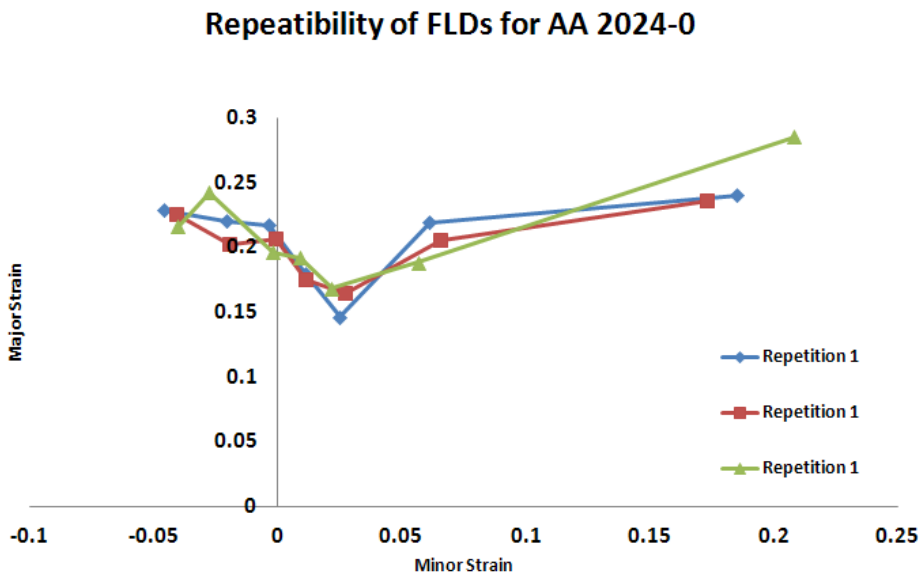

Figure 40: Three repetitive FLD curves of AA 2024-0

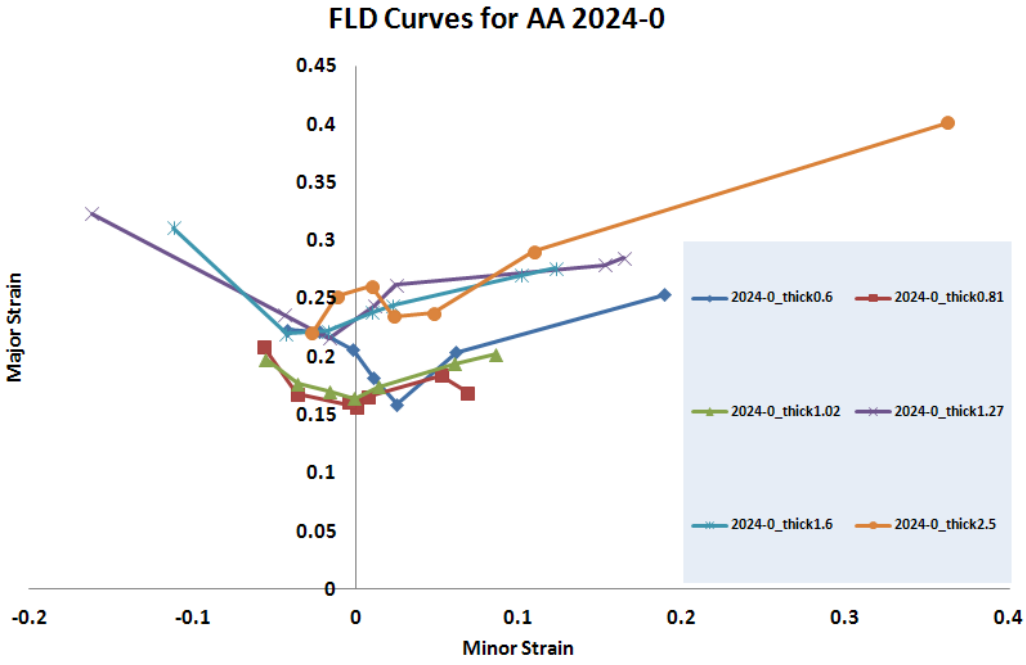

Figure 41: FLD curves of AA 2024-0 for different thicknesses

3.1.2.4 Stack Compression Test

Stack compression test is a simple material characterization test used to determine onset of plastic yielding and flow behavior of the workpiece material under uniaxial compression loads. Although compression test has been known for many years, its application for sheet materials is quite new method so that only a few studies can be found in the literature related with this subject. Since this test is not standardized yet, experimental procedure for the test is generally adapted to standard compression test [57]. The studies related with compression test for sheet materials are generally target to obtain flow curves, hardening behaviors and biaxial anisotropy of the specimens. Addition to this, studies using stack compression tests is also performed to express friction coefficient numerically with reverse finite element applications [58]. In this study, sheet materials in 10 mm diameter are used. On the other hand, usage of optical measurement device during the stack compression test results with more reliable and accurate determination of deformation behavior [59].

Experimental procedure for compression test is quite simple. The one of the most important issues is the preparation of the test specimens. Thicknesses and dimensions of the test specimens are completely required to be homogeneous. During the tests, sheets with 1 mm thickness are used. Six sheets are superimposed so that specimen length can be considered as 6 mm. Circular sheet specimens are 15 mm in diameter. As the test performed using stacked sheet parts, it is essential to assure the same orientation with respect to the rolling direction. Test specimens are compacted using selobant in order to prevent any priori and early slippage of the stacked sheets. Teflon based lubricant is sprayed on the test specimen and the test specimen is centered of the forming plates. The test is performed using 30 tons capacity Zwick/Roell compression test machine (Figure 42).

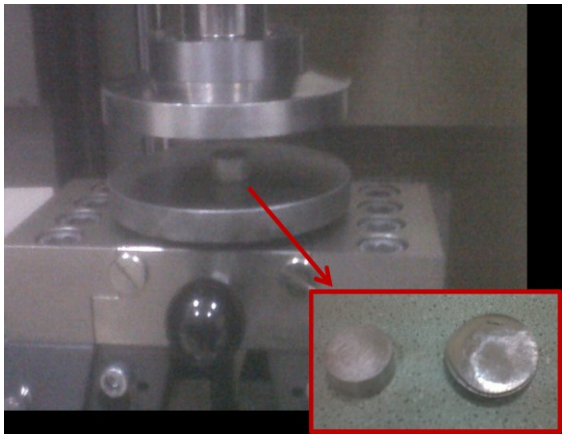

Figure 42: Stack compression test set-up and test specimen

In this study, layer compression test is performed for aluminum alloys such as AA 2024, AA6061 and AA 7075. Each test is performed using 5 mm/min punch speed. Tests are accomplished using 3 repetitions. As it is shown in the Figure 43, flow curve obtained by stack compression test, tensile test and hydraulic bulge test display similar trends for AA 7075-0 up to 0, 1 plastic strain. The reason behind the decreasing trend of the flow curve obtained by stack compression test is directly related with Bauschinger effect. The repeatability of the test results is quite good for low range of compressive strains.

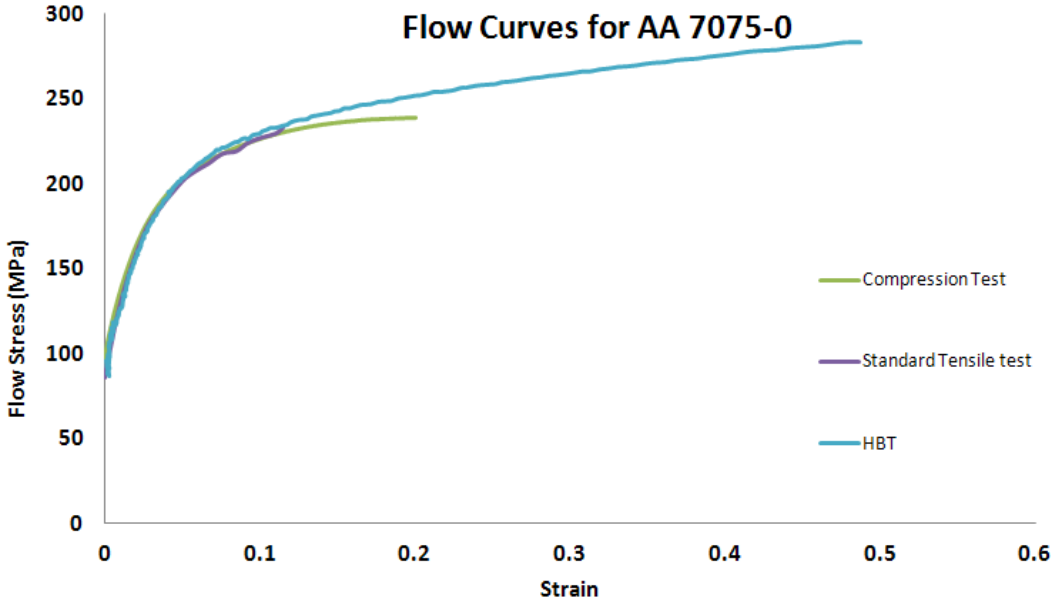

Figure 43: Flow curves of AA 7075-0 which are obtained by different MCTs

CHAPTER 4

DETERMINATION OF FRICTION COEFFICIENT FOR DIFFERENT LUBRICATION CONDITIONS IN STRETCH FORMING PROCESS

4.1 Introduction

Friction plays an important role in sheet metal forming processes. Especially in processes such as stretch forming process in which contact area between tool-blank interfaces is quantitatively large, the influence of friction directly affects the quality of the operation. In stretch forming operation, friction exists in two regions. These are;

- Form die and sheet metal,
- Jaws and sheet metal interfaces.

In stretch forming operation, friction affects the shear stresses at the tool and sheet metal interfaces, tensile stress in the plane of the sheet and local strains over the deforming section of the blank. In order to reduce the influence of friction, appropriate lubrication has to be applied to reduce coefficient of friction. In stretch forming process, lubrication is performed by brushing or spraying of the lubricant over the die, however, brushing is generally preferred in stretching processes because this method offers uniform distribution and high lubricant savings rather than spraying. The lubricant selection is quite important to achieve required strain values and it is determined by considering the geometry and surface properties of form die and sheet material and also the amount of applied force. According to the above mentioned variables, several types of lubricants are available in industry for stretch forming process. Water soluble oils are commonly used due to the ease of removal from the workpiece. On the other hand, in lighter works in which the required force is low, heavier oil can be used. Also, in some SF operations where high friction coefficient values exist, there is a need for applying different types of lubricants to reduce friction. For example, tool surface can be coated with silicon film or nylon where lower friction coefficient is required.

In the literature, there are many studies performed to identify the influence of friction acting during sheet metal forming processes and these studies mostly cover design of specific test

equipments or inverse engineering analyses where the number of analytical studies are comparatively quite less.

One of the analytical approaches is provided by Kaftanoğlu [60]. He developed two methods to determine friction coefficient. The first method is suitable to obtain friction coefficient in radial drawing zone and the second method is applicable to obtain friction coefficient in stretch forming zone using analytical equations which include some quantities such as loads, stresses and strains (Figure 44). He concluded that, friction coefficient changes with continued plastic deformation.

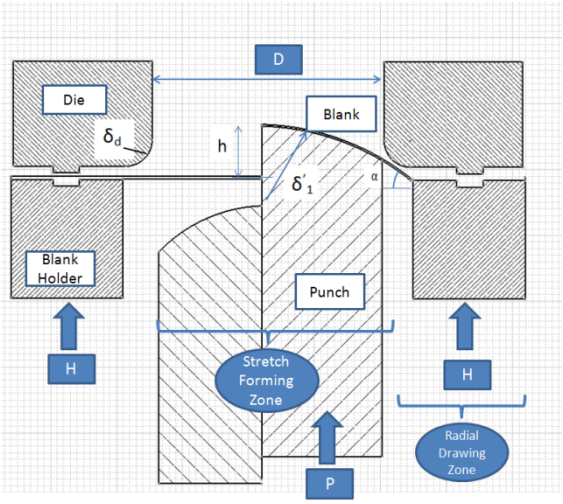

Figure 44: Illustration of test set-up to determine friction coefficient [60]

According to this study, friction coefficient for radial drawing zone can be calculated by;

$$\mu = \frac{\delta P \cot a}{2\delta H + \delta P} \qquad (Eq\ 44)$$

Where H is the blank holder load, P is the punch load and μ is the friction coefficient

Friction coefficient in the stretch forming zone is expressed by the following equations;

$$k = \frac{\sigma_3}{\sigma_1} \qquad (Eq\ 45)$$

k is the stress ratio, σ_3 is the thickness and σ_1 is the meridional stress

$$x = \frac{d\varepsilon_2(2k-1) + d\varepsilon_3(R+k)}{d\varepsilon_2 + d\varepsilon_3(R+1)} \qquad (Eq\ 46)$$

Where ε_2 and ε_3 are the circumferential and thickness stresses, R is the plastic anisotropy in tension

$$\mu = \frac{(1-x)sin^2\theta}{(1+x)(\theta - sin\theta cos\theta)} \qquad (Eq\ 47)$$

Where θ is the angle that normal to an element of shell wall makes with the vertical axis.

On the other hand, many inverse mathematical methods are performed to obtain representative friction coefficients. Using numerical models of the process, results are established with different friction coefficients and results are then compared with the actual process in order to determine corresponding coefficients of the friction conditions [61-64]. The basic and most important part of friction study is based on the same methodology. This will be discussed in "Inverse Method Based on FEM" section.

Also, there are numerous studies related with limiting done height and draw bead tests [65] which are also used to identify friction coefficient. As the common alternative of these tests, strip draw test is one of the most important tribology test for sheet metals but requires a special testing equipment. A further disadvantage that must be mentioned is that no bulk deformation is present in strip-draw test.

As it is mentioned in the previous chapters, this study focuses to visualize possible defects that can appear during stretch forming process before the real manufacturing phase by the help of FEM. It is a well-known fact that FEM requires well identified input variables. Since the friction coefficient is a significant input to those type of analyses, identification of accurate friction coefficient (μ), values are perquisites in order to accomplish successful numerical analyses.

For the analysis of deep drawing and stretch forming of sheet metals, there are approaches to measure friction coefficients where either specific test equipment or an inverse engineering analysis is necessary. In this study, we show that a new approach conducted on an existing Nakajima testing facility used to investigate the friction behavior with inverse engineering analysis is appropriate for the anaylsis of stretch forming process.

In this study, friction studies are performed at two steps. First step is the numerical verification of a well-known analytical equation to stretch forming process in which a sheet material is stretched over a cylindrical die. Validation of this equation is evaluated by the

simulation of the test. The second method is based on inverse analysis technique. Friction tests are performed in different die lubrication conditions and the results are matched with simulation results in which the same strain distribution is obtained. In the experimental side of this study, different lubrication conditions including dry, oil, nylon and silicon film coated situations are evaluated. These conditions are (Figure 45);

- No lubricant-Dry condition,
- Oil lubricated (Drawsol 1050E® is a blend of solvent refined mineral oils, extreme pressure additives, corrosion protection additives and emulsifiers – compound to form a medium viscous drawing lubricant),
- Nylon + Oil lubricated condition,
- Silicon film coated condition.

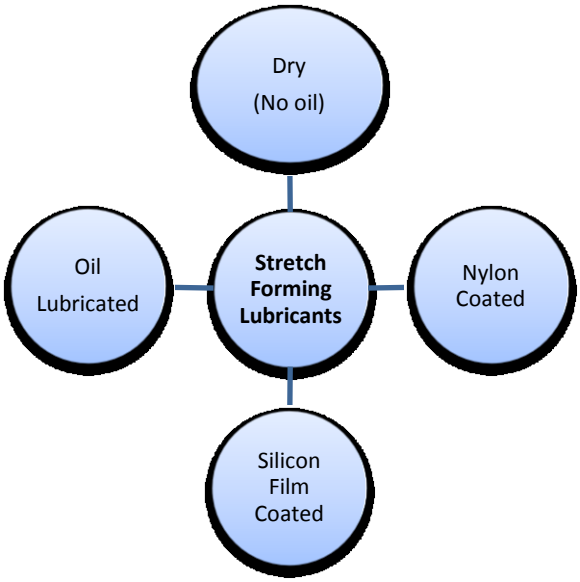

Figure 45: Lubrication conditions being analyzed for stretch forming process

4.2 Analytical Method

In the analytical part of the friction study, the success and convenience of an analytical equation (Equation 55) for stretch forming process is evaluated. In this study, numerical modeling of a new testing facility is conducted and in certain increments of the analysis, Equation 55 is used to identify friction coefficient. The illustration of test set-up and the test methodology is shown in Figure 48.

During stretch forming process, sheet metal is curved on the forming die as shown in the Figure 46. Since the forming tool is in contact with the sheet material while tensile forces are exerting by jaws, there exists contact pressure in the normal direction, P. The frictional shear stress is expressed with μP where μ is the coefficient of friction. If an infinitesimal element, ds, is taken from a curved section, the length of the arc is defined by the following equation;

$$ds = Rd\theta \qquad (Eq\ 48)$$

As it is known, friction affects both tension and the flow of the sheet material. Therefore, equilibrium equation can be written for the Figure 47 which illustrates the free body diagram of a stretched sheet metal.

$$PRd\theta = T_1 \sin\frac{d\theta}{2} + (T_1 + dt)\sin\frac{d\theta}{2} \qquad (Eq\ 49)$$

After assumption of, $\sin\frac{d\theta}{2} \approx \frac{d\theta}{2}$ is made, Eq 49 becomes;

$$PRd\theta = T_1\frac{d\theta}{2} + (T_1 + dt)\frac{d\theta}{2} \qquad (Eq\ 50)$$

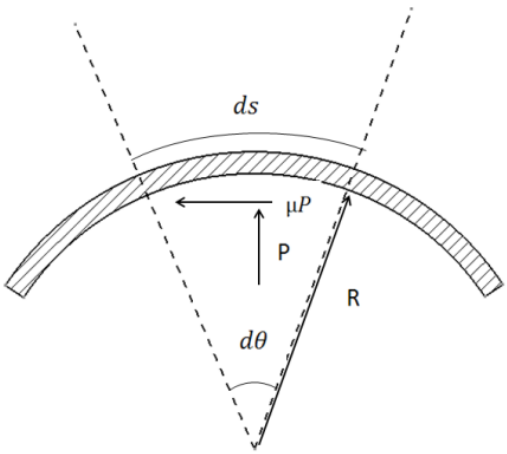

Figure 46: An exagerated illustration of the infinitesimal element of a stretched sheet

Finally the equation reduced to;

$$T_1 = PR \qquad (Eq\ 51)$$

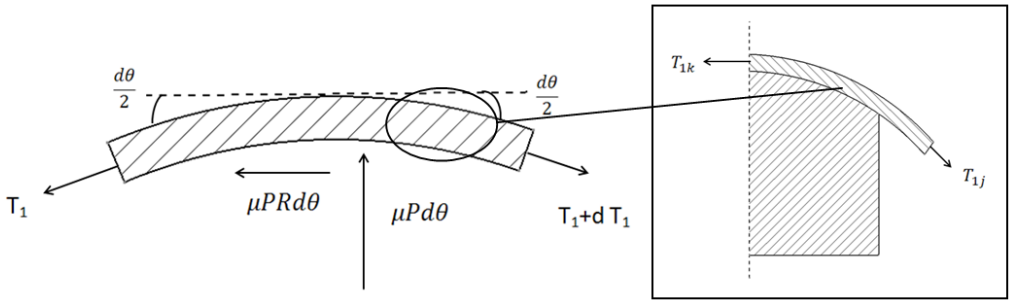

Figure 47: Corresponding free body diagram of a sheet segment

The equilibrium condition shown in the Figure 47, for forces along the sheet blank can be expressed by;

$$(T_1 + dT_1) - T_1 = \mu PRd\theta \qquad (Eq\ 52)$$

Substituting Equation 51 into 52 gives;

$$\frac{dT_1}{T_1} = \mu d\theta \qquad (Eq\ 53)$$

By taking the integral of both sides,

$$\int_{T_{1j}}^{T_{1k}} \frac{dT_1}{T_1} = \int_0^{\theta_{jk}} \mu d\theta \qquad (Eq\ 54)$$

As a result, coefficient of friction acting in stretch forming operation can be found as;

$$\mu = \frac{\ln(\frac{T_{1k}}{T_{1j}})}{\theta_{\mathrm{jk}}} \qquad (Eq\ 55)$$

Numerical validation is performed to check the reliability of the analytical approach. A commercial finite element code Msc. Marc® is used for the analyses. FLC testing facility with a cylindrical punch is used. The blank geometry is a standard tensile test geometry specified in ASTM E8-04 [39]. During the analyses half symmetry is used to reduce CPU time. Simulations are repeated using different coefficient of friction which are; 0.05, 0.1, 0.25, 0.5 respectively.

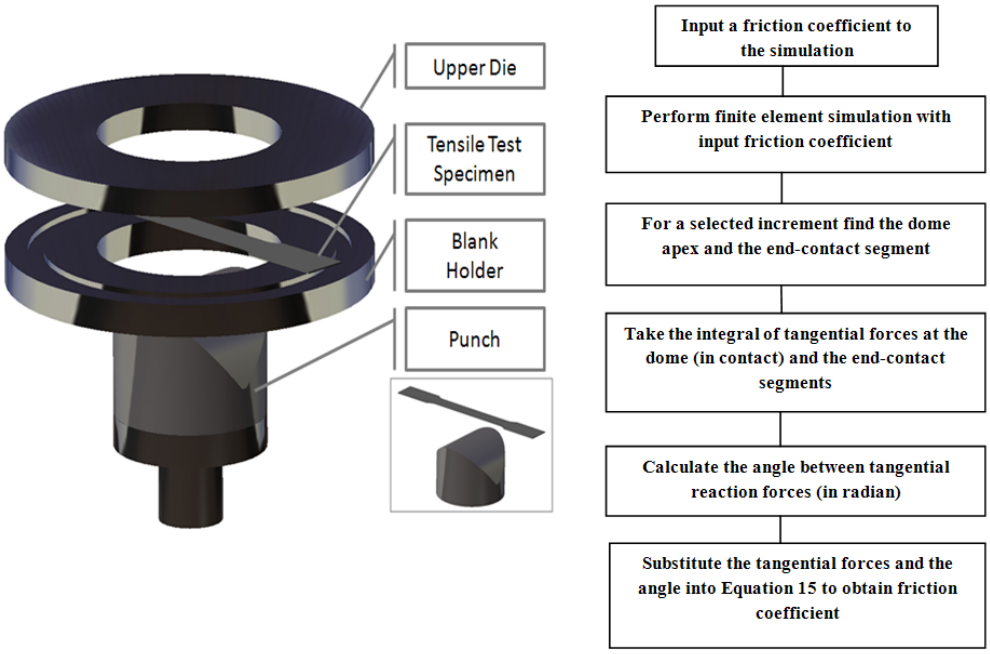

Figure 48: An illustration of FLC testing facility and the flow chart to describe the method to find friction coefficient

S1 and S2 (Figure 49) are the sections taken from the dome apex and from the end of the contacting region of the strip. Tangential forces are calculated by taking force integral over these sections. Then, the angle between tangents of the line segments is calculated for each increment. Substituting these variables into Equation 55 gives coefficient of friction for the corresponding increment.

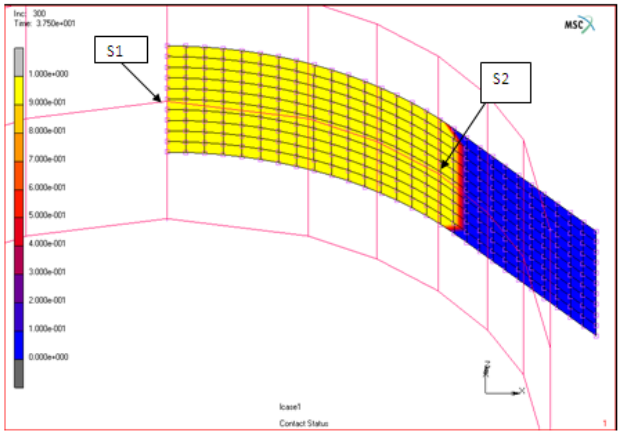

Figure 49: Finite element simulation and the illustration of segments S1 and S2

In numerical validation part of this study, analyses are repeated with different input coefficients of friction. Coefficients of 0.05, 0.1, 0.25 and 0.5 are used in the finite element

simulations. As it is shown, good agreement is obtained for a specific range of the simulative experiment (Figure 50) with the results taken from analytical model and the input coefficients of friction especially in certain increment ranges.

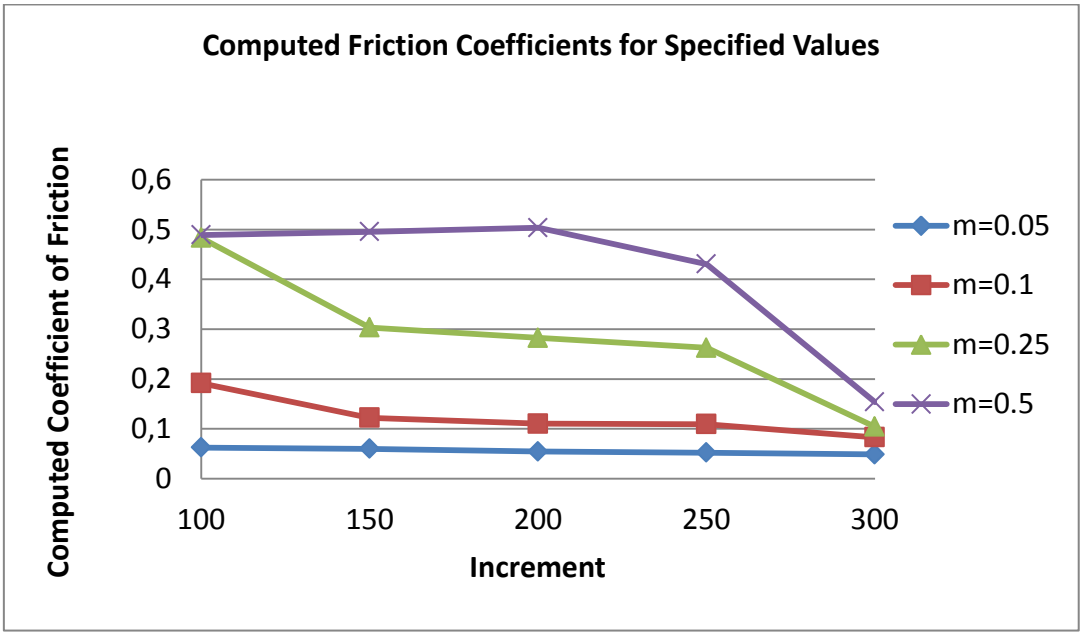

Figure 50: Computed coefficients of friction using finite element simulation to validate analytical model

4.3 An Inverse Method Based on FEM

Due to its involved physical and difficult to model phenomena, friction is preferably characterized under environmental conditions specific to the process being analyzed. Therefore, in this study specific test equipment is designed and inverse engineering approach is used.

Identification of realistic Coulomb friction coefficient is a prerequisite to accomplish successful numerical analyses. For this purpose, inverse engineering analyses are performed to find these friction coefficients to be used in stretch forming simulations. In this study, stretching operation and simulations are performed under different lubrication conditions and with different coefficients of friction. Experimental and numerical results are compared considering the distribution of major and minor strains and best fitting results give the most appropriate coefficient for stretching. Experimental trials and numerical modeling phase of this study are explained below.

4.3.1 Experimental Set-Up

In the experimental side of this study, Zwick /BUP600 Erichsen test device (Figure 51) is used. A new cylindrical punch (Figure 52) is designed for stretching purpose and standard tensile test specimen (Figure 53) is used as blank [39]. 150.000 N blank holder force is applied to the ends of sheet specimen and is stretched over the cylindrical punch until it fractures. The important point is that, cylindrical punch has the same manufacturing history with conventional stretch forming dies to reflect the same surface properties. Each test are performed repetitively for different types of aluminum alloys including; AA 2024-0, AA 6061-0 and AA 7075-0 with their solution heat treated and Clad coated circumstances. Also, different lubrication conditions for die such as dry, oil, nylon and silicon film are used to identify friction coefficient for each case.

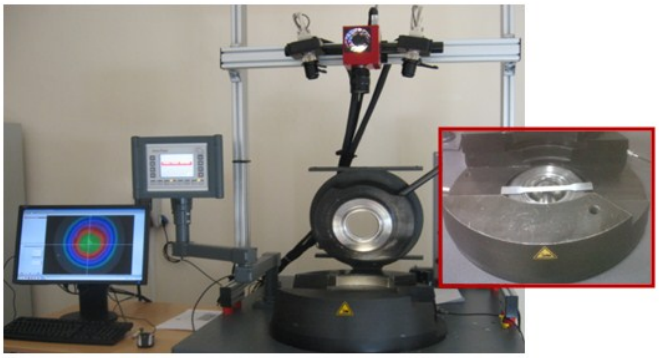

Figure 51: Experimental setup for friction tests – Zwick/BUP600 Erichsen Cupping test device and illustration of sheet specimen

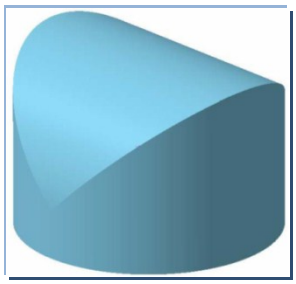

Figure 52: Specific-designed punch which has the same pre-manufacturing history with an actual stretch forming die

Technical drawing of specific designed punch which has the same pre-manufacturing history with an actual stretch forming die is given in APPENDIX B-Figure 114.

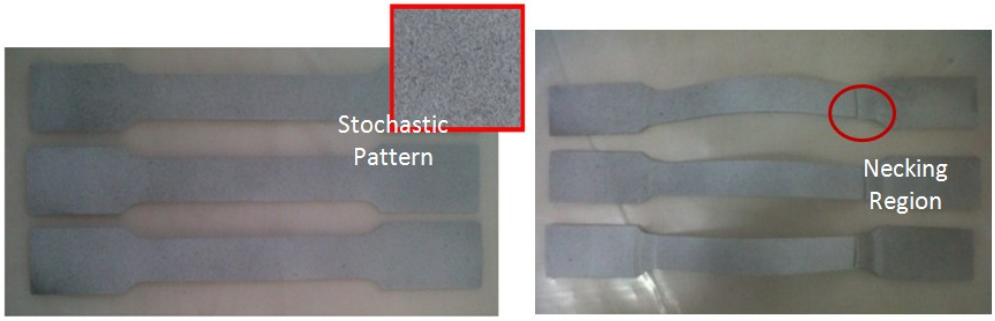

Figure 53: Illustration of initial and final geometry of standard tensile test specimen with stochastic pattern

3-D optical measurement system (GOM-Aramis®) is integrated to system in order to obtain deformation history of the sheet specimen. Deformation is recorded by CCD cameras (10 frames per second) as shown in the Figure 54.

Three repetitive stretching tests are conducted with dry, oil lubricated, nylon and silicon film covered die conditions. For each lubrication condition, major-minor strain over the section, which is drawn through the centerline of sheet specimen, is obtained to compare with numerical analyses. Figure 54 illustrates the camera view of specimen on die and the section on it. The output obtained with experimental deformation measurement is the graphs shown in the Figure 55 – 56. These results will then be used to compare with numerical analyses performed by different friction coefficients. The best-fitting curve is associated with the most appropriate coefficient of friction as will be discussed in Result and Conclusion part of this Chapter.

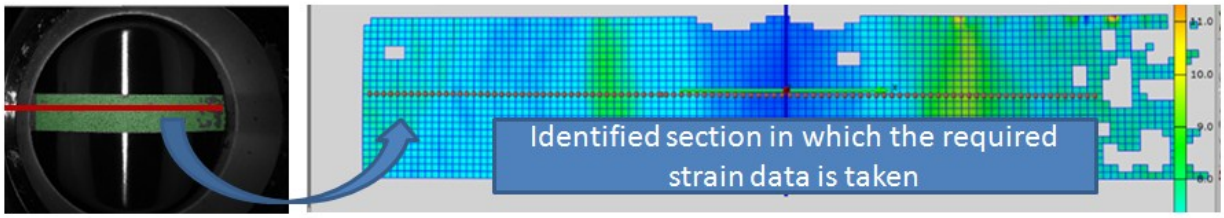

Figure 54: Experimental strain information taken from the optical measurement and illustration of identified section

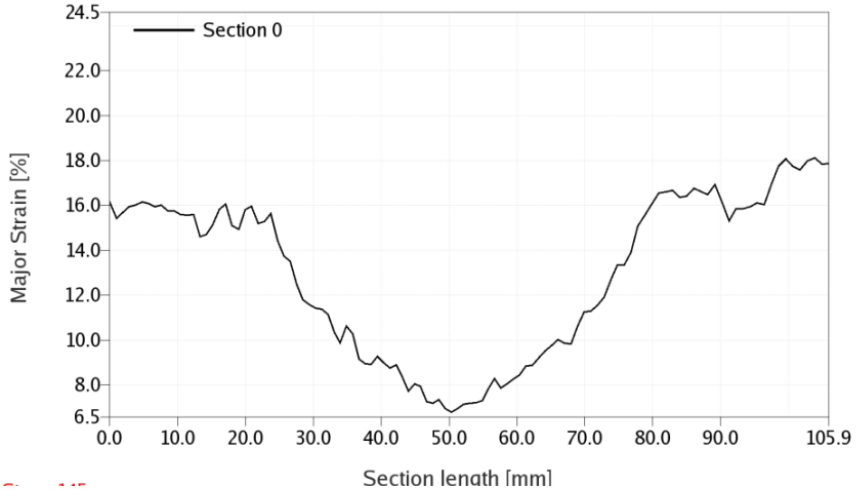

Figure 55: Major strain over the arc length calculated from experimental optical analysis

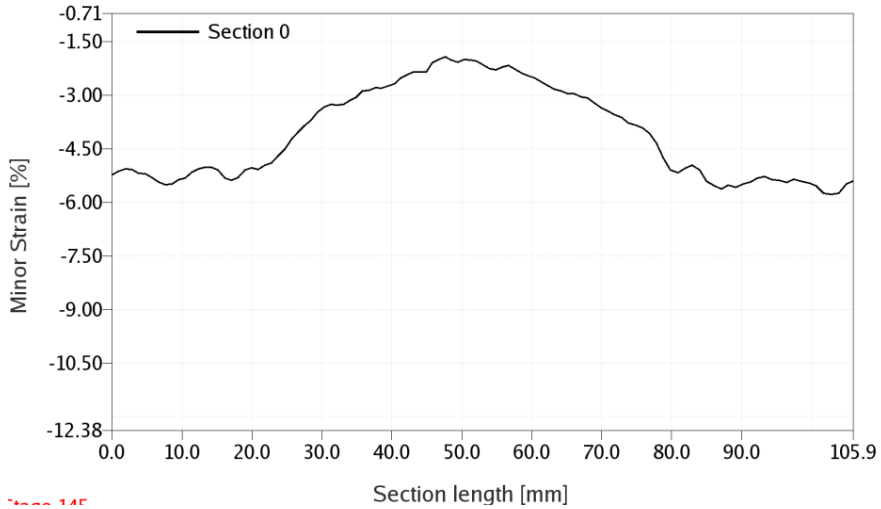

Figure 56: Minor strain over the arc length calculated from experimental optical analysis

4.3.2 Numerical Modeling

Numerical modeling is done in the LS-Dyna® environment, which is dynamic-explicit finite element software. All tooling used in the experimental testing facility is modelled exactly in the FE software environment. Analyses are performed for different coefficient of frictions Figure 57 shows the three bodies in the model: The form die (rigid), the sheet (plastically deformable) and the punch (rigid). The process is modeled utilizing quarter symmetry.

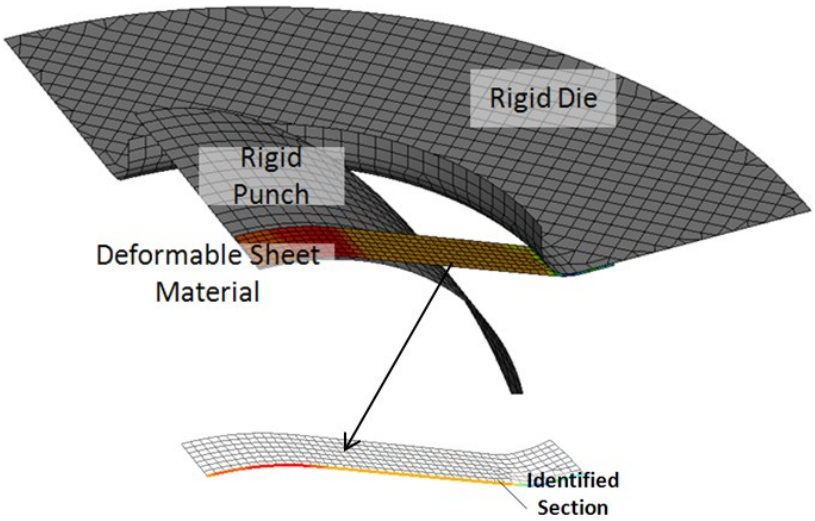

Figure 57: ¼ quarter model for friction testing facility

The sheet is discretized with Belytschko-Tsay shell elements using 5 integration points through the thickness. The penalty method is used as the contact algorithm and Coulomb model is used to handle friction. 0.05, 0.075, 0.10, 0.15, 0,20,0.25, 0.30, 0.35 friction coefficients are used to repeat numerical analyses.

Numerical analyses duplicates exactly the same tool motions performed during the experimental studies. Consistency between the simulation results and the experimental measurements are given in the next section.

4.4 Results and Discussions

The aim of this study is twofold. Firstly, the validity of the experimental setup is proven numerically. This also opens the way for an analytical computation of the friction coefficients directly from experimental measurements. Another aim of the study is to determine friction coefficients in stretching of aluminum alloys with a new testing facility under different lubrication circumstances.

For the first work, required data obtained from the numerical analyses of a new testing facility. Then, this data is implemented to Equation 55 and as shown in the graphics given in Figure 50, for a certain range of deformation, computed friction coefficient converges to the utilized friction coefficient during the simulation. In the second work which has higher importance for further studies, finite element analyses are conducted for various aluminum alloys repeating the analyses with different friction coefficients. For the integration scheme,

explicit solution procedure is used. Meanwhile, 3-D optical measurement experiments are accomplished with GOM-Aramis®. Friction coefficients under certain circumstances are determined by comparing the experimental and numerical results considering strain and geometrical features of the bulged specimen.

After 3-D optical measurements and finite element analyses are performed, the strain results are compared and matched considering the strain and bulged specimen from dome apex region. Since quarter symmetric analyses are performed using different friction coefficients, the comparison is made in the second half length of the section which was drawn in experimental evaluation. As it is shown in the Figure 58 given below, dry condition in other words the condition which is not lubricated, friction coefficient reaches to its maximum value, 0.2. Oil lubrication, nylon and silicon usage remarkably decreases the friction coefficient acting during the process. As shown in the following Figures 59-61, 0.15 friction coefficient is obtained in oil lubricated process, 0.10 in nylon coated and finally 0.05 in silicon film coated situation. The one of the most surprising point is that; solution heat treated aluminum alloy 2024-W and annealed alloy 2024-0 gives 0.2 coefficient of friction in dry condition as shown in the Figure 62. Therefore, during the simulation steps, the same friction value will be implemented for solution heat treated and annealed conditions of aluminum alloys. However, as summarized in Table 6, the variation of aluminum alloy causes different value of friction coefficient.

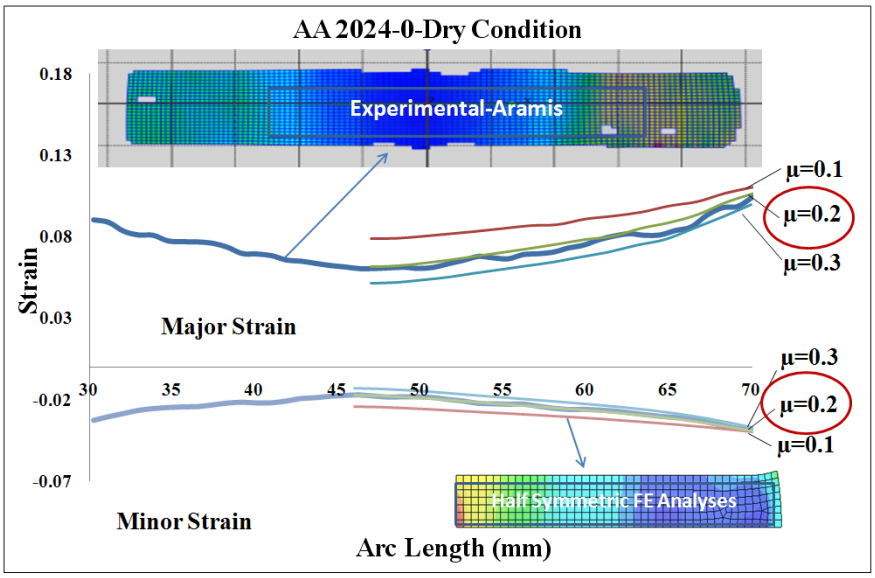

Figure 58: Comparison of major-minor strain over the section taken from the optical measurements and numerical analyses to determine friction coefficient in dry condition. (For dry condition, the most suitable friction coefficient is found as 0.2 for AL 2024-0)

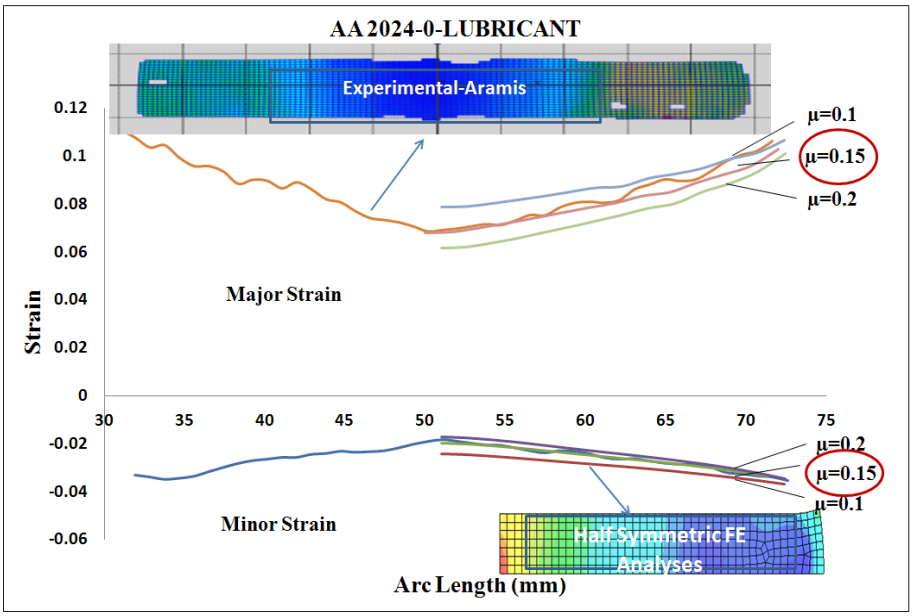

Figure 59: Comparison of major-minor strain over the section taken from the optical measurements and numerical analyses to determine friction coefficient in oil lubricated condition. (For dry condition, the most suitable friction coefficient is found as 0.15 for AL 2024-0)

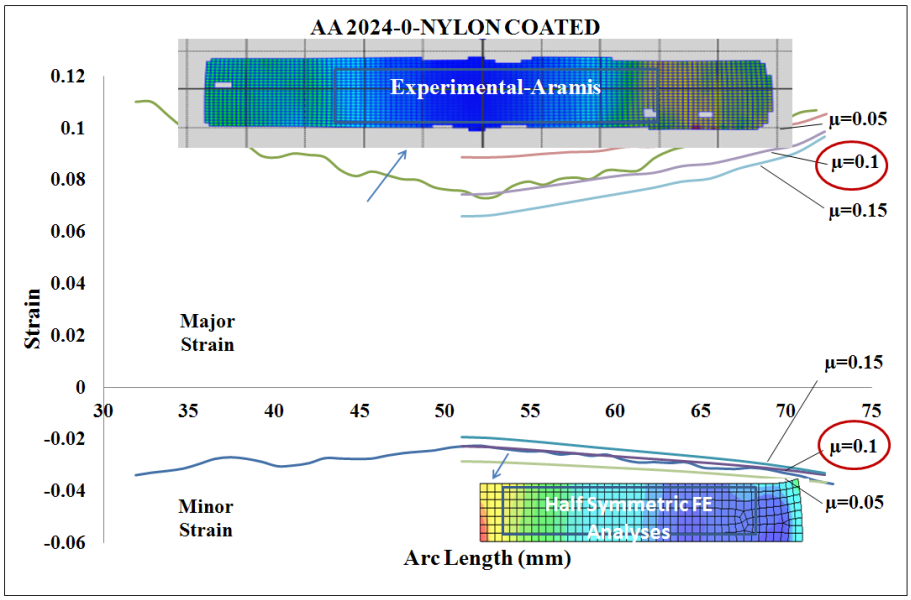

Figure 60: Comparison of major-minor strain over the section taken from the optical measurements and numerical analyses to determine friction coefficient in nylon coated condition. (For dry condition, the most suitable friction coefficient is found as 0.1 for AL 2024-0)

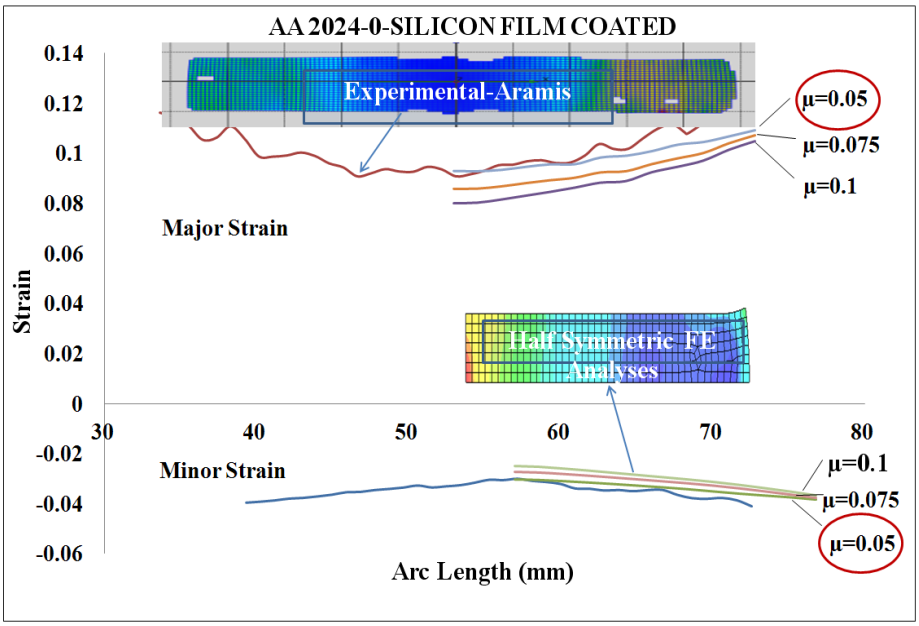

Figure 61: Comparison of major-minor strain over the section taken from the optical measurements and numerical analyses to determine friction coefficient in silicon film coated condition. (For dry condition, the most suitable friction coefficient is found as 0.05 for AL 2024-0)

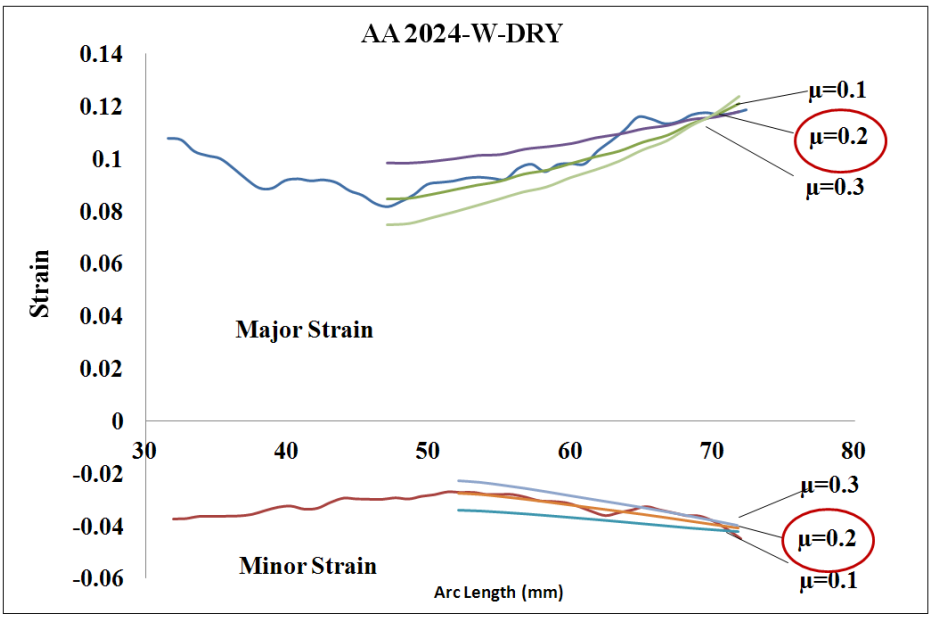

Figure 62: Comparison of major-minor strain over the section taken from the optical measurements and numerical analyses to determine friction coefficient in dry condition. (For dry condition, the most suitable friction coefficient is found as 0.2 for AL 2024-W)

Table 6: Friction coefficients (μ) obtained in inverse based analysis method for different types of aluminum alloys

Lubricants	*2024-0*	*2024-0-CLAD*	*6061-0*	*7075-0*	*7075-0-CLAD*
Dry	0.2	0.25	0.2	0.175	0.2
Oil	0.15	0.15	0.15	0.15	0.15
Nylon+Oil	0.1	0.125	0.1	0.1	0.1
Silicon+Oil	0.05	0.05	0.05	0.05	0.05

CHAPTER 5

EXPERIMENTAL STUDY

5.1 Introduction

In the experimental side of the studies, optical deformation measurement device (GOM-Argus®) is used to find plastic deformation behavior of aluminum alloys during stretch forming process. The results will then be used to calibrate and validate the finite element simulations for this process.

In experimental studies, 750 tons capacity Cyril – Bath stretch forming press is used. As a blank material, AA 2024-0 rectangular sheet material is used and its deformation behavior during stretch forming process is investigated through optical measurements. 3-D optical deformation analyses are conducted using GOM-Argus® Module. Three basic stretch forming motions are investigated during experimental trials. First of all, stretching process is accomplished by only horizontal movement of jaws in reverse directions. Secondly, the rectangular sheet is stretched with the vertical raise of form die while jaws remain constant. Finally, form die – jaw synchronized motion which was derived from the simulations, is implemented to NC unit of the stretch press. During the studies, the process is stopped and optical measurements are performed at a certain level of deformation in order to compare the strain and force data with the measurements taken from simulation in the same level of deformation. The list of the experimental trials is given in the Figure 63 and optical measurement procedure is summarized in Figure 64 below.

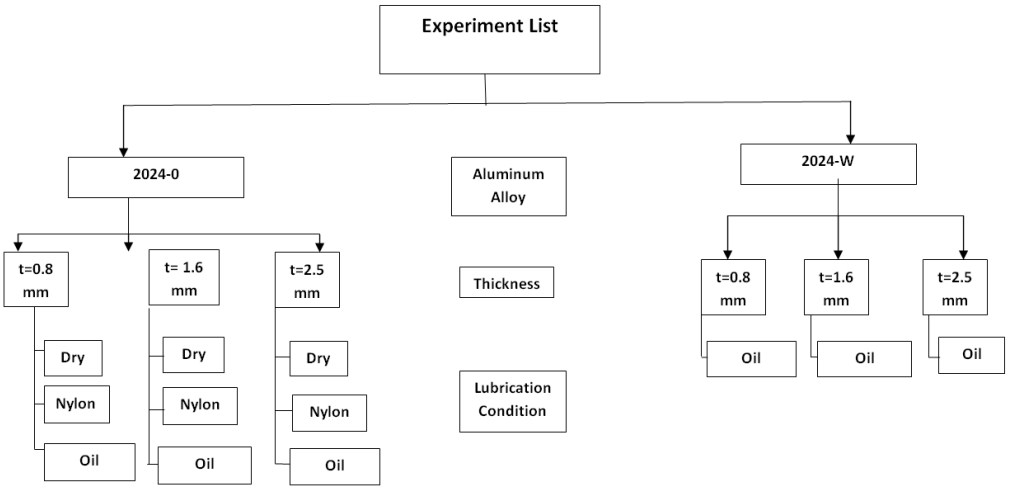

Figure 63: The list of experimental trials

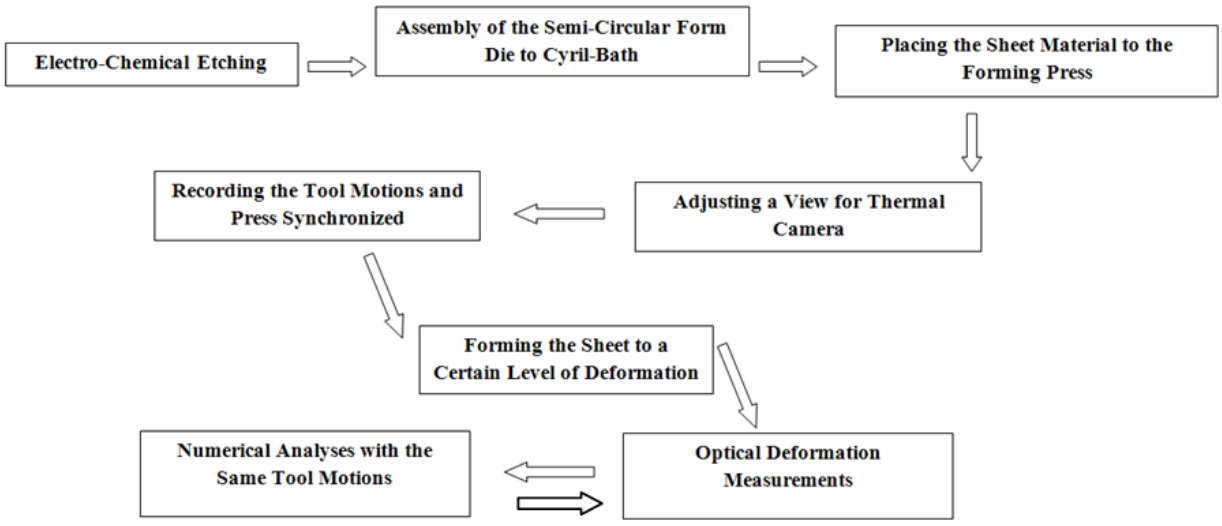

Figure 64: Experimental procedure for optical deformation measurement to the stretched form parts

This procedure is repeated for three modes of experiments which includes; stretching by jaws, stretching by form die and synchronized motion of form die – jaw trajectory. In the next section, experimental setup and methodology is explained in detail.

5.2 Experimental Set-Up

Experimental set-up consists of 750 tons capacity Cyril-Bath stretch forming press, GOM-Argus® 3-D optical measurement device, etching equipment, thermal camera, semi-circular forming die and a rectangular aluminum sheet metal (Figure 66). The influence of forming parameters and tool trajectories are examined using this equipment. In order to obtain non-complicated results in which direct results can be taken, semi-circular stretch form die is designed and manufactured. Technical drawings and details for the specific purpose designed die is given in the APPENDIX B-Figure 115.

Before starting optical measurements, the sheet material has to be subjected to etching process in order to form grid pattern on the region in which the optical deformation measurements will be taken (Figure 65).

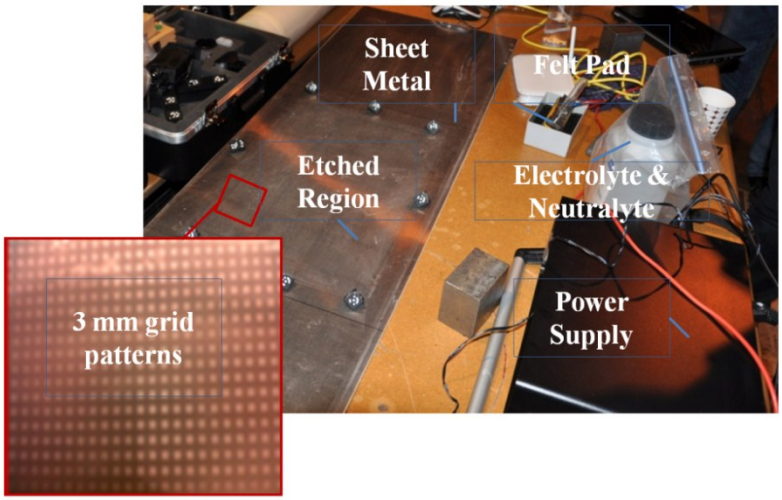

Figure 65: Electro-chemical etching apparatus and 3 mm grid pattern after etching process

After etching procedure has completed, the sheet material is located on stretch forming press as shown in the Figure 67 and the locations of jaw and die are set to initial conditions from the NC unit of the press. The sheet is clamped with jaws from both ends carefully considering the middle of etched region becomes exactly on the dome apex section of the semi-circular die. Except of the real experiment list, one specimen is used before the optical measurements in order to find out how much the sheet can be deformed. After the fracture location is identified, the deformation process is stopped in certain levels in the next trials. Experimental trials are performed for AA 2024-0 and 2024-W for different thicknesses and lubrication conditions. Three different modes of press capabilities are used. First of all, uniaxial tensile operation is conducted using the stretching the sheet material by reverse motion of jaws. Secondly, form die is used to stretch sheet metal fixed by jaws.

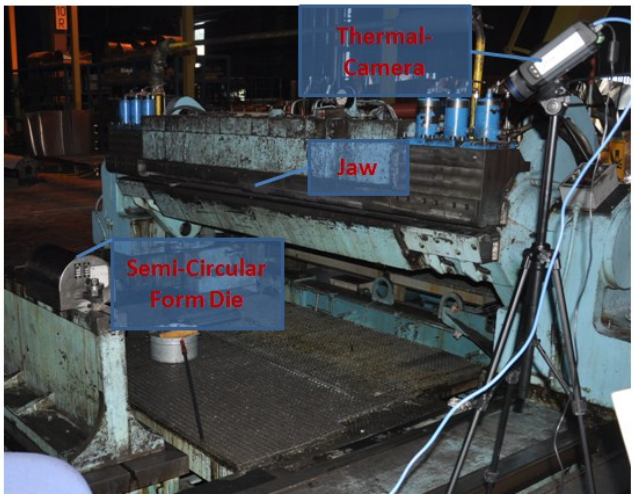

Figure 66: Experimental set-up including thermal camera

Thirdly, tool motions taken from the simulation results are implemented using the NC unit of the press in order to determine whether the simulation is performed successfully or not.

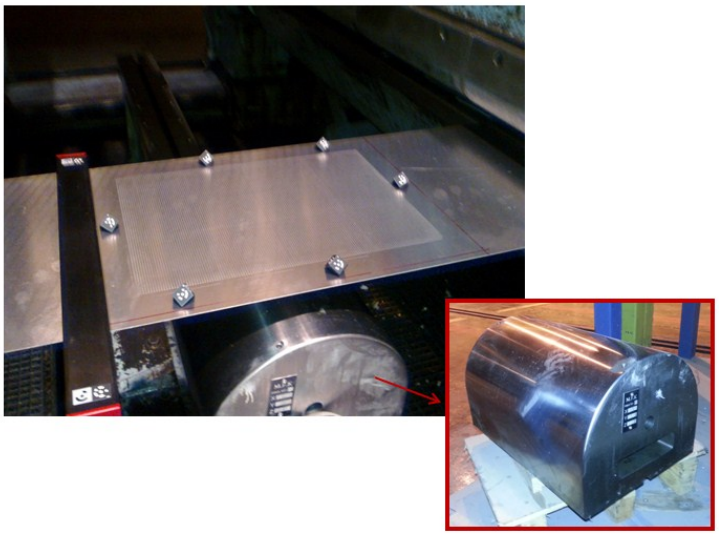

Figure 67: Illustration of the position of sheet metal specimen in stretch forming experiments

Two video cameras are used to record tool motions from the NC unit and sheet metal deformation from the press concurrently as shown in the Figure 68 given below. All of the press motions are tracked from the control unit in order to implement these process parameters to numerical simulations.

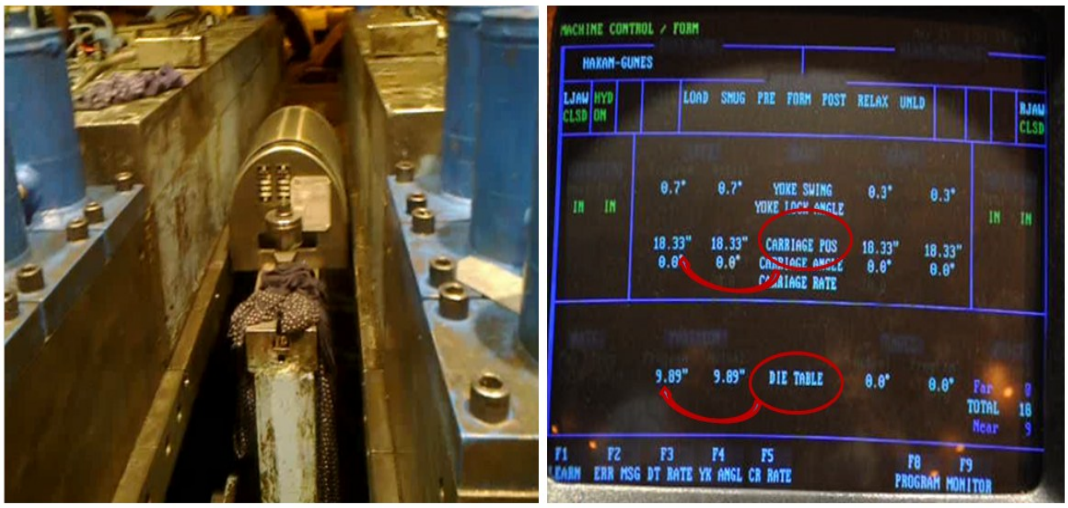

Figure 68: Illustration of two camera records. First figure is the, instantaneous recorded sheet metal stretching operation and second Figure shows tool motions which can be controlled and traced from the NC unit of the press

In certain levels of deformation, the process is interrupted and application of photogrammetric method starts (Figure 69). Formed sheet material is recorded with a digital camera and with a resolution of 1280x1024 pixels. In this study, NIKON D300 is used [66].

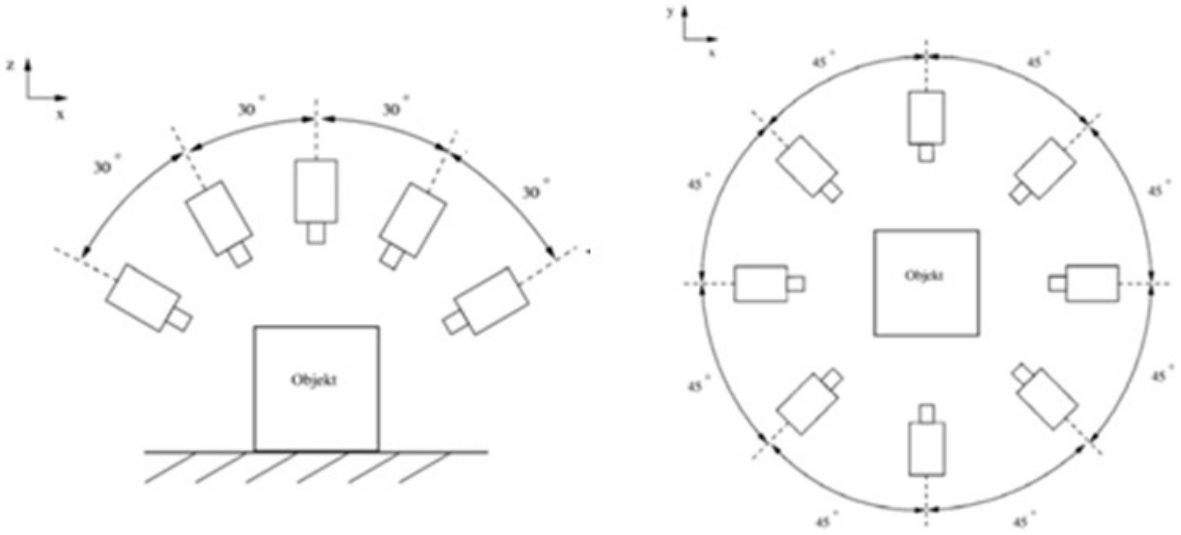

Figure 69: Strategy of taking photographs of deformed sheet material [66]

5.3 Basic Experiments

Three basic tool motions are used to form sheet material in stretch forming process. The sheet material is generally subjected to synchronized jaw and tool trajectories, however, one of these motions which are described below can be used. These three basic stretch forming motions can be described as follows (Figure 70);

- Deforming the sheet material by jaws,
- Deforming the sheet material by form die,
- And finally deforming the sheet material by synchronized trajectories of tool and jaws.

Experimentally, above mentioned tool motions are applied separately in order to form sheet material. In certain level of deformation, the press is stopped and optical measurements are conducted. The experiment methods are similar for these three cases except the lubrication condition, thickness of the sheet and the application of tool motions.

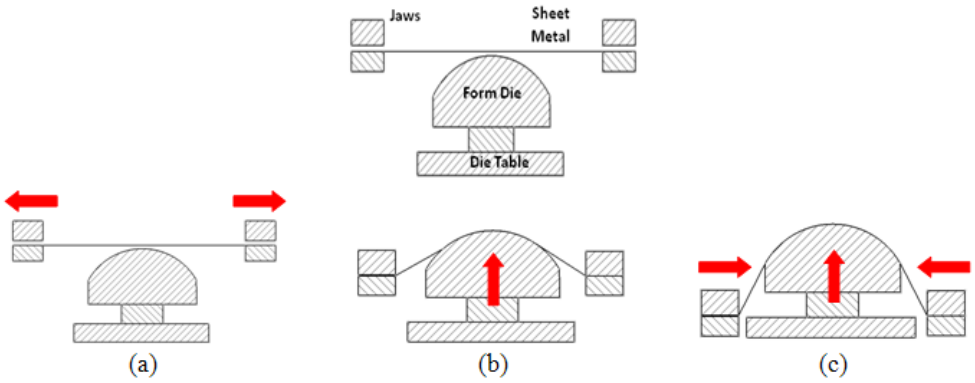

Figure 70: Modes of the experiments: (a) stretching by jaws, (b) stretching by form-die, (c) stretching by combined movement

5.3.1 Stretching Sheet Material by Jaws

Stretching aluminum sheet material by jaws refers to clamping the sheet from both edges and stretching using only the horizontal movement of jaws (Figure 71). In this type of experiments, semi-circular shaped form die isn't used. Therefore, the sheet is formed under uniaxial tensile loading. The rectangular aluminum sheet plate is stretched 1 inch (totally 2 inches) from both edges and then the deformation over the etched region is measured using optical device.

Although 2024-0 aluminum alloy shows approximately 20% elongation during standard tensile test, in stretch forming operation this elongation limit cannot be achieved because of the process nature. Any improperness such as knurl on the sheet causes early tearing of the material. In order to prevent early tearing, the edges of the sheet material are deburred. This experiment is repeated for 3 different thicknesses which are; 0.8 mm, 1.6 mm, and 2.5 mm.

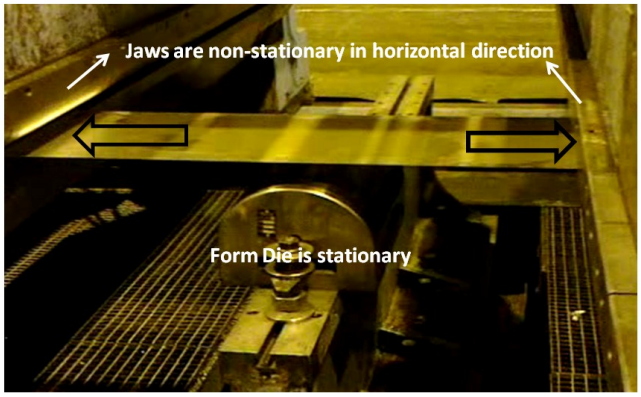

Figure 71: Experimental stretching of blank by using jaws

5.3.2 Stretching Sheet Material by Form Die

In these experiments, the sheet is clamped from edges using stationary jaws and formed by the vertical rise of form die (Figure 72). The deformation limit for this type of forming is identified and the process is interrupted just before the failure in order to measure deformation over the etched region. Stretching the sheet material by forming die experiment is repeated for three different lubrication condition and three different thicknesses. As it is mentioned in the previous chapter, the lubrication condition can differ according to the material and part geometry. Dry, oil and nylon coated conditions are used to lubricate the interface between form die and sheet material.

Each result taken from the experiments will then be compared with numerical studies in order to validate the success of the modeling of stretch forming process.

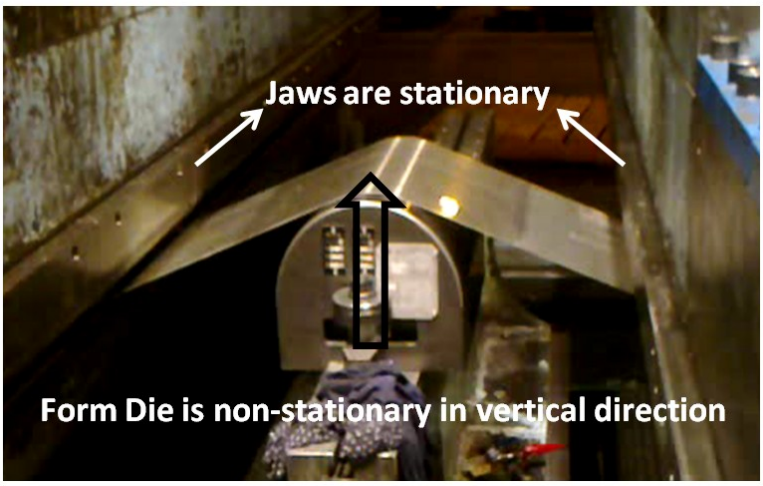

Figure 72: Experimental stretching of blank by using form die

5.3.3 Stretching Sheet Material by Synchronized Trajectories of Jaws and Form Die

After simple stretching by jaw and form die are accomplished separately, synchronized trajectories of jaw-form die is handled (Figure 73). The sheet materials with complex geometries are generally formed using this type of tool trajectories. In order to use this type of motion, the experience oriented methods are used to keep sheet stretched during the process. However, this procedure requires careful control when the material is formed and therefore additional labor cost is increased. In this study, it is aimed to determine tool motions which end up with required stretching over the sheet and also which keep the sheet material

stretched during the process. Therefore, in the first phase, inverse based analyses have to be performed in order to calibrate the strains obtained from experimental and numerical studies. After it is accomplished, a new method will be introduced to determine tool trajectories using finite element method.

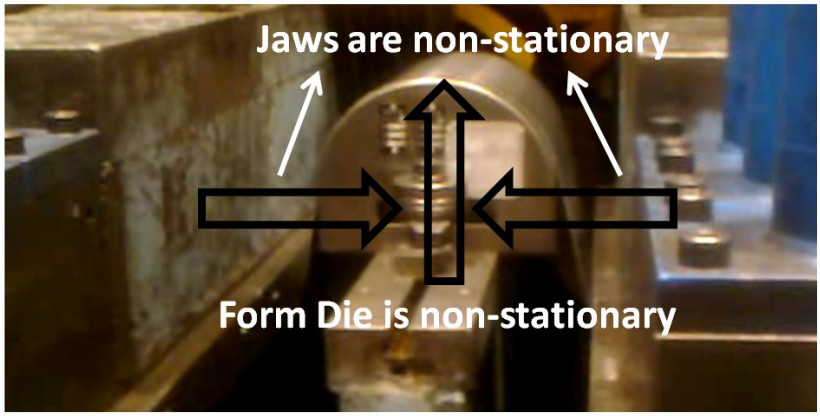

Figure 73: Experimental stretching of blank by using synchronized tool motion

The sheet material is formed with combined movement of jaw and form die which is applied using the NC unit of the Cyril-Bath press. The determination of the tool trajectories is identified by the operator and the process is stopped when the required stretching is achieved. While the sheet is stretched with semi-circular form die, the distance between the jaws is decreased in order to give the semi-circular form of the die to the sheet material as shown in the Figure 73. After that, the sheet is experimentally analyzed with optical measurement device. This type of experiment is also repeated for different thicknesses and lubrication conditions.

5.4 Results & Discussions

As it is mentioned above, experiments are conducted using three basic tool motions for stretch forming process. Measurement results taken from the ARGUS® are imported to Sview program in order to obtain and evaluate strain distribution on the test specimens for comparing with numerical studies.

In the first experiments in which the only jaw motions are used, ARGUS® measurements are transferred to Sview program. Totally 10 sections (5 sections in horizontal direction-5 sections in vertical directions) over the etched region are identified. Then major-minor strain

distribution over the section length is calculated. In the Figure 74, sections in 50 mm distances are shown.

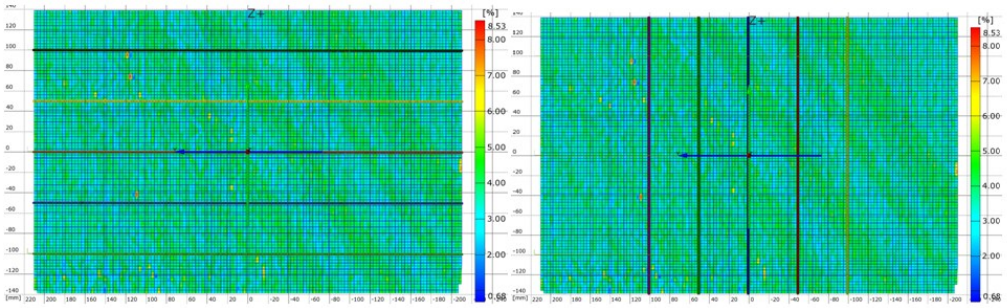

Figure 74: Horizontal and vertical sections over the etched region of the test specimens in which only jaw motion is used.

For each section, major-minor strain distribution over the section length is calculated and plotted in Figure 75-76. Approximately 0.080 major strain is obtained on the section where 0.020 minor strain value is obtained. Although 0.15 plastic strain value can be obtained for simple tensile test, for stretch forming process this value is limited up to 0.1. If this amount of plastic strain is exceeded, tearing on the sheet material can occur. The reason behind the limited strain amount can be summarized as follows;

- Weakening of the workpiece from the contact areas with the jaw because of the knurled jaw interface(s).
- Insufficient deburring from the edges of sheet metal to prevent notch effect.

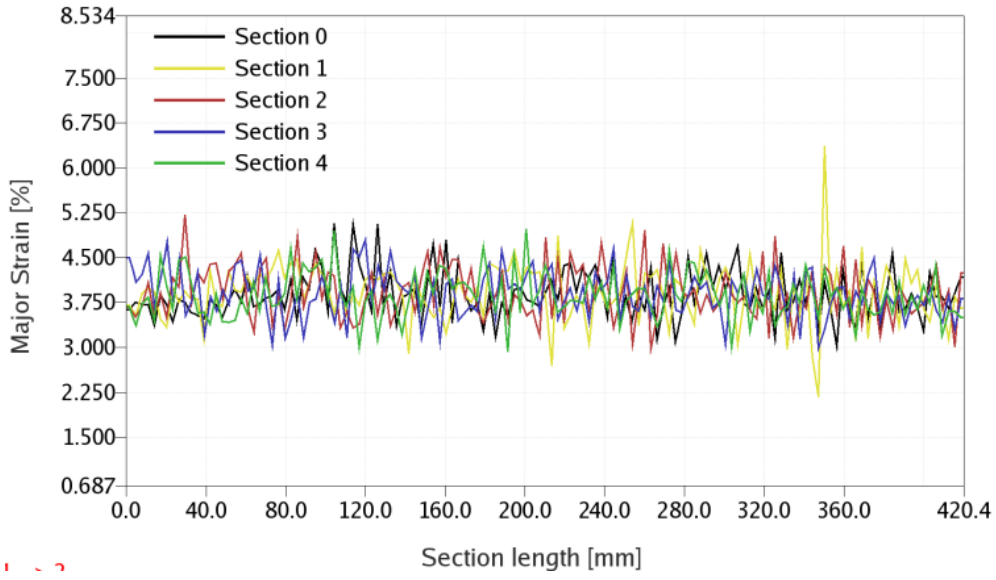

Figure 75: Major strain over the section length for each section which lies in the horizontal direction

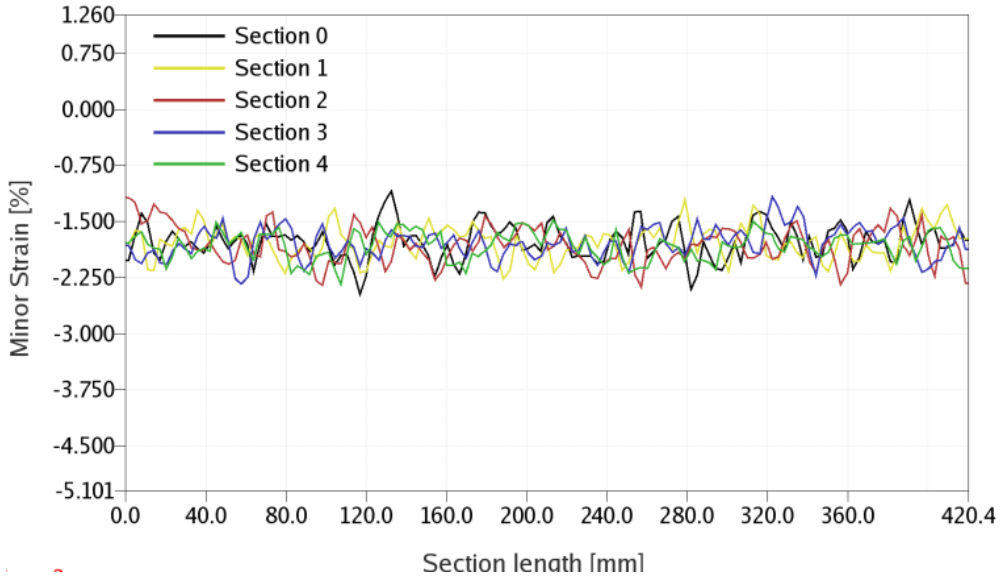

Figure 76: Minor strain over the section length for each section which lies in the horizontal direction

In the second stage of experimental trials, stretching experiments are conducted using only die motion. Similar to the first experiments, sections (both in major-minor directions) are assigned on the etched region of the sheet metal as shown in the Figure 77.

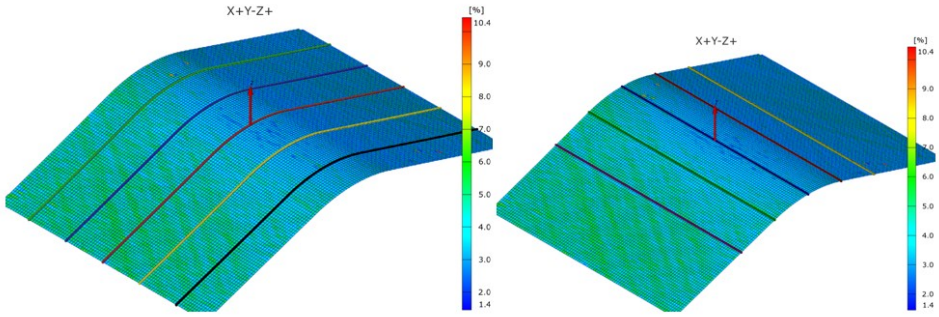

Figure 77: Horizontal and vertical sections over the etched region of the test specimens for the experiments in which only die motion is used.

In the graphics given below, major-minor strains over the arc length are given (Figure 78-79). Section 2 refers to the line assigned in the middle of the specimen. In the dome apex region, minimum major strain value is obtained because of the friction effect. Minor strain in the dome apex is approximately equal to 0.015 whereby the major strain is measured as 0.04. Throughout the section line, the least value for both major and minor strain can be obtained in

dome apex area. Plastic strain values for each section are increasing while getting further away from dome apex.

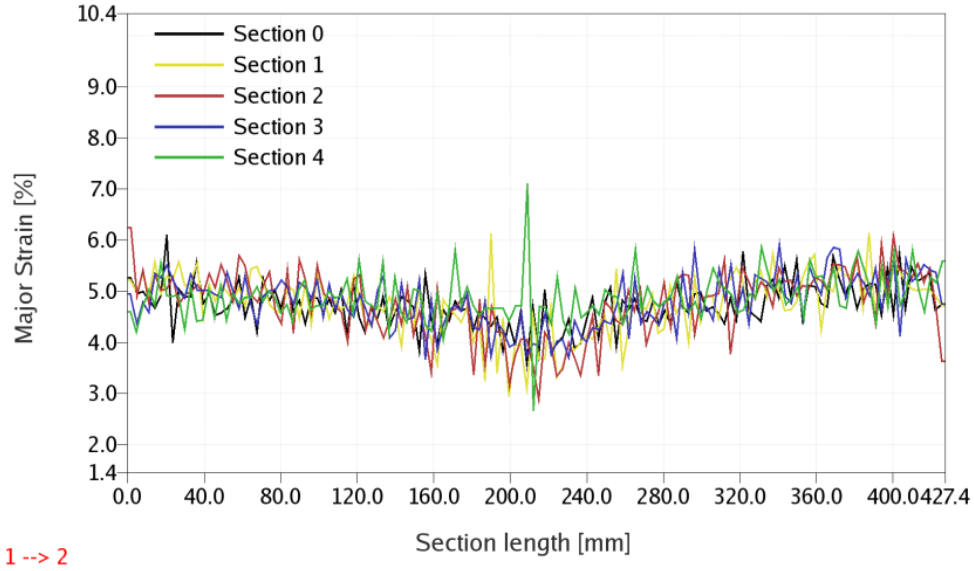

Figure 78: Major strain over arc length for each section which lies in the horizontal direction

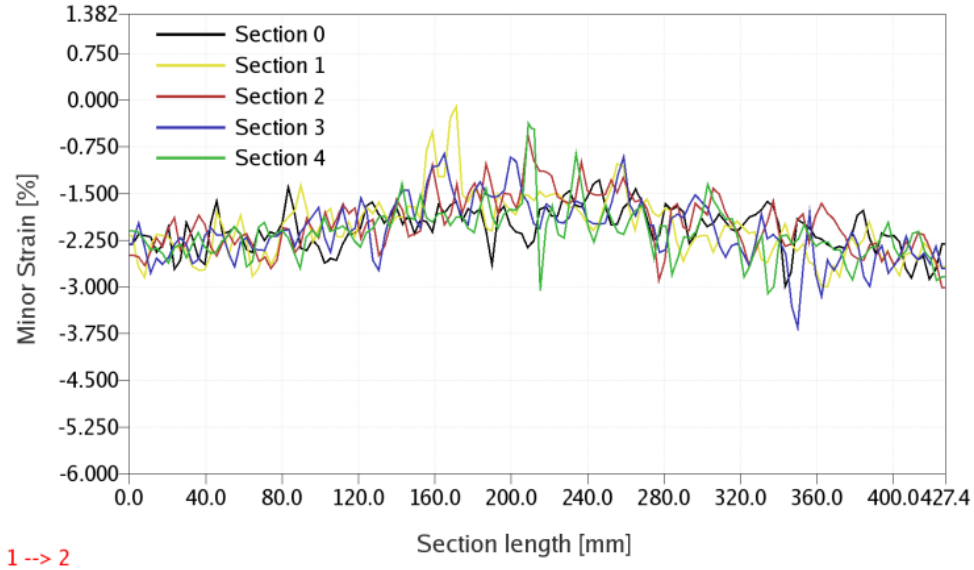

Figure 79: Minor strain over the section length for each section which lies in the horizontal direction

Finally, plastic strain distribution over the test specimen for synchronized motion of both jaw-form die is evaluated. Different from other experiments, jaw's and form die's motion are used together to form the sheet material. As shown in the Figure 80, semi-circular form of the die is given directly to the sheet material with combined tool motions.

In these experiments, tool motions are determined according to the trial-error procedure. After desired form for the sheet material is obtained, additional stretching is applied using the

vertical motion of form die. The process is stopped when the sheet material is subjected to sufficient stretching. Optical measurement results show that; 0.01 major strain amount is achieved where by this amount rises up to 0.04 values towards the end of etched regions. It can be easily seen that, minor strain through the horizontal sections are also decreasing towards the dome apex of the semi-circular shape (Figure 81-82).

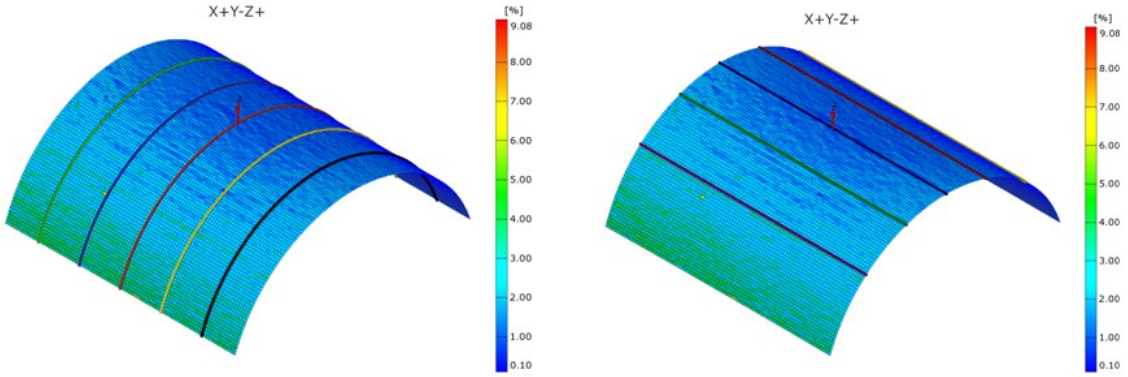

Figure 80: Horizontal and vertical sections over the etched region of the test specimens for the experiments in which both form die and jaw motions are used.

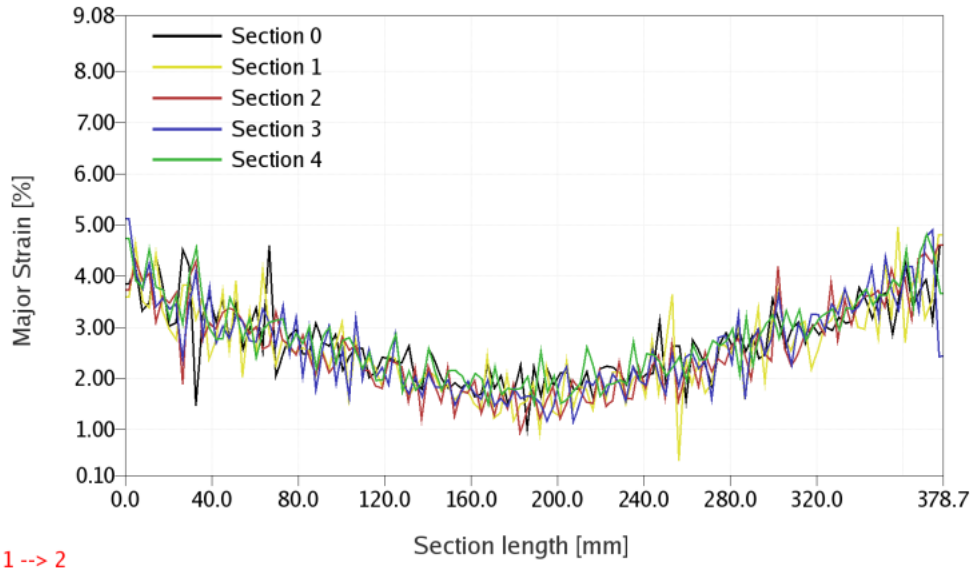

Figure 81: Major strain over arc length for each section which lies in the horizontal direction.

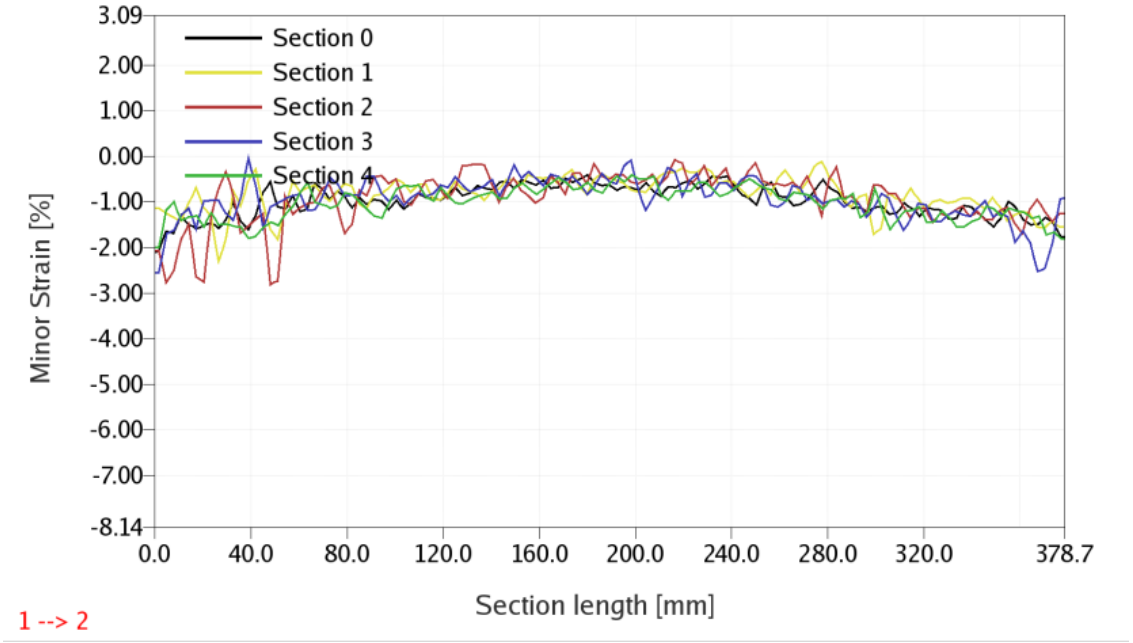

Figure 82: Minor strain over the section length for each section which lies in the horizontal direction

On the other hand, some important conclusions are obtained by chance during the experimental trials. As it is mentioned before, thermal camera is used to identify accurate starting time of deformation in certain tool positions. However, Lüders band appearance is observed just before the sheet fractures. It is a well-known fact that, deformation energy causes heat increase on the workpiece. Since Lüders band, also known as slip band, are localized bands in metals experiencing larger amount of tensile stress, fracture firstly occur from the regions in which these bands are observed. Therefore, sufficient stretching judgment is always given by the operator using visual inspection of Lüders bands so that the process is stopped and it is said that the workpiece is sufficiently stretched when Lüders band appears. However, it has been observed that Lüders band existence on the sheet material can be observed by thermal camera long before it has been detected by a normal human eye. So forming parameters can remain in safe region to prevent unexpected tearing on the sheet material. As it is shown in the Figure 83, tensile stresses cause Lüders bands in local regions and because of larger deformation thermal camera can easily detect the slip lines on sheet material.

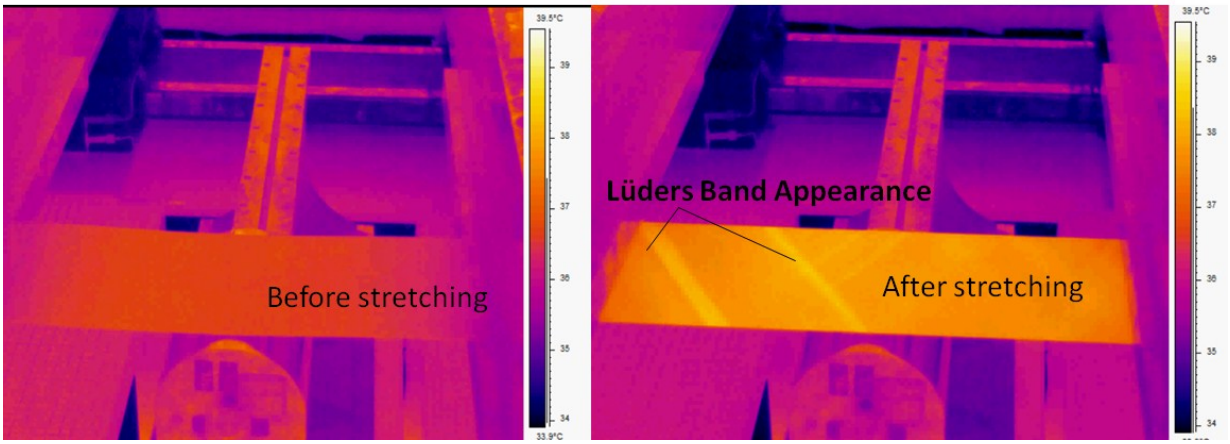

Figure 83: Detection of Lüder's Band by using thermal camera during stretching process

To sum up, experimental studies are accomplished using three basic tool motions. Strain distributions on the etched areas are measured and evaluated. During the studies, tool motions are recorded using a video camera in order to dublicate tool motions numerically. Numerical simulations will be performed for the same parameters with experimental trials. Deformation information and geometrical form of the final workpiece will be used to compare numerical results with the experimental findings. After the same deformation information is obtained for each trial, a real aircraft part will be manufactured with the information taken from the numerical analyses without any trial-error procedure.

CHAPTER 6

NUMERICAL MODELING OF STRETCH FORMING PROCESS

6.1 Introduction

In this chapter, numerical modeling method for stretch forming process is considered in detail. Same process parameters such as; tool motions, material properties that used in experimental trials are implemented to the numerical modeling. Numerical modeling is done in the LS-Dyna® environment, which is dynamic-explicit finite element software.

The aim of this chapter is two-fold. Firstly, best numerical model to predict strain distribution on the blank material during stretch forming process is obtained. Secondly, tool motions are obtained by using FEM and the success of pre-determination of tool motions with numerical analyses is evaluated and then these findings will be compared with experimental measurements and applications. Therefore, during the process the sheet will remain stretched on the form die and any failure (wrinkling-tearing) possibility will be prevented in the case of minimizing trial and error procedure.

First of all, numerical modeling for simple stretching operation is performed in which the blank material is deformed only by jaw motion. After that, deformation information is taken from the simulation results and compared with the optical measurement results. Then, in the second phase, sheet metal is clamped by jaws and deformed with the vertical movement of form die as same as it is in actual process. Finally, synchronized form die and jaw motions are implemented into commercial FE package program Ls-Dyna®, and results taken from the simulation is compared and calibrated with the actual strain distribution that is previously measured using ARGUS®. After compatible results are obtained for both numerical and experimental studies which are performed using semi-circular form die, real aircraft parts are manufactured using the tool motion information taken from the FE analyses.

6.2 Stretch Forming Simulation for Basic Tool Motions

In this section, simulations for basic tool motions are performed. Plastic strain taken from the experimental studies will be compared with numerical studies. Each simulation for different tool motions is considered in detail below.

Figure 84 shows the three bodies in the model: The form die (rigid), the sheet (plastically deformable) and the jaw (rigid). The process is modeled utilizing half symmetry. The sheet is discretized with Belytschko-Tsay shell elements using 5 integration points through the thickness. Penalty method is used as the contact algorithm and Coulomb model is used for friction. FORMING_ONE_WAY_SURFACE_TO_SURFACE contact type is used in which only blank nodes are checked for penetration to the die surface. Then penalty forces are applied to those nodes proportional to the penetration depth and contact is simulated. This model is used for the numerical analyses of the mentioned experiments. Consistency between the simulation results and the experimental measurements are given in this section.

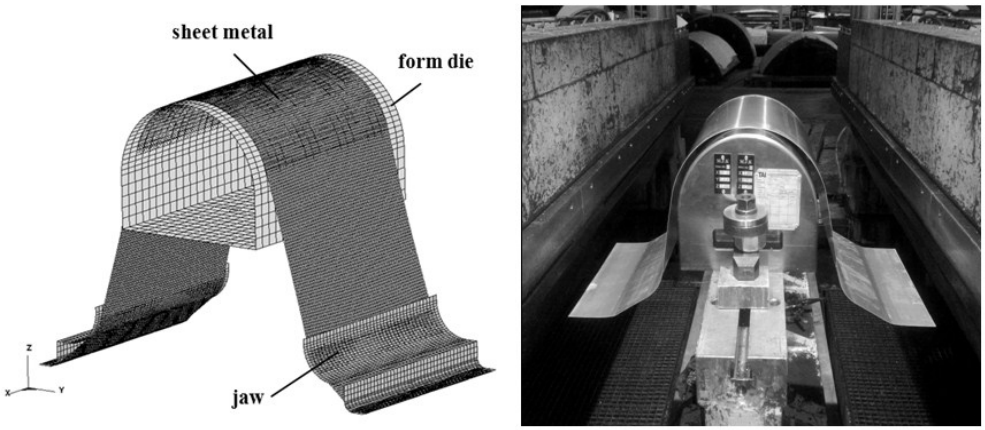

Figure 84: An illustration of numerical model and experimental setup for stretch forming process.

6.2.1 Modeling of Stretching Sheet Material by Jaws

In this mode, the sheet material is clamped by jaws and stretched with jaw motion. Tool motions are directly taken from experimental trials and implemented to FE software. In order to decrease CPU time, process is modeled half-symmetrical. Comparison difficulties of the quarter symmetrical FE model with the full 3-D measurement of the test specimen during the geometrical best-fit operations prevent preparing quarter-symmetrical models.

As it is shown in the Figure 85, two bodies are used in the model: The jaw (rigid) and sheet material (plastically deformable). Since the process is performed in order to stretch sheet material by only jaw motion, form die is not modeled for these types of numerical models.

Ls-Dyna® offers many element formulations for four node isoparametric shell elements including Hughes-Liu (ELFORM2), Belytschko-Tsay (ELFORM2), Belytschko-Leviathan

(ELFORM8), Belytschko-Wong-Chiang (ELFORM10) and fast co-rotational Hughes-Liu (ELFORM11). All of these elements employ one point quadrature and hence, are very efficient. In this study, Belytschko-Tsay shell element definition is used to discretize the sheet material. It is a well-known fact that, element geometry is flat and the results in warping can become inaccurate, however, it is a very efficient element which gives good results at large strains in bending. On the other hand, in order to obtain more accurate results, gauss integration type with 5 integration points through the thickness of the sheet material is used.

"MAT_3-PARAMETER_BARLAT" model is used to define material properties (MAT 36 in Ls-Dyna® refers to this type of material model) [67]. This model is developed by Barlat and Lian (1989) for modeling sheets with anisotropic materials under plane stress conditions. This material model allows the use of Lankford parameters for the implementation of anisotropy. The effective stress as a function of plastic strain for uniaxial tension in the rolling direction is implemented to define plastic deformation behavior of the sheet metal.

Boundary conditions (BC) are also applied to the model. Since the process is simulated utilizing half-symmetrical model, symmetry plane (in XZ plane) is used. Also, node set is defined for the nodes on the blank where it is in contact with jaw. Displacement BC is defined by using the jaw motion that is taken from experimental studies.

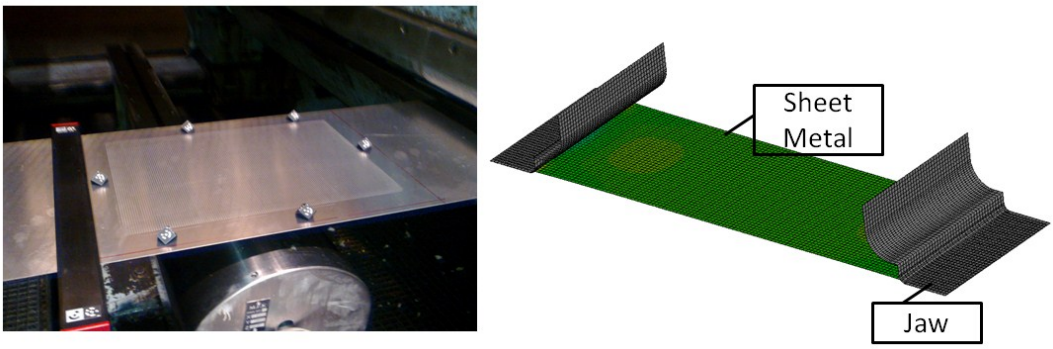

Figure 85: Numerical modeling of stretching using jaws

Figure 88 shows the comparisons of the strain distributions (major & minor strain values taken from the half section of the sheet) between the experiments and the simulations for the first (stretching by jaws) and second (stretching by form-die) stretching modes, respectively. Since the accuracy of the optical strain measurement system is around 0.5 %, scattered data is obtained from the experiments, whereas smooth distribution is obtained from the simulations. Results show good agreement.

6.2.2 Modeling of Stretching Sheet Material by Form Die

Studies on modeling of stretching sheet material by using only form die are also accomplished. Same process parameters such as tool geometry, material properties, jaw-die trajectories and lubrication conditions with the experimental studies are used in the analyses. Modeling procedure for this mode is quite similar with stretching only by jaw. The only difference between these two modes is that the modeling of die in order to give the semi-circular shape to sheet material (Figure 86). Contrary to the analyses in the first mode, accurate contact description is required in order to define frictional effects between form die and sheet material. Coulomb friction coefficients which are found by experiments are implemented according to the lubrication application. As a result, after the same tool motions in experimental trials are implemented to analyses, equivalent strain distribution which is shown in Figure 87 is obtained.

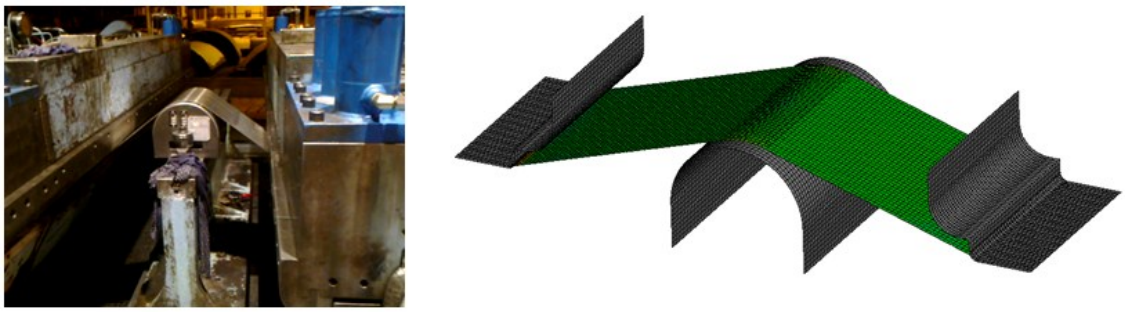

Figure 86: Numerical modeling of stretching using form die

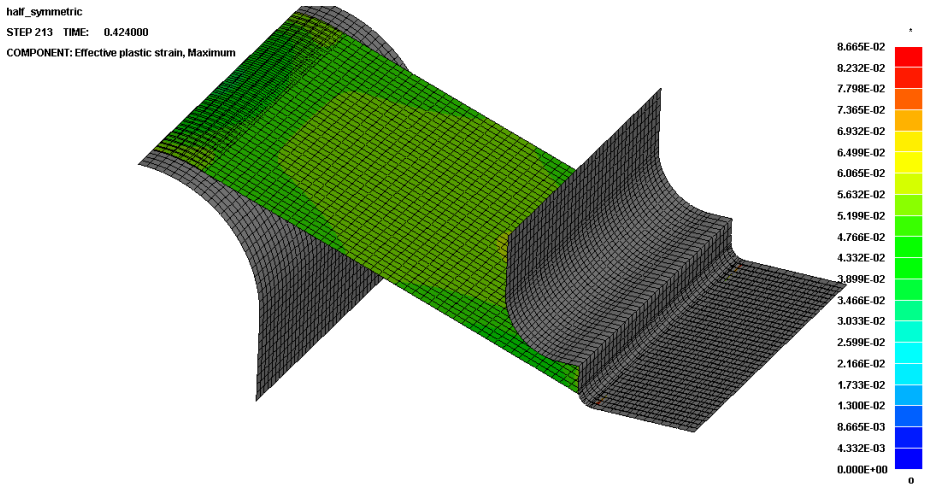

Figure 87: Equivalent plastic strain distribution of AA 2024-0 in stretching operation by form die

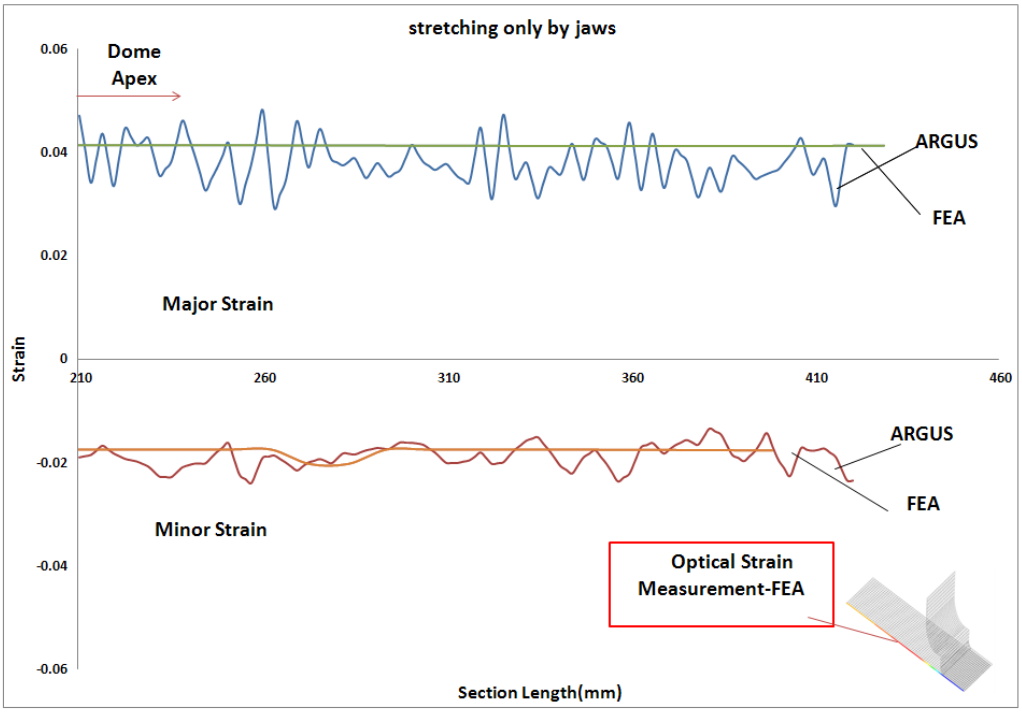

(a)

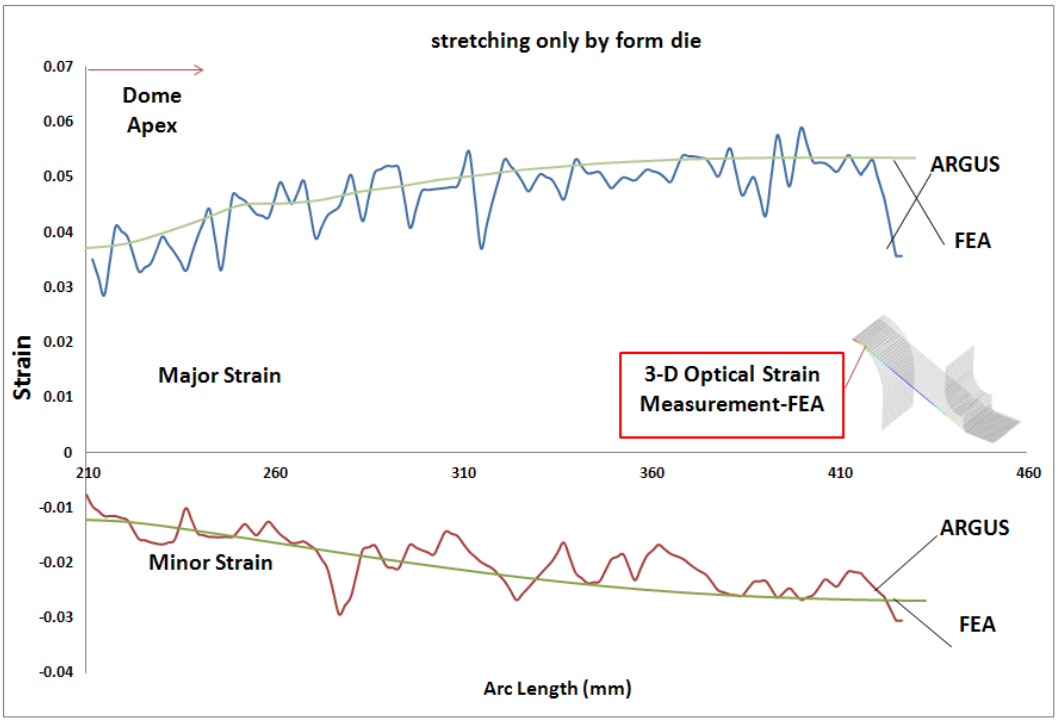

(b)

Figure 88: Comparison of ARGUS®-FEM measurement for stretching operation (a) only by jaws (b) only by form die

Addition to strain comparison between optical measurement and analysis result, geometrical comparison is also evaluated. As shown in Figure 89, experimental (obtained by optical measurement) and analysis results are geometrically matches.

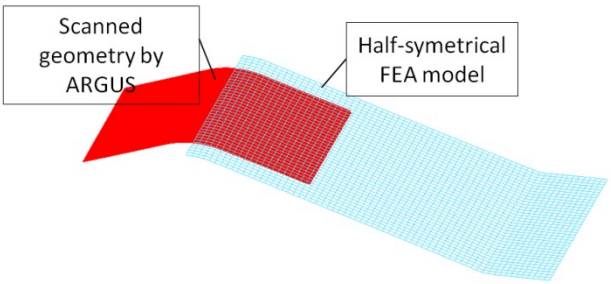

Figure 89: Geometrical comparison of sheet material between experimental ARGUS® measurement and FE analysis

6.2.3 Modeling of Stretching Sheet Material by Synchronized Trajectories of Jaws and Form Die

In the third stretching mode, two different case studies are accomplished. In the first trial, the tool trajectories obtained from the simulation are used for the forming of the sheet part. Simulation result shows that, at the end of the process, failure (tearing) is observed at the side wall. For the same parameters in simulation, experimental trial has been performed and the sheet is fractured from the region which is also well predicted by simulation (Figure 90). As it is shown in FLD curve given in Figure 90, the side wall region in identified tool location exceeds the formability limit and numerical identification of tearing is validated through experimental case.

In the second study, tool motions are improved by considering the sufficient stretching of sheet material without any fracture by the help of FLD curves. After new tool motions are taken from simulation in which the sheet part can be obtained with sufficient stretching numerically, a second trial has been performed with these tool motions. As expected, no fracture over the sheet material is observed. At the end of the process, maximum equivalent plastic strain reaches to the value of 0.09 in side wall of sheet metal (Figure 91).

On the other hand, 3-D optical strain measurements are taken from the part which is sufficiently stretched. Major-minor strains over an identified section are taken and compared with simulation result. Figure 92 shows that both major and minor strains over this section are consistent.

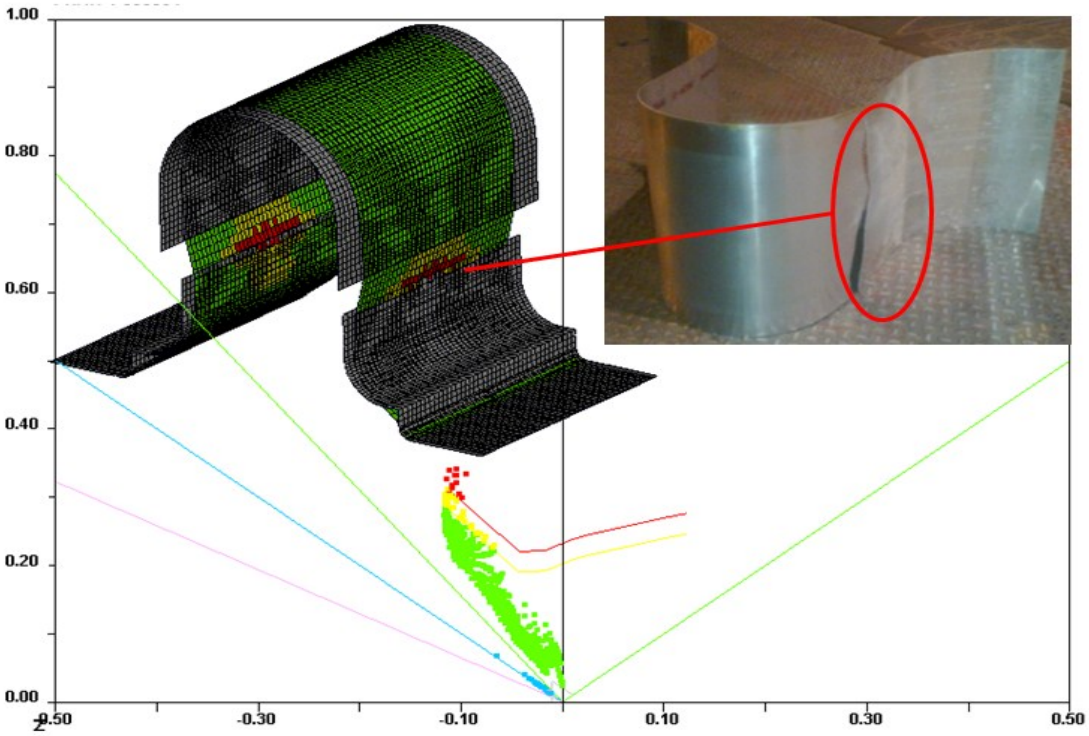

Figure 90: Failure area in numerical and experimental study

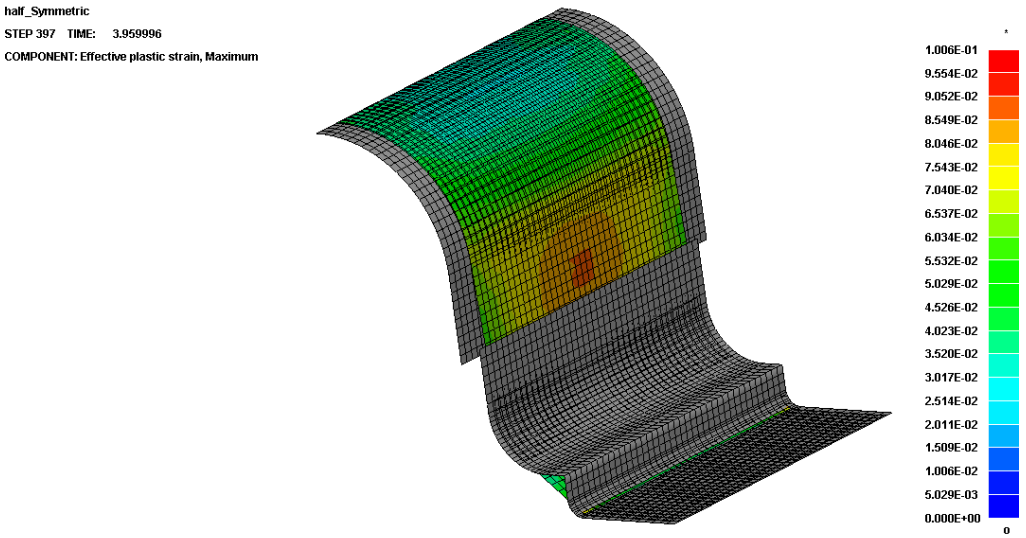

Figure 91: Equivalent plastic strain distribution of AA 2024-0 in stretching operation by synchronized tool motions

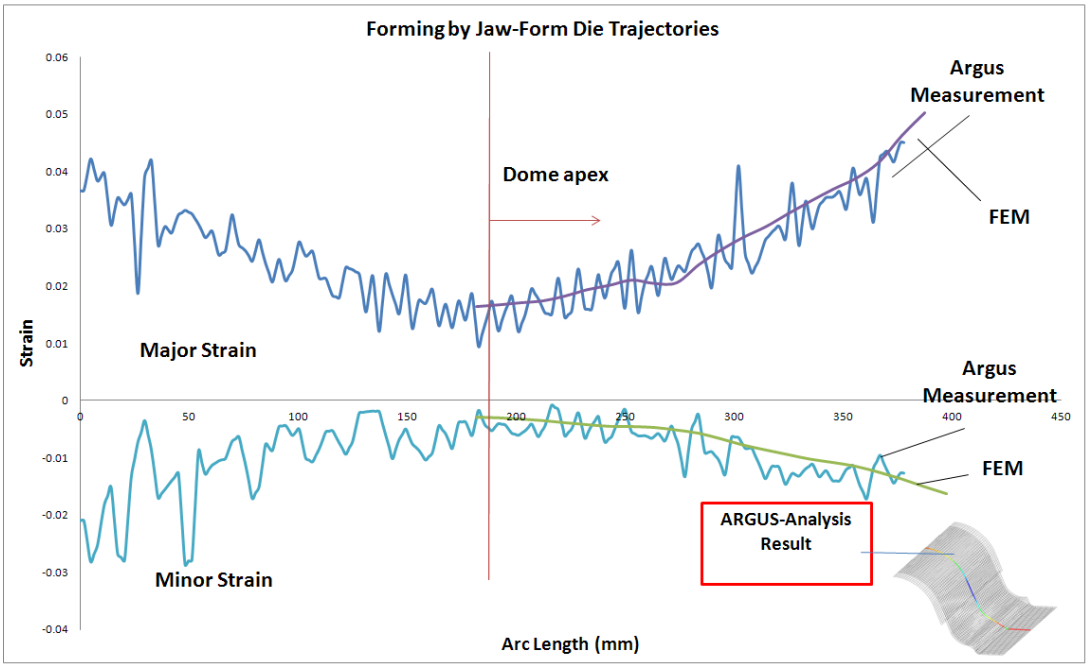

Figure 92: Comparison of ARGUS®-FEM measurement for stretching operation which is performed using synchronized tool motions

In this study, it is aimed to create a reliable basis for the FEM modeling of the stretch forming process in order to minimize trial-error procedure which includes re-work times, additional costs that arises due to labor and machining. Addition to this, products which has higher quality can be obtained by a operation whose parameters are previously identified by FEM. Mechanical material characterization is done to obtain a realistic material model. Friction coefficients are determined using a new approach where inverse analysis is performed. 3-D optical strain measurements are performed for different stretch forming tool trajectories to validate the reliability of the corresponding FE simulations. With these systematical experiments, it is also demonstrated that, a reliable FE model can be used to determine the limits of the stretch forming process before the actual manufacturing phase.

CHAPTER 7

CASE STUDIES

7.1 Introduction

In the previous chapters, the numerical analyses of simple experiments using semi-circular stretch forming form die are conducted successfully. Although strain comparisons between numerical and experimental studies give good results, more complex shaped products are required to be investigated in order to prove the success of stretch forming model. For this purpose, real aircraft parts are used to examine both numerical and experimentally. In the first case study, prediction of material formability is analyzed using FEA. Then the result is compared with experimental analysis. In the second study, usage of FLD to visualize the geometrical aspects is examined. And finally, the prediction of tearing using FLD in finite element analyses is conducted both experimentally and numerically. In short, this chapter is devoted to real applications.

7.2 Case Study 1: Experimental and Numerical Investigation of Wrinkling Phenomena

"The Front Cockpit" part of Turkish Basic Training Aircraft (Figure 93) is manufactured using stretch forming process. As a workpiece material, AA 2024-0 is used and then the material is subjected to heat treatment operation after forming in order to transform W (water) condition.

Figure 93: Front cockpit part on HÜRKUŞ (Basic Training Aircraft)

The thickness of sheet material is 1.6 mm. The form die is designed to manufacture two pieces at an operation. Therefore, manufacturing time required to complete the part number is automatically minimized. The CAD model of form die and final product is shown in Figure 94. As it is mentioned before, form die is designed to form two products at the same operation. And Punching tools are inserted on form die in order to identify tooling holes on sheet material. Tooling holes will then be used to trim sheet material in secondary operations using NC program.

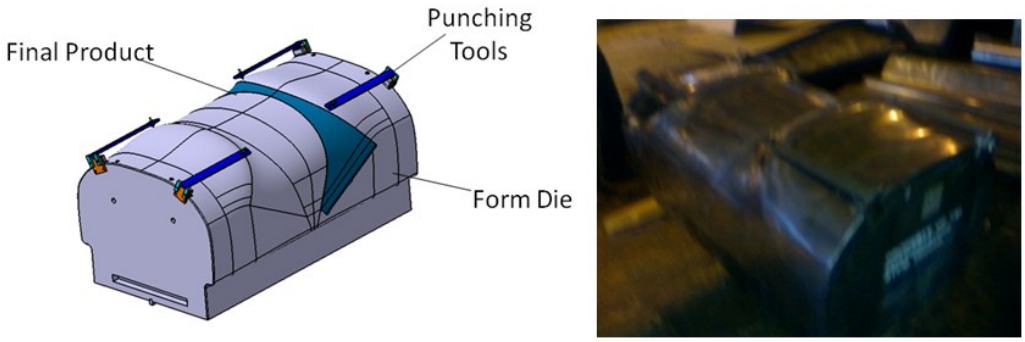

Figure 94: CAD model of form die and its actual isometric view

First of all, finite element modeling of cockpit part is established. In order to decrease CPU time, the process is modeled utilizing quarter-symmetric1/4 model as shown in Figure 95. The form die is modeled as rigid, whereby blank is modeled elasto-plastically deformable and the jaw is modeled also rigid. No contact is identified for final product and it is only used to visualize whether the sheet material takes the desired form or not. The blank material is discretized by 4-noded Belytschko-Tsay shell elements. Five integration points through thickness are used.

Boundary conditions of the process can be described as; since quarter-symmetric1/4 model is used, X-Z and Y-Z symmetry boundary conditions are used. Initial and final configurations are identified in CAD model and displacement BCs are adjusted using these values.

Contacting elements of blank with rigid jaw is only subjected to constraint in all directions except of stretching direction. So that compressed edges of blank material by jaw, can be modeled as a section which is not subjected to deformation. These regions then show only rigid movement together with jaw trajectory.

Geometrical BC which is used to determine where to start and stop the analysis is determined by the CAD modeling.

Penalty method is used as contact algorithm and Coulomb friction coefficient is implemented into the Ls-Dyna®. Coulomb friction coefficient is taken from the friction studies for the AA 6061-0 and dry lubrication conditions which equals to 0, 2.

Plastic deformation behavior of AA 6061-0 sheet material is implemented to finite element program using anisotropic deformation definition which is called "MAT-3-Parameter-Barlat" model. The mechanical properties of AA 6061-0 are given below in Table 7.

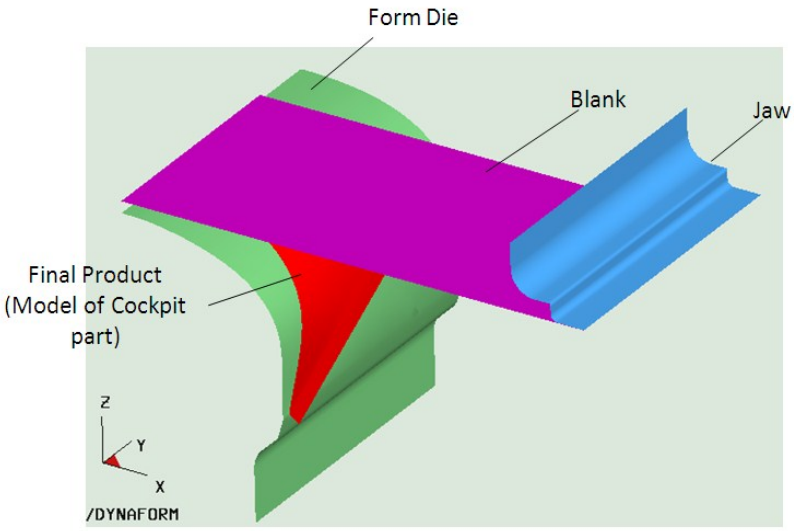

Figure 95: CAE model of ¼ symmetric model of stretch forming process

Table 7: Mechanical Properties of AA 6061-0

Yield Strength (Mpa)	Ultimate Strength (Mpa)	Elastic Modulus (Mpa)	Poisson's Ratio	Density (tonnes/mm^3)	R0	R45	R90	K (Mpa)	n
56	121	68900	0.33	2.70E-09	0.65	0.65	0.58	211.7	0.20

In stretch forming analyses, determination of relative tool motions is the most complex and important issue. As it is known, forming die raises to stretch sheet material while the jaws are getting closer in order to form side walls of the product. Therefore, synchronization of tool trajectories has to be balanced as the sheet is kept uniformly stretched during the process and the process is stopped when the required stretching amount is achieved. In this analysis, tool motions are defined using following functions. Using these jaw and form die trajectories, the stretching of sheet material during the process is satisfied and using FLD curves the process is

stopped when the required stretching is achieved. The initial and final configurations of tool locations are adjusted using the CAD model and their relative positions as shown in Figure 96.

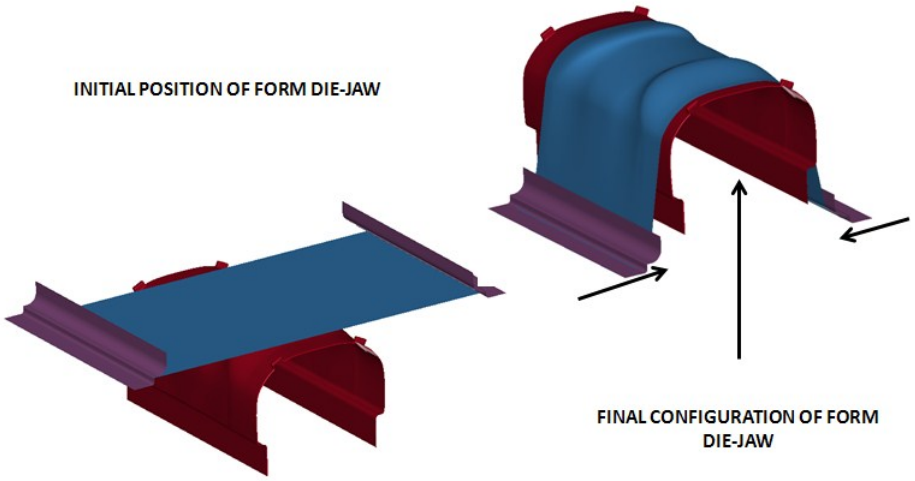

Figure 96: Initial and final configuration of tools and blank to form desired component

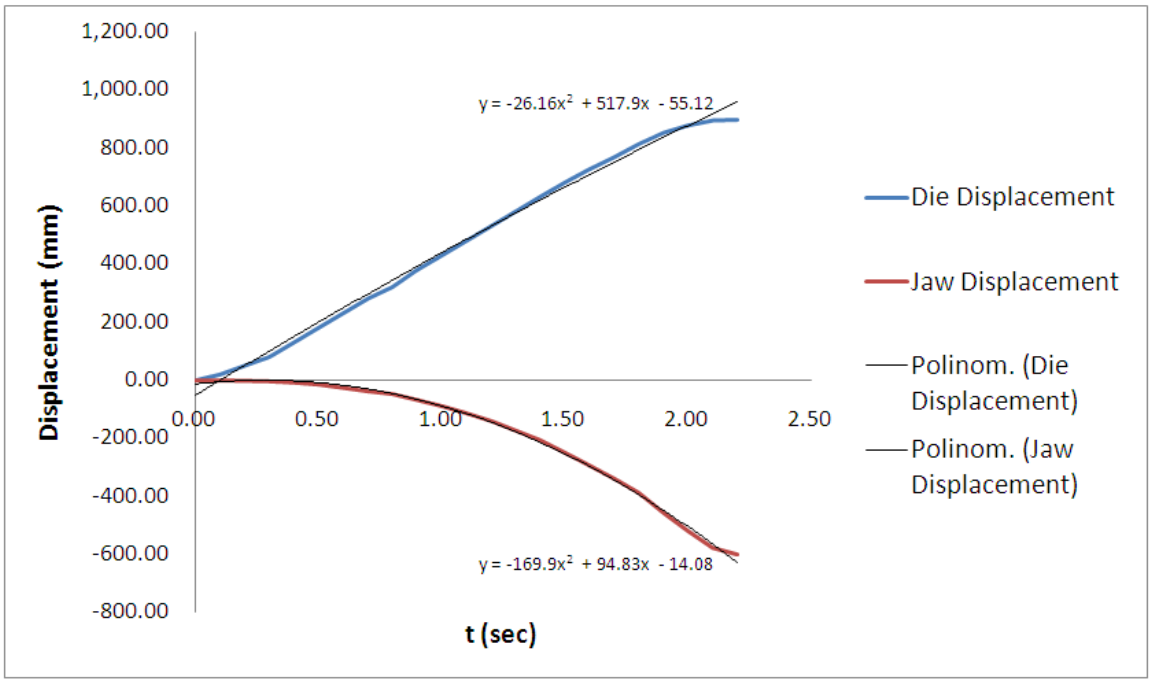

Figure 97: Tool motions which are implemented to finite element software (Ls-Dyna®)

After the analysis is performed using the above mentioned inputs, the results are visualized using FLD curves. It is observed that; the edge of part is successfully obtained with these tool

motions (Figure 97) and process parameters. The blank material achieves the required stretching condition; however, out of the edge of part wrinkle tendency is identified by using the FLD curves. In such a case, a second analysis can be performed in which the form die is raised to provide more stretching while minimizing the wrinkle tendency. But the tool motions are directly taken from the simulation and implemented into NC control unit of Cyril-Bath stretch forming press to validate the simulation result in actual condition. In the experimental validation, the form die is not lubricated. Because in the simulation, the friction coefficient value is implemented as 0,2. 1220 x 2585 mm rectangular blank (1.6 mm in thickness) geometry is clamped to forming press by jaws and piecewise linear jaw and tool motions are implemented into NC unit of hydraulic stretch forming press (Figure 98). AA 6061-0 sheet metal is formed with the same process parameters which are implemented into finite element software. As it shown in the Figure 99-100, although desired form is obtained in actual process, wrinkling occurs outside of the EOP (edge of part) as it was previously obtained in FEM analysis.

Figure 98: Experimental trial to form cockpit part in 750 tons capacity Cyril-Bath press

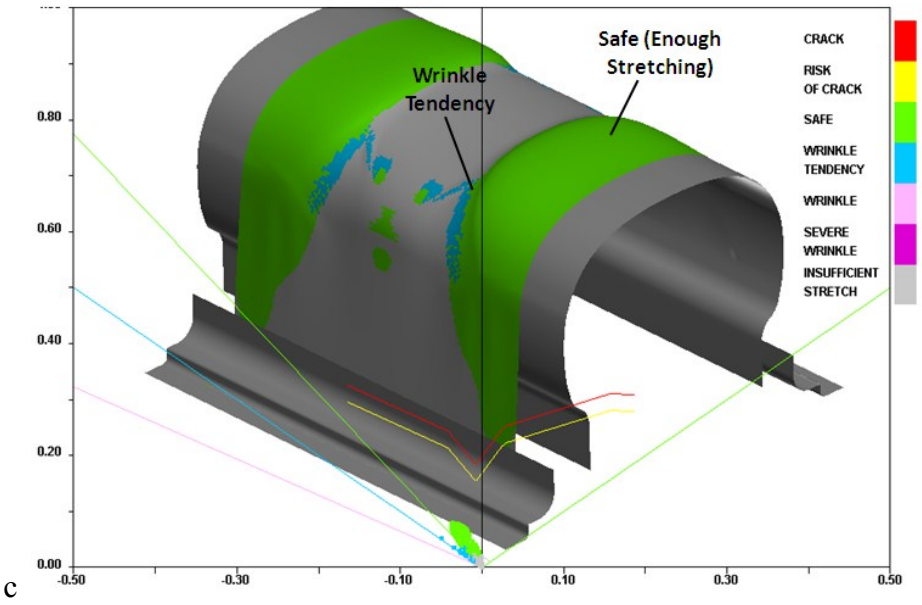

c

Figure 99: Visualization of simulation result with FLD curve of AA 6061-0 which has 1.6 mm thickness

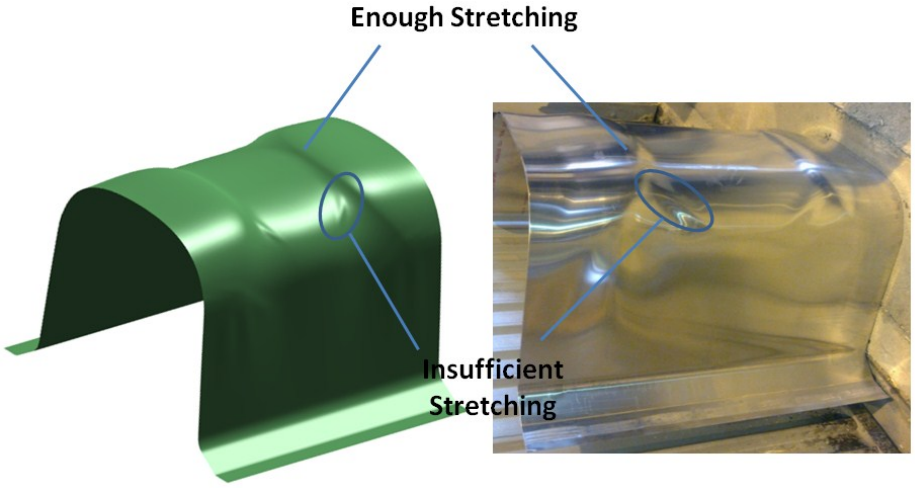

Figure 100: Comparison of simulation and experimental result

In this study, strain distributions and its difference are compared between the results which are taken from 3-D optical measurement device and ¼ quarter symmetric finite element analyses which have been performed with different friction coefficients. As it is shown in Figure 101, equivalent plastic strain difference is maximum 0, 02. Since the experiments are performed in lubricated conditions with AA 2024-0 (t=1.6 mm), the analysis which is performed with 0, 15 friction coefficient gives the best match with experimental deformation measurements. In this situation (μ= 0, 15), the difference strain value minimizes up to 0.002.

As a result of this study, reliability of finite element model for stretch forming process and the accuracy of Coulomb friction coefficients are validated through experimental measurements.

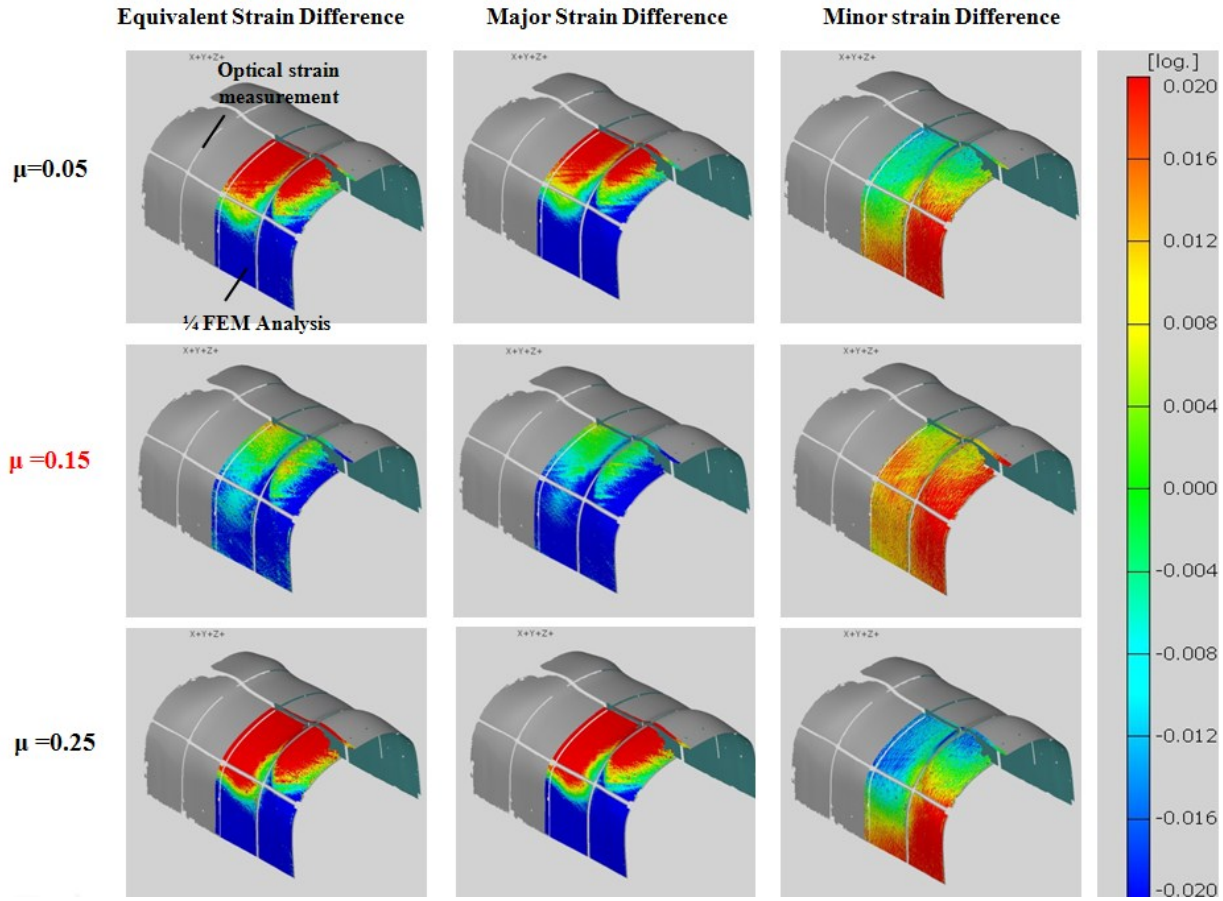

Figure 101: Strain difference between 3-D optical strain measurement and finite element analyses which are performed with several friction coefficients

Technical drawing of forming die which is related with this case study is given in APPENDIX B-116.

7.3 Case Study 2: Tearing Prediction by Using FEM

In the second case study, numerical and experimental study on stretch forming operation of "The Exhaust Pipe" of AW 139 helicopter is handled (Figure 102). Exhaust pipes are generally manufactured in complex forms. Since formed hollow tubes are used in exhaust pipes, it is preferred to manufacture lower and upper sides separately and then these details are assembled using welding operation. This detail part is commonly made out of titanium; however, in this case study aluminum alloy is used. 1250 X 690 mm rectangular aluminum alloy (AA 2024-0) is used as blank material. The thickness of sheet metal is 0, 65 mm.

Figure 102: Exhaust pipe location in AGUSTA AW-139 Helicopter

In this case study, specially purpose designed jaws are used to obtain desired geometry. The CAD model and actual form die are shown in the Figure 103.

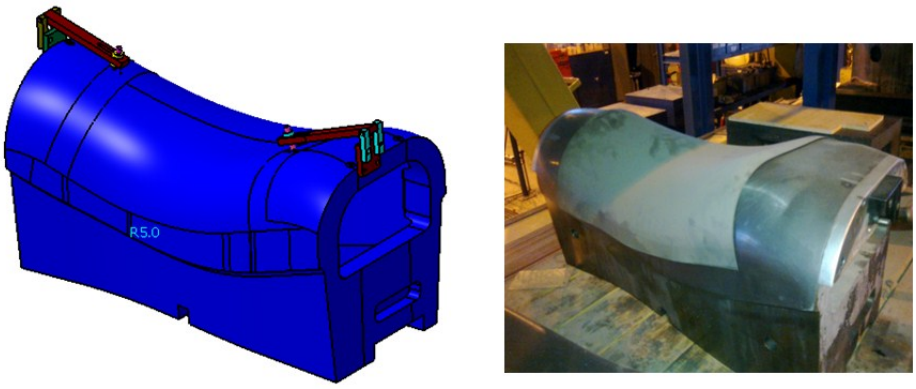

Figure 103: CAD model and actual view of form die

Since the part is not symmetric, full finite element model is prepared. Special jaws are modeled and it is observed that the sheet material buckles while the tearing begins from the region which has larger contact interface with form die. Same tool motions, material and contact parameters are used in the actual validation of simulation. It is observed that, the sheet material wrinkle and tears in the same tool location with the simulation (Figure 104-105). This study also validates the reliability of FLD curves in the evaluation of formability in stretch forming analyses.

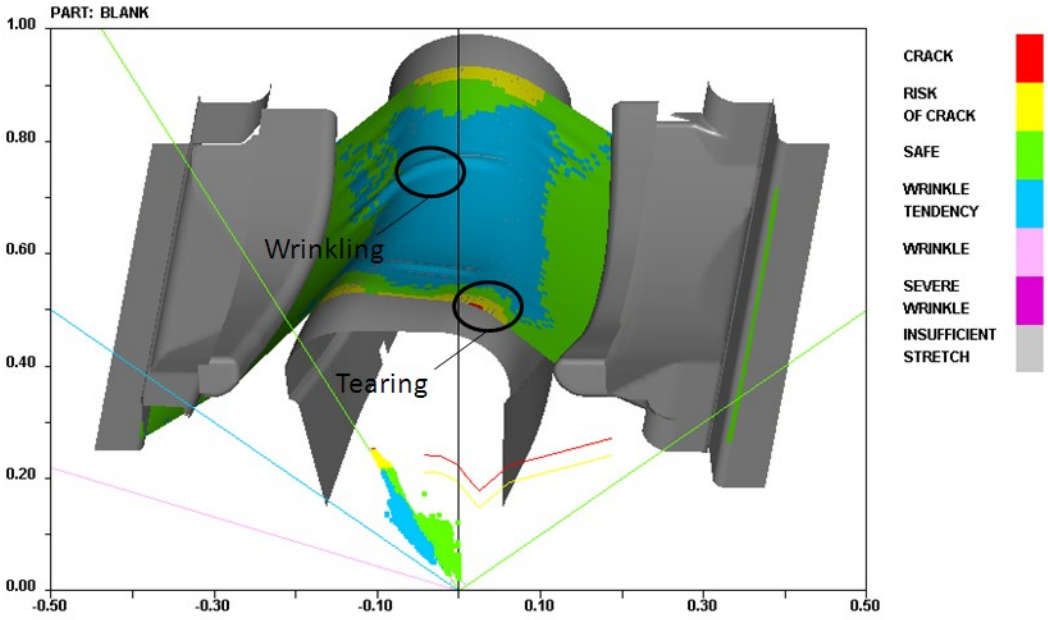

Figure 104: Visualization of FEM analysis result for Case 2

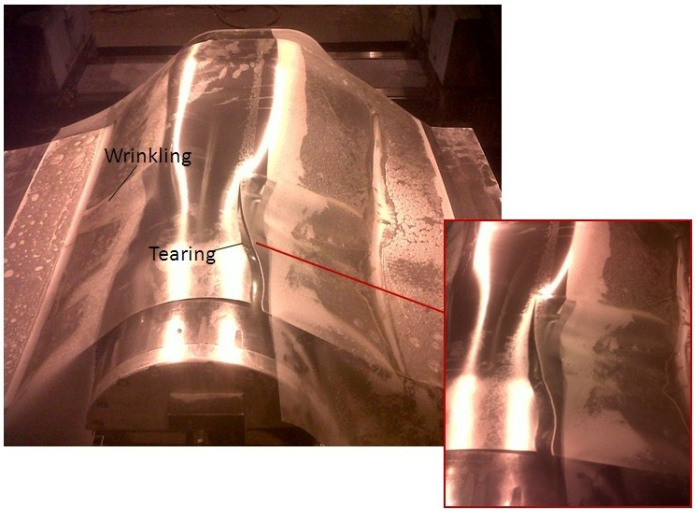

Figure 105: Experimental validation of failures obtained in finite element simulation

7.4 Case Study 3: Usage of FLD to Visualize the Formability

The final case study is related with modeling of stretch forming process of a wing component of KAI KT-1. The sheet material is AA 2024-0 and the thickness is 0, 81 mm. In this study, only modeling side of stretch forming operation is handled. As it is shown in the Figure 106, the form of wing component varies through the section. Although the product has smaller circumference in the front, in the back it reaches to its maximum value. In other words, the

circumference of the stretched material is not uniform through the part length. On the other hand, the sharp region in the apex of form die increases the tearing possibility due to non-uniform stretching. Therefore, two different CAD models are used in the analyses of stretch forming process. Technical drawing of forming die for this case study is given in APPENDIX B-Figure 117.

Agonic jaws and form die are used in CAD modeling to compare with the simulation performed with angled case. The non-conventional jaws in 1.5 ° angle and form die in 1° angles are used in CAD modeling in order to obtain uniform deformation during the process (Figure 106).

Tool motions are previously identified by press operator and these values are implemented to both FE models. It is proved that; required form of sheet material can only be obtained by the parameters which are mentioned in the second analysis.

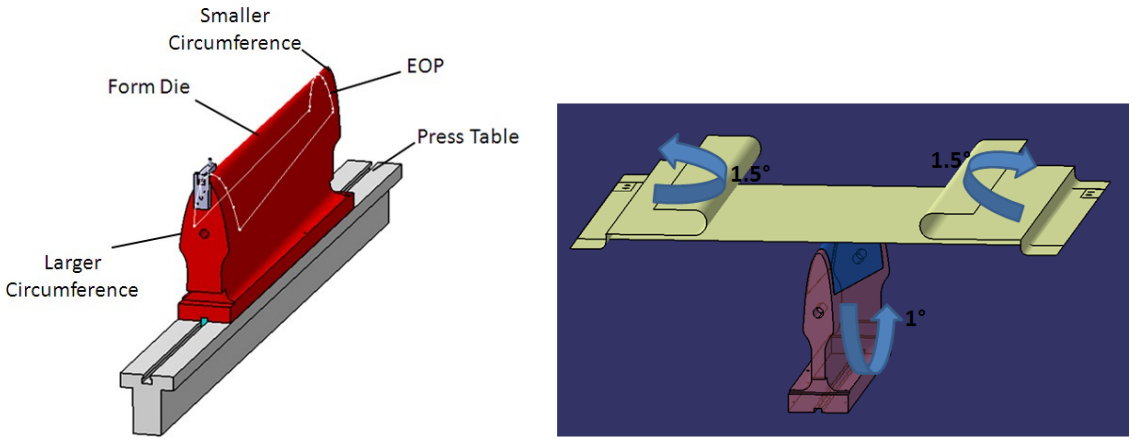

Figure 106: CAD model of form die to obtain wing component (Illustration to angled tool locations)

In the first analysis, agonic tools are used. When the result of numerical analysis is evaluated using FLD curves, it is seen that the sheet achieves required stretching (Figure 107). However, geometrical expectations cannot be fulfilled with agonic locations of tools as it is shown in Figure 108. Although it is observed that the sheet has sufficient stretching at the end of the process, the sheet material does not lie on the form die. Blank – tool distance in normal direction reaches approximately 18 mm in some regions inside the EOP. So that it is concluded that; visualization of analyses with FLD to evaluate formability is an important tool but it is also important to evaluate the geometry using the contact interface with form die and blank material.

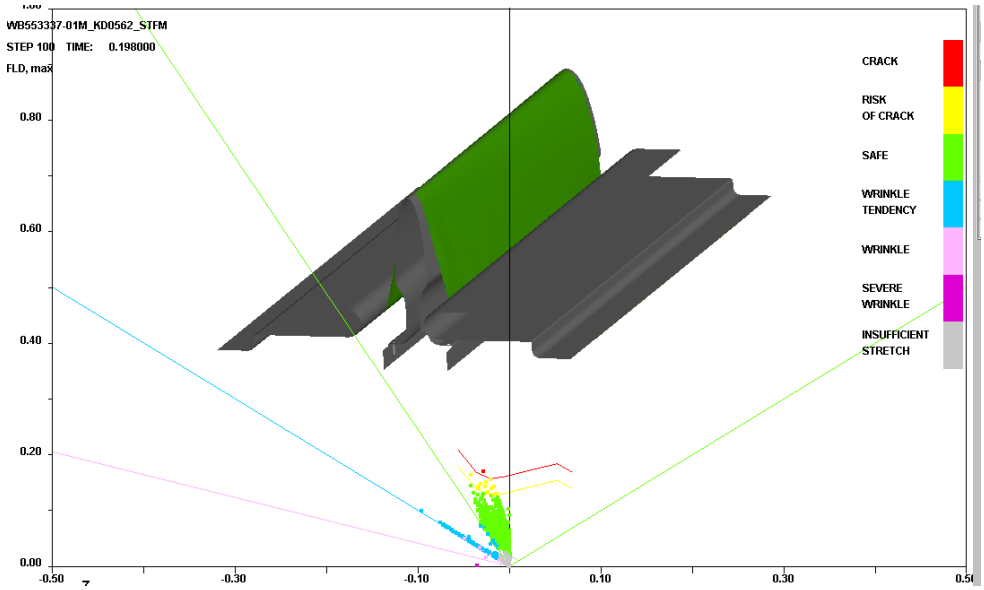

Figure 107: Visualization of simulation using FLD for agonic tools. The blank material achieves required stretching

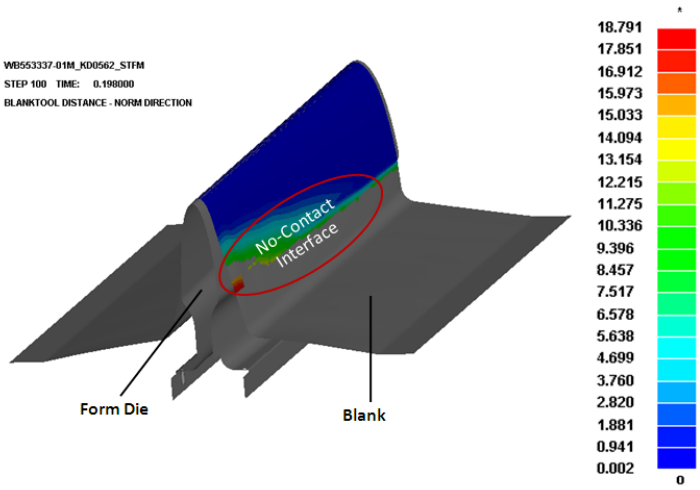

Figure 108: Illustration to blank-tool distance in normal direction (Some region of blank has no contact with form die- approximately 18 mm differences)

In the second finite element model, analysis consists of two angled jaws in 1.5° and form die in 1°. Analysis is re-modeled using same tool motions, material and contact models. FLD curve for AA 2024-0 in 0, 81 mm thickness shows that, sheet material achieves sufficient stretching condition (Figure 109). On the other hand, geometrical expectations are also validated using blank-form die distance in normal direction. As it is shown in Figure 110, sheet material lies on form die considering the edge of part.

In this case study, the importance of using FLD curves to evaluate analysis result is emphasized. However, FLD curves alone are not sufficient. Also, the necessity of geometrical

comparison between the desired forms of the product with the analysis result is highly important to obtain successful finite element analyses.

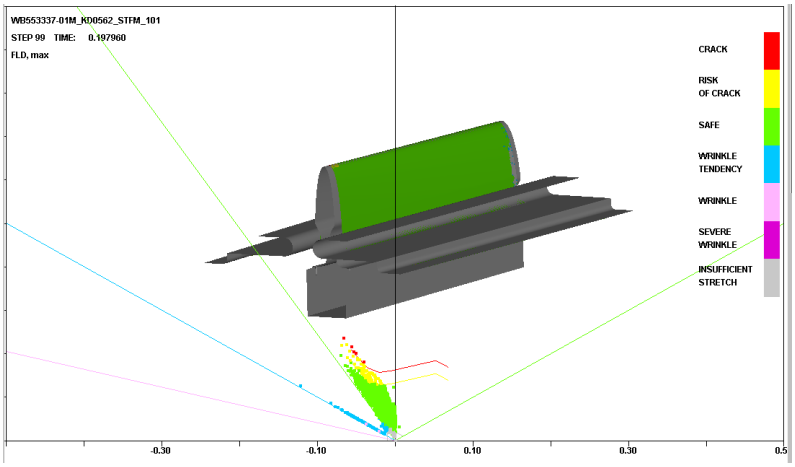

Figure 109: Visualization of simulation using FLD for angled tools (The blank material achieves required stretching)

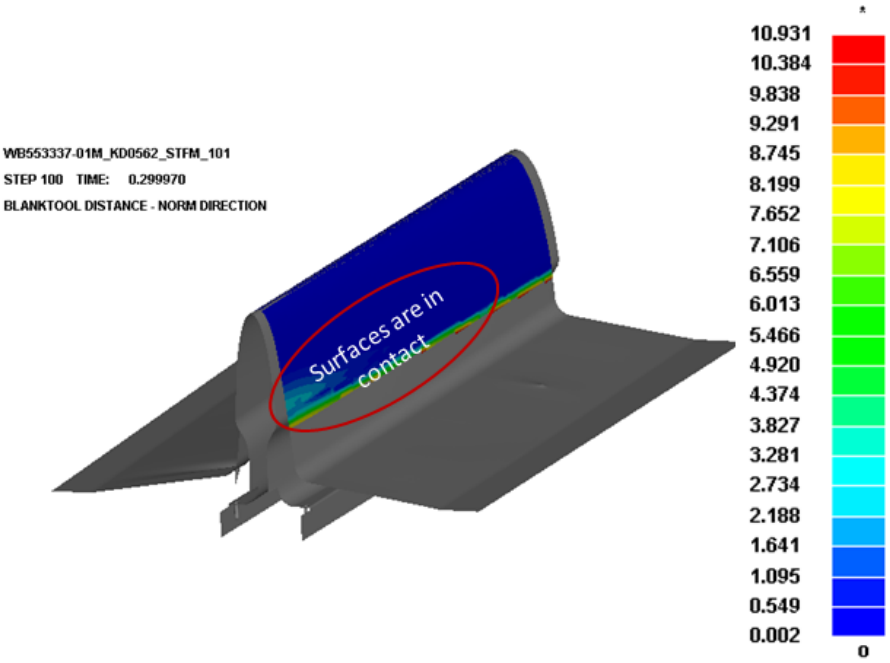

Figure 110: The contact interface in normal direction obtained by FEM analysis which is modeled using angled tools (0.003 mm through the part EOP)

To sum up, experimental and numerical studies showed that; analyses which are performed with accurate material modeling with reliable friction coefficient give good results and shows similarity with experimental trials. It is proved that, formability and instability of sheet material caused by wrinkling and tearing can be observed with numerical modeling by using

FLD curves. In addition to evaluate the results with FLD curves, the importance of making a comparison between numerical simulated blank with desired geometry is emphasized. To conclude, finite element method is a reliable tool to visualize deformation before real manufacturing to adjust the process parameters. As it is mentioned in Case Studies , each process detail such as wrinkling, tearing, sufficient stretching, even the changes in material deformation due to 1° tool location can be obtained with FEM.

CHAPTER 8

CONCLUSIONS AND FUTURE WORKS

Stretch forming process is commonly used in the aircraft industry for the manufacturing of large sheet panels. The success of this process is highly dependent on the tool motions during forming. These motions are determined by trial-error procedure and it is costly. This study aims to optimize the stretch forming process by determining the necessary tool motions, predicting formability defects and adjust process parameters before real manufacturing to identify suitable design changes to achieve required form with numerical analysis. Material characterization and friction tests of mostly used aluminum alloys are conducted for input to the model. In order to improve the model and validate the analyses results, experimental work is performed in which the deformation of the sheet is measured optically.

HBT, standard tensile, compression and FLD tests are performed for different aluminum alloys including AA 2024, AA 6061 and AA 7075. The results and findings which obtained from mechanical tests are summarized as follows;

- Mechanical properties such as, yield point, UTS, elastic modulus and anisotropy coefficients are obtained for aluminum alloys using standard tensile test.
- Plastic flow curves are obtained using three different test methods, which are; tensile, compression and HBT respectively. It is shown that, plastic strain up to a limited level can be obtained using tensile test. However, HBT and stack compression test gives data in higher plastic strains. The main reason behind this fact is that, HBT and compression tests give deformation data for biaxial stress state while only uniaxial stress data can be obtained by tensile test. Material modeling by using flow curve obtained by compression or HBT does not require flow curve extrapolation and this situation minimizes the errors occurred in mathematical material modeling. For aluminum alloys, up to maximum 0, 2 strain value can be achieved, although HBT or compression test give data up to 0, 5 strain value.
- The repetitions showed that, repeatability of HBT and standard tensile test is quite high, however, the repetitions in stack compression test can be considerably different. It is concluded that, in order to obtain repeatability, the sliding effect between the layers should be minimized by locating the specimens carefully. It is also observed

that, if the stack compression test is performed carefully, the flow curve shows similarity with the other test results.

- FLD (Forming Limit Diagram) curves are obtained for different aluminum alloys in different thicknesses. These forming limit windows are used to visualize the formability of blank material in virtual environment. In other words, forming defects such as wrinkling, tearing or over-stretching are predicted using FLDs.

In this study, inverse based analyses are performed to identify Coulomb friction coefficients for different thicknesses, lubrication conditions and aluminum alloys. The detail of this study is explained in previous chapters. As a summary, following results are obtained;

- For the purpose of identifying friction coefficient, a new testing apparatus is used. Further case studies showed that, reliable friction coefficients are obtained for different aluminum alloys and lubrication conditions.
- The higher value of friction coefficient is obtained in dry (no-lubrication) condition and it is followed by; oil lubricated, nylon and silicon covered cases respectively.
- Surprisingly, no difference in frictional coefficient is obtained between solution heat treated (W condition) and annealed (0 condition) specimen for the same aluminum alloy.
- On the other hand, numerical calculations showed that the equation which is derived to identify friction coefficient gives good result, however, success of this equation has not been tested experimentally yet.

After material characterization and determination of friction coefficient studies are accomplished, an effort has been made on modeling of stretch forming operation using FEM. In the numerical and experimental studies, both strain and geometrical comparison are considered. First of all, a new form die for stretching purpose is designed and manufactured. Since the die has semi-circular form, it is planned to perform initial studies on a blank material which can be uniformly formed. Three modes of stretching which are; stretching by jaw, stretching by form die and stretching by synchronization of tool motions together are considered. 3-D optical measurement system, ARGUS®, is used for experimental strain measurements. Having obtained similar results from both numerical and experimental trials, real airplane parts, which have more complex shapes, are formed by using stretch forming operation. Experimental results show good agreement with numerical analyses. Results and

findings of numerical and experimental study on stretch forming process are summarized below.

- The material is modeled anistropic by using 3-Parameter-Barlat material model. In the modeling phase of stretch forming process, it is observed that anisotropic modeling gives better results with experimental optical measurements.
- Experimental optical measurement studies show that, strain comparison between simulation and experimental trials give similar results. Since the accuracy of the optical strain measurement system is around 0.5 %, scattered data is obtained from the experiments, whereas smooth distribution is obtained from the simulations. Results show good agreement.
- It is proved that formability of sheet material and possible defects such as tearing and wrinkling can be predicted by FEM with the usage of FLD curves.
- Additionally, it has been proved that jaws and form die trajectories can be determined and optimized using FEM analyses.
- Also, Lüders bands, in other words, slip bands can be observed with thermal camera during the actual process. Therefore, enough stretching judgment can be easily done with thermal camera before they appear physically visible to a normal human eye. In this study, it is aimed to create a reliable basis for the FEM modeling of the stretch forming process in order to minimize trial-error procedure. 3-D optical strain measurements are performed for different stretch forming tool trajectories to validate the reliability of the corresponding FE simulations. It is also demonstrated that, a reliable FE model can be used to determine the limits of the stretch forming process before the actual try-out phase. Therefore, problems which are encountered in stretch forming process such as; manufacturing time, labor cost, waste material and modifications on die design can be minimized using FEM.

In the future works, aluminum sheet material will be modeled using kinematic hardening rule. On the other hand, optimization studies will be performed to adjust best tool motions by FEM. The optimization of the synchronized tool motion by FEM will eliminate trial-error procedure completely.

REFERENCES

[1] Smith B., Advanced Material & Processes/September 2003, 41-44

[2] Groover M., Fundamentals of Modern Manufacturing Materials, Processes and Systems Third Edition, 2007.

[3] Tekkaya E., Lecture Notes, MFGE 303, Atılım University

[4] Schuler, Metal Forming Handbook, Springer, 1988

[5] Alumatter, last retrieved 2012 January, http://aluminium.matter.org.uk

[6] TALAT, Training in Aluminium Application Technologies, last retrieved in 2011 March, http://www.alueurope.eu

[7] Lange K., Handbook of Metal Forming, Society of Manufacturing Engineers (SME), First Edition, U.S.A., 1975.

[8] W. H. Cubberly., Tool and Manufacturing Engineers Handbook, SME, 1984

[9] Kaufman J. G., Introduction to Aluminum Alloys and Tempers, ASM International, 2000.

[10] Marciniak Z., Duncan J. L., Hu S. J., Mechanics of Sheet Metal Forming, 2002.

[11] Jung M-H., Stretch forming analysis for skin of aircraft, model. B717-200. 2001-89.

[12] JIN H-X., Basic experiment research and numerical simulation on mirror aluminum alloy skin stretch forming. Beijing: Beijing Universit of Aeronautics and Astronautics, 2006 :12-23.

[13] He D-H., Li X-Q., Li D-S., Yang W-J., Process design for multi-stage stretch forming of aluminium alloy aircraft skin. Trans. Nonferrous Met. Soc. China 20 (2010) 1053-1058.

[14] He D-H., Li D-S., Li X-Q., Jin C-H., Optimization on springback reduction in cold stretch forming of titanium-alloy aircraft skin. Trans. Nonferrous Met. Soc. China 20 (2010) 2350-2357.

[15] Wade D., Accurate FEA prediction of extrusion forming to improve aircraft design and manufacturing, Boeing Publication 4B00 #002

[16] Huang C., Torng C., Chang H., Effects of springback on the stretch forming of the aluminum saddle-shaped skins. Steel Research International Vol.79 pp.85-90

[17] Hardt D. E., Norfleet W. A., Parris A., In process control of strain in a stretch forming process, Journal of Engineering materials and technology, Vol. 123, October 2001

[18] Yoshida M., Yoshida F., Konishi H., Fukumoto K., Fracture limits of sheet metals under stretch bending. International Journal of Mechanical Sciences 47 (2005) 1885-1896

[19] Luo M., Wierzbicki T., Numerical failure analysis of a stretch bending test on dual phase steel sheets using a phenomenological fracture model. International Journal of Solids and Structures 47 (2010) 3084-3102

[20] Rajiv S., Kevin O., Variation modeling for a sheet stretch forming manufacturing system. CIRP Annals, Vol. 48, Issue 1, 1999, pages 397-400

[21] Keum Y. T., Wagoner R. H., A finite element program for simulating sheet metal stretch forming process, KSME Journal, Vol. 6, No.1, pp. 6-15, 1992

[22] Corona E., A simple analysis for bend stretch forming of aluminum extrusions, International Journal of Mechanical Sciences, 46 (2004) 433-448

[23] Panda S. K., Kumar D. R., Kumar H., Nath A. K., Characterization of tensile properties of tailor welded IF steel sheets and their formability in stretch forming, Journal of Material Processing Technology, 183 (2007) 321-332

[24] Feng X., Zhongqin L., Shuhui L., Weili Xu., Study on the influences of geometrical parameters on the formability of stretched curved flanging by numerical simulation, Journal of Material Processing Technology 145 (2004) 93-98

[25] Gilmour K. R., Leacock A. G., Ashbridge M. T. J., The influence of plastic strain ratios on the numerical modelling of stretch forming. Journal of Materials Processing Technology 152 (2004) 116-125

[26] Moon Y. H., Kim D. W., Tyne C. J., Analytical model for prediction of sidewall curl during stretch-bend sheet metal forming. International journal of Mechanical Sciences 50 (2008) 666-675

[27] Panda K. S., Kumar D. R., Experimental and numerical studies on the forming of tailor welded steel sheets in bi-axial stretch forming, Materials and Design 31 (2010) 1365-1383

[28] Cai Z-Y., Li M-Z., Chen X-D., Digitized die forming system for sheet metal and springback minimizing technique. Int J Adv Manuf Technol (2006) 28:1089-1096

[29] Paunoiu V., Teodor V., Epureanu A., Spring back compensation in reconfigurable multipoint forming. World Scientific and Engineering Academy and Society, Pages 180-185

[30] Cai Z-Y., Wang S-H., Xu X-D., Li M-Z., Numerical simulation for the multi-point stetch forming process of sheet metal.Journal of Material Processing Technology 209 (2009) 396-407

[31] Liu W., Yang Y., Li M-Z., Numerical simulation of multi-point stretch forming and controlling on accuracy of formed workpiece. Int J Adv Manuf Technol (2010) 50:61-66

[32] Wang S., Cai Z., Li M., Numerical investigation of the influence of punch element in multi-point stretch forming process. Int J Manuf Technol (2010)49: 475-483

[33] Papaioanu A., Liewald M., Further development of the SCS stretch forming technology with assitance of forming simulation. Int J Mater Form (2010) Vol. 3. Suppl 1:155-158

[34] Papaioanu A, Schleich R., Liewald M. Improved tool development process for novel SCS technology for aluminum sheet metal, 7th European Ls-Dyna Conference

[35] Araghi B., Manco G., Bambach M. Hirt G., Investigation into a new hybrid forming process: Incremental sheet forming combined with stretch forming. CIRP Annals-Manufacturing Technology 58 (2009) 225-228

[36] Kurukuri S., Miroux A., Wisselink H., Boogaard T. Simulation of stretch forming with intermediate heat treatments of aircraft skins. Int J Mater Form (2011) 4:129-140]

[37] TAI Process Standard PS. 35.42

[38] K. Siegert, S. Vagner. Formability characteristics of aluminum sheets, TALAT Lecture 3701, European Aluminum Association, 1994

[39] ASTM E8-04,: Standard tensile test methods for tension testing of metallic materials", July U.S.A., 2003.

[40] S. Kunaporn and M. Ramulu, Ultra high pressure waterjet peening, 2001 WJTA American Waterjet Conference August 18-21, 2001

[41] Stachowicz F., Biaxial Stress-Strain Relationship of Sheet Metal From Hydraulic Bulge Test. 5th International Multidisciplinary Conference

[42] Gleyzal, A., Plastic deformation of a circular diaphragm under pressure. J. Appl.Mech.70,1948,288–296

[43] Brown, W.F., Thompson, F.C., Strength and Failure Characteristics of Metal in Circular Bulging. Trans. Am. Soc. Mech. Eng. 71, 1949, 575–585

[44] Koç M et al. An experimental study on the comparative assessment of hydraulic bulge test analysis methods. J. Mater Design (2010), doi:10.1016/j.matdes. 2010.05.057

[45] Gutscher G., Wu H. C., Ngaile G., Altan T., Determination of Flow Stresses for Sheet Metal Forming Using the Viscous Pressure Bulge (VPB) Test, Journal of Materials Processing Technology, 146 (1), 2004, 1-7.

[46] Chakrabarty J., Alexander J. M., Hydrostatic Bulging of Circular Diaphragms, the Journal of Strain Analysis for Engineering Design, 1970, 155-161

[47] W. Panknin, Der hydraulische Tiefungsversuch und die Ermittlung von Fließkurven (The hydraulic bulge test and the determination of the flow stress curves), Dissertation, Institute for Metal Forming Technology, University of Stuttgart, Germany, 1959.

[48] Atkinson, M., 1996. Accurate determination of biaxial stress–strain relationships from hydraulic bulging tests of sheet metals. Int. J. Mech. Sci. 39 (7), 761–769.

[49] A. Güner, A. Brosius, A. Tekkaya. Analysis of the HBT with FEA concerning the accuracy of the determined flow curves. Key Engineering Materials Vols. 410-411 (2009) pp 439-447

[50] Mutrux A., Hochholdinger B., Hora P. A procedure for the evaluation and validation of the hydraulic biaxial experiment. Numisheet 2008

[51] Diehl A., Staud D., Engel U.: Investigation of the mechanical behaviour of thin metal sheets using hydraulic bulge test. In: 4th Int. Conference on Multi. Material

[52] Gagov V., Feschiev N., Comsa D. S. Comsa, Minev V.: Strain hardening evaluation by bulge testing of sheet metals. 12th International Scientific Conference, Achievements in Mechanical & Materials Engineering

[53] S.P. Keeler: SAE Paper No. 650535, 1965 S.P. Keeler: SAE Paper No. 650535, 1965

[54] G.M. Goodwin: SAE Paper No. 680093, 1968

[55] D. Banabic, Sheet metal forming processes: Constitutive modeling and numerical simulations. Springer, 2010.

[56] ISO 12004-2, "Determination of Forming Limit Curves in the Laboratory". 2008-10-15.

[57] Norm DIN 50106: Prüfung metallischer Werkstoffe: Druckversuch. Berlin: Beuth-Verlag, 1978

[58] S. Coppieters, P. Lava, H. Sol, A. Van Bael, P. Van Houtte, D. Debruyne. Determination of the flow stress and contact friction of sheet metal in a multi-layered upsetting test. Journal of Materials Processing Technology, 210 (2010), 1290-1296.

[59] M. Merklein, A. Kuppert. A method for the layer compression test considering the anisotropic material behavior. Int J Mater Form (2009) Vol. 2 Suppl 1:483–486

[60] Kaftanoğlu B., Determination of coefficient of friction under conditions of deep-drawing and stretch forming, Wear, 25 (1973), pp. 177-188

[61] Hatipoglu H., Polat N., Köksal A., A methodology to determine friction coefficient in Fluidcell forming process. Steel research Int 81 (2010) No:9 (640-642),2010.

[62] B. H. Lee, Y.T.Keum, R. H. Wagoner, Modeling of the friction caused by lubrication and surface roughness in sheet metal forming. Journal of Material Processing Techonology, 130-131 (2002) 60-63.

[63] R. Grueebler, P. Hora. Temperature dependent friction modeling for sheet metal forming.Int J Mater Form (2009) Vol. 2 Suppl 1:251-254.

[64] Kim H., Altan T., Yan Q., Evaluation of stamping lubricants in forming advanced high strength steels using deep drawing and ironing tests., Journal of Materials Processing Technology 209 (2009) 4122–4133.

[65] Wojtowicz W. J., Sliding friction test for metalworking lubricants. Lubrication Engineering, 11 (1955) 3, 174-177.

[66] GOM-ARGUS, User Information. Braunschweig, Germany, 2009.

[67] LS-DYNA 971 Theory Manual, Livermore Software, U.S.A., 2007.

APPENDIX A

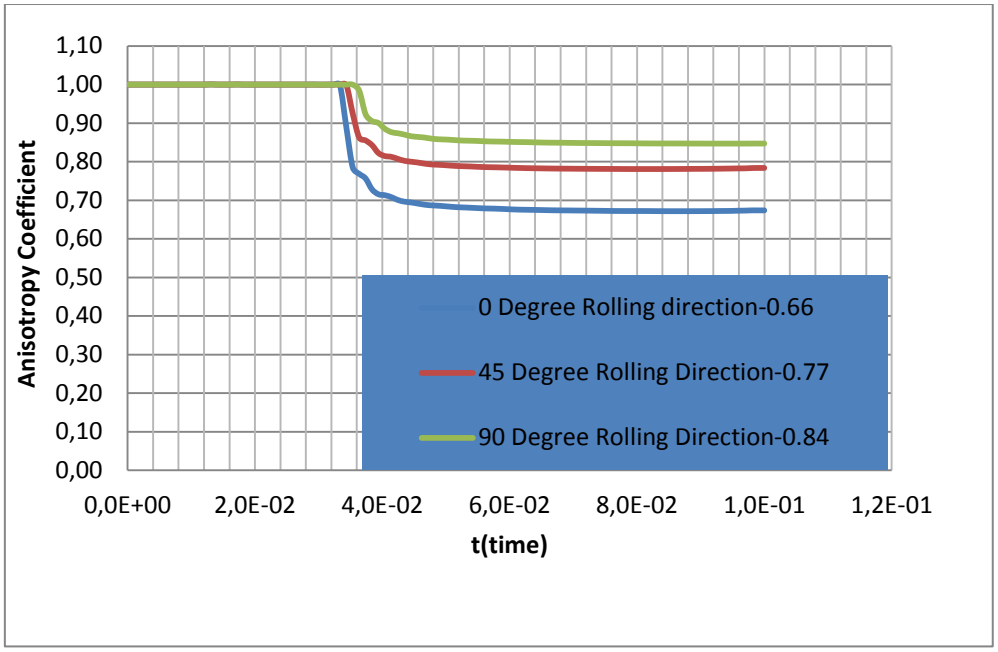

Figure 111: Results of FEM modeling (performed by Ls-Dyna) which show the proportion of width strain to thickness strain for AA 6061-0. As it is shown, anisotropy coefficient converges to the value implemented to software.

Table 8: Main alloying elements of wrought aluminum

Alloy	Main Alloying Element
1xxx	Mostly pure aluminum
2xxx	Copper
3xxx	Manganese
4xxx	Silicon
5xxx	Magnesium
6xxx	Magnesium and Silicon
7xxx	Zinc
8xxx	Other elements

Table 9: Advantages of aluminum [9]

PROPERTY	DETAIL
Light weight	Specific gravity of aluminum (≈2.7 gr/cm3) is almost 35% of steel and iron and this makes aluminum more suitable for light vehicle, aircraft and light equipment manufacturing.
Good corrosion resistance	By the nature of aluminum, thin oxidized surface is created at the surface of the aluminum and due, corrosion of aluminum is good. This resistivity can be improved by thicken this oxidized film artificially.
Suitable for further processes	Aluminum is a suitable material for the further application such as welding, machining and casting.
Strong Under various conditions	Aluminum is not very fragile in low temperatures. So it can be used under cold weather conditions. Various properties can be obtained by alloying and heat treating the aluminum
Suitable for various surface treatment	In harsh environment when the natural surface protection film of aluminum is not enough,thickening the oxidized film by the anode oxidization treatment gives abrasion resistance. Various surface treatments are used and the technologies of plating have been recently developed.
Not fragile at low temperatures	The properties of aluminum, makes it resistant to ultra low temperatures. Therefore it is suitable for LNG transportations, making storage tanks and other structures or equipments for low temperature plants.
High recycling value	It has a beautiful silver color and unlike iron, red rust would not appear damaging its clean appearance.
Good appearance	Small elastic coefficient of aluminum brings about good shock absorption effects. It also has the advantage of reducing the stress caused by heat.

Table 10: Solution heat treatment procedure for aluminum alloys

Material	Thickness	Heat Treatment (C^0-min)	Transition Time (in sec)	Quenching(C^0-min)
2024-0	0,81	493-35	6	25 -3
	1,02	493-35	6	25 -3
	1,27	493-35	6	25 -3
	1,6	493-35	6	25 -3
2024-0 Clad	0,81	493-35	6	25 -3
	1,02	493 -35	6	25 -3
	1,27	493 -35	6	25 -3
	1,6	493 -35	6	25 -3
6061-0	0,81	529 -35	6	25 -3
	1,02	529 -35	6	25 -3
	1,27	529 -35	6	25 -3
	1,6	529 -35	6	25 -3
7075-0	1,02	493 -35	6	25 -3
	1,27	466 -35	6	25 -3
	1,6	466 -	6	25 -3
7075-0 Clad	0,81	493 -35	6	25 -3
	1,02	493 -35	6	25 -3
	1,27	466 -35	6	25 -3
	1,6	466 -35	6	25 -3

Table 11: Heat treatment control procedure by using TAI Process Standard [36]

	Tensile Test Specimen	HBT Specimen	FLD specimen
Aluminum Alloy	2024-T42	2024-T42	2024-T42
Thickness (mm)	1	1,2	1,27
Brinell Hardness (HRB) (specified in the standard)	63,0-83,5	63,0-83,5	63-83,5
Brinell Hardness HRB (measured value)	66-67	68-70	65
Conductivity (IACS) (specified in the standard)	30,5-34,0	29,0-32,5	29,0-32,5
Conductivity (IACS) (measured value)	31,6-32,0	32,0 max.	31,5 max.

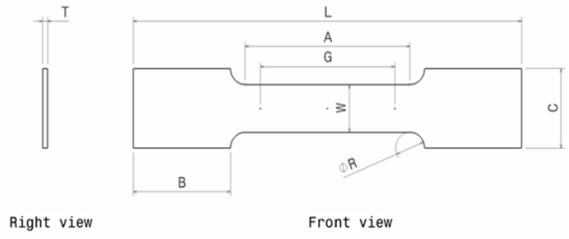

G: The length of extensometer	80±0.010 mm
W: Width	20±0.25 mm
R: Fillet radis	Thickness of the specimen
L: Total length	15.0 mm
A: Parallel length	120.0 mm
B: Gage length	50.0 mm
C: Gage width	30.0 mm

Figure 112: Tensile test specimen and its dimensions according to ASTM E8-04

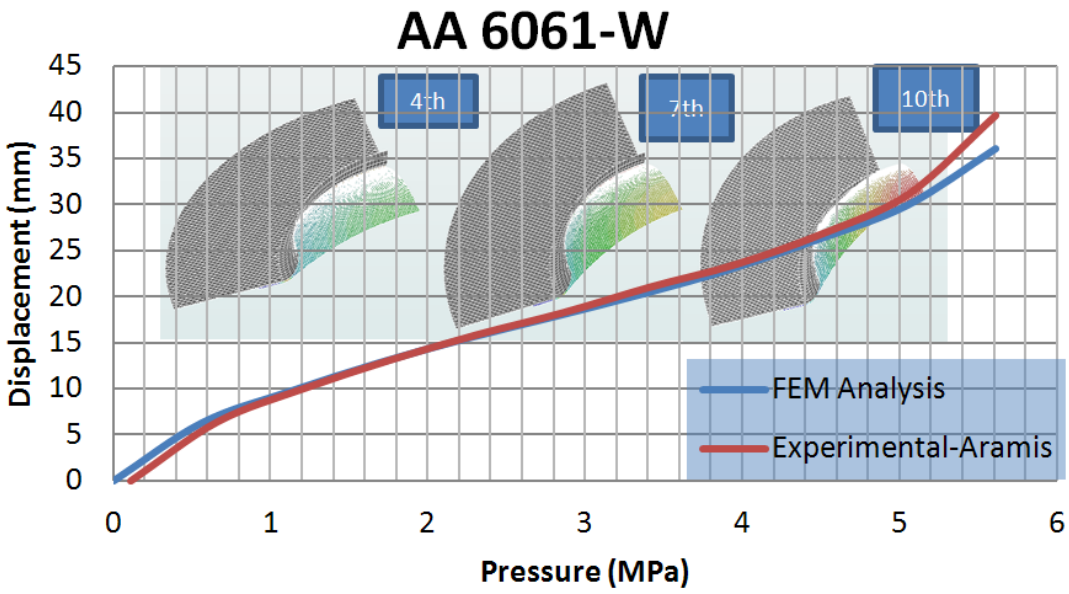

Figure 113: Displacement-Pressure curves which are taken from experiment and simulation

APPENDIX B

TECHNICAL DRAWINGS

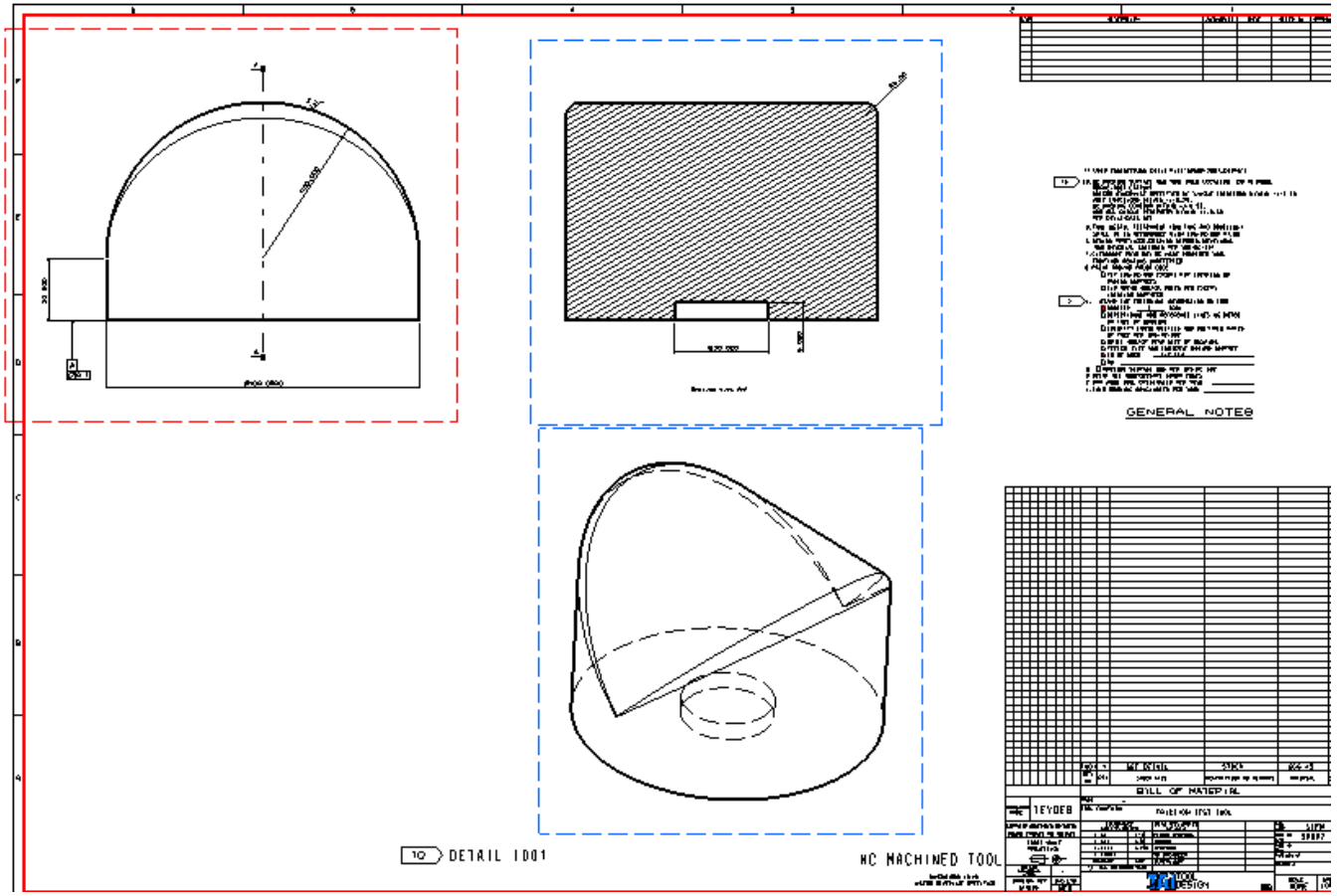

Figure 114: Technical drawing of a cylindrical punch which is used to form sheet specimen to identify friction coefficient under stretching

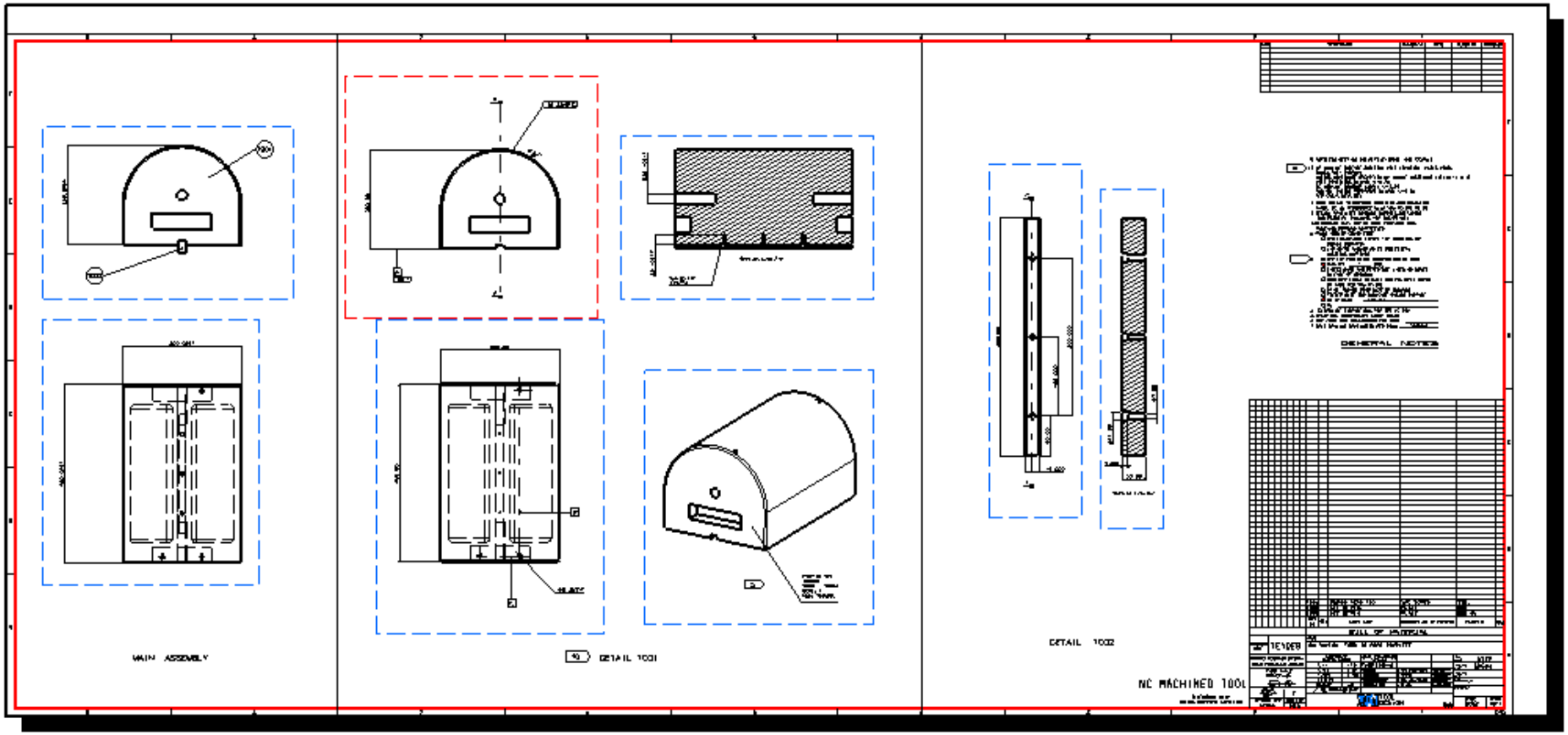

Figure 115: Technical drawing of semi-circular stretch forming die which is used in systematical experiments

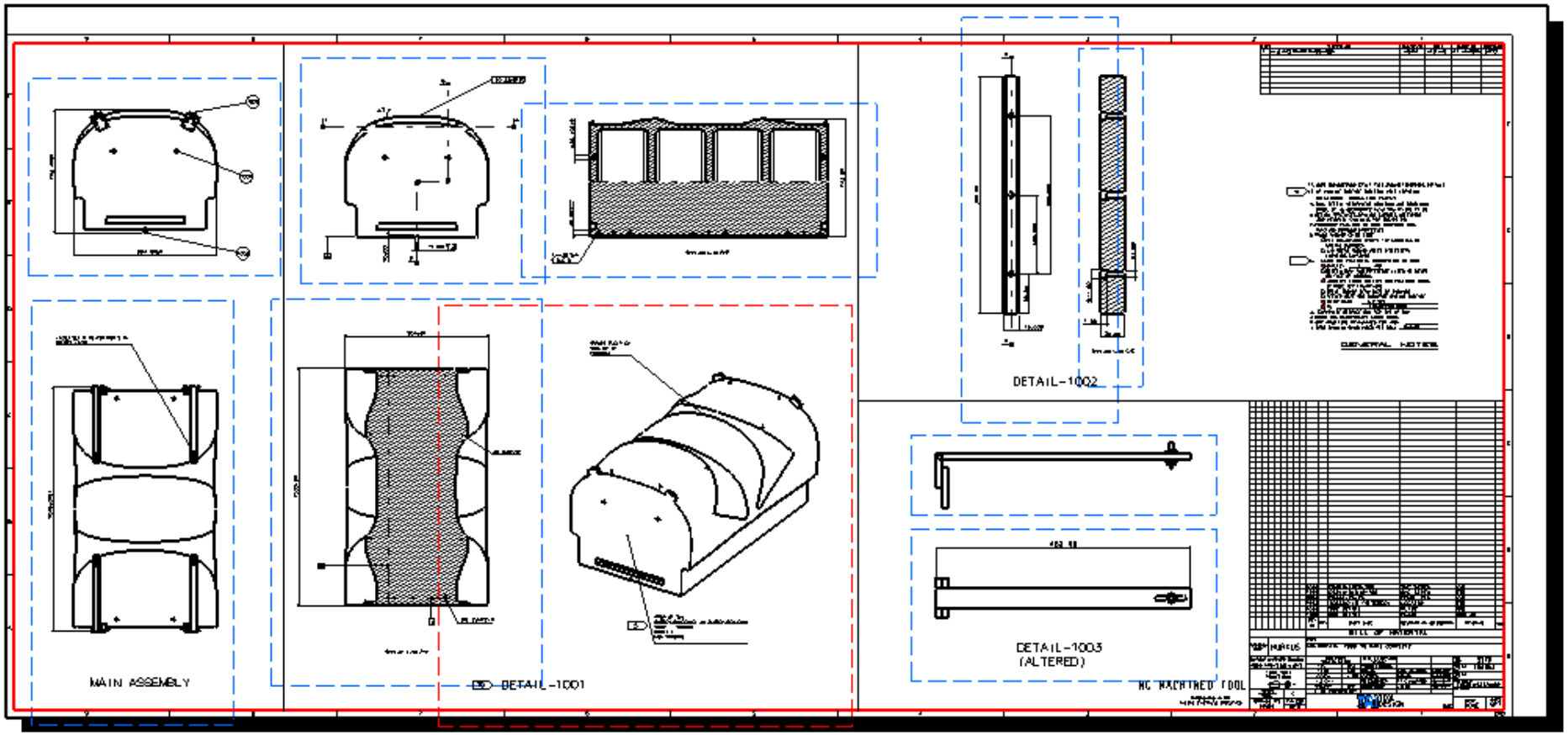

Figure 116: Technical drawing of a form die which is used to form HURKUS-Basic Training Aircraft's cockpit part

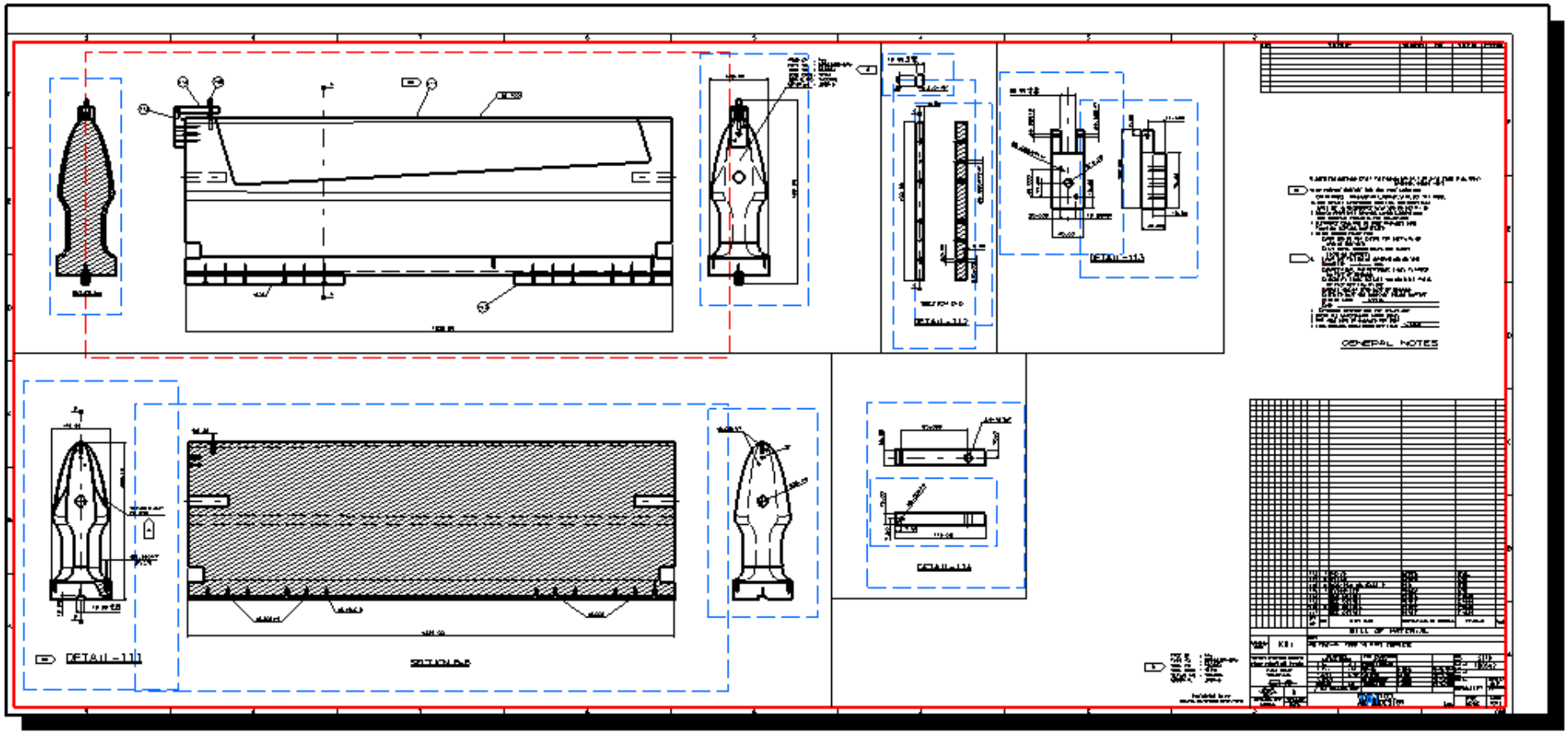

Figure 117: Stretch forming die which is used to form wing component of KAI, KT-1